ABSTRACT

Title of Dissertation: THE NEURAL BASES OF LATERALIZATION EFFECTS IN VISUAL FREQUENCY PROCESSING: A COMPUTATIONAL MODELING INVESTIGATION

Mary Flaherty Howard, Doctor of Philosophy, 2005

Dissertation directed by: Professor James A. Reggia
Department of Computer Science

This study develops a hypothesis on the origin and nature of spatial frequency lateralization that is grounded in the biology of the visual system, and demonstrates its potential validity using a neural network model. Computational experiments show that differences in the timing of development of the magnocellular and parvocellular systems coupled with asynchronous maturation of the hemispheres could result in the development of hard-wired asymmetry that biases the processing of spatial frequencies. The results provide evidence that this hard-wired asymmetry has the potential to explain both the absolute and the relative frequency lateralization effects observed in psychophysical experiments. This evidence is utilized to support a theoretical model that explains the relative frequency lateralization effect in terms of an interaction between task-driven

spatial attention and eccentricity-dependent frequency lateralization. Both the computational model demonstrating the basis of asymmetric development and lateralized spatial frequency processing, and the theoretical model illustrating the basis of the relative frequency lateralization effect, are specified in terms of neural structures and processes in the visual system. Two theories previously developed at an abstract level, namely, the Hellige theory on lateralized spatial frequency development and the Ivry and Robertson Double Filtering by Frequency theory of relative frequency lateralization (as applied to the visual system) are effectively made operational by this biological specification.

The hard-wired asymmetry that develops in the computational experiments exhibits a hemispheric bias based primarily on spatial frequency. There is also evidence of a secondary bias related to the visual pathways. The pathway bias happens to be opposite in direction from that proposed by other researchers to explain temporal frequency lateralization effects observed in electrophysiological investigations on visual frequency processing. This contradiction is addressed by postulating that the electrophysiological lateralization effects arise from known anatomical asymmetries in the vicinity of the occipital poles rather than from actual processing differences. This contention is supported through computational modeling of the dipole potential-VEP wave relationship. The model results demonstrate that dipole asymmetry attributable to anatomical differences could produce the observed lateralization effects.

The Neural Bases of Lateralization Effects in Visual Frequency Processing:

A Computational Modeling Investigation

by

Mary Flaherty Howard

Dissertation submitted to the Faculty of the Graduate School of the
University of Maryland, College Park in partial fulfillment
of the requirements for the degree of
Doctor of Philosophy
2005

Advisory Committee:

Professor James Reggia, Chair/Advisor
Professor Avis Cohen
Professor José Contreras-Vidal
Professor Bonnie Dorr
Professor David Poeppel

ACKNOWLEDGEMENTS

This work was supported in part by NIH award NS35460.

Contents

List of Tables

List of Figures

Chapter 1

Introduction

1.1 Overview

Much of neuroscience research is devoted to understanding the neural mechanisms underlying cognitive function. In this effort, research on differences between the right and left cerebral hemispheres is of special interest because of its potential to relate lateralized functionality, such as that associated with language and visuospatial processing, to specific neurobiological asymmetries. This potential is realized through the construction and testing of linking hypotheses, which attempt to explain data acquired in experiments on functional lateralization in terms of known, or proposed, anatomical and physiological asymmetries. Because it is often difficult or impossible to test these hypotheses empirically, computational modeling is commonly employed to examine their plausibility. In this study, I seek to contribute to this research by developing novel hypotheses on the neural bases of several empirically-observed visual lateralization effects and establishing their potential validity using computer models.

The lateralization effects considered in this study are related to the processing of the frequency components of a visual stimulus. A visual stimulus is a pattern or wave formed by changes in luminance across space and time. Any waveform, including a visual pattern, is composed of sine waves of various frequencies, amplitudes, and phases (for more on this, see Section 2.1). In the spatial domain, the sine waves, as distinguished on the basis of frequency, comprise the spatial frequency components of the visual stimulus. Similarly, in the temporal domain, the sine waves comprise the temporal frequency components. A decomposition of a visual pattern into its low and high spatial frequency components is illustrated in Figure 1.1.

Figure 1.1: The picture in the center contains the full range of spatial frequencies present in the visual image depicted. The picture on the left is composed from only the low frequencies contained in the image, while the picture on the right is composed from only the high frequencies in the image.

The main topic that I address in my investigation is the neural basis of lateralization in the processing of *spatial* frequency information. This lateralization is characterized as the more efficient processing of low frequency

information by the right hemisphere and of high frequency information by the left hemisphere. Its significance in visual asymmetry research is based on its two-fold potential to a) explain a variety of seemingly unrelated visuospatial lateralization effects, and b) be explained by asymmetries involving the basic components of the visual processing system. Past model-based research has concentrated primarily on the first of these two elements (for review, see Section 2.7). In contrast, I focus my research on the latter element, examining two hypotheses that together explain the nature and origin of spatial frequency lateralization in terms of a specific neurobiological asymmetry. In addition, I examine a third hypothesis that explains the neural basis of several *temporal* frequency lateralization effects that, on first consideration, appear to be inconsistent with this neurobiological asymmetry. Using models to examine the explanatory power of these hypotheses, I accomplish the following specific aims:

1. Establish that hemispheric asymmetry impacting spatial frequency processing can develop solely as the result of the timing of maturational processes affecting the visual system.

2. Provide evidence that this asymmetry can account for spatial frequency lateralization effects observed in psychophysical experiments.

3. Demonstrate that the spatial and temporal frequency lateralization effects obtained in electrophysiological experiments are consistent with known morphological and topological asymmetries in the visual cortex, and therefore may not be reflective of, or consistent with, the asymmetry that actually affects spatial frequency processing.

The lateralization effects I consider in this study are limited to the processing of frequency information in the visual system; however, the principles on which I base my hypotheses are not. Rather, it seems likely that these principles apply to other modalities and cognitive tasks. This prospect gives the research a relevance to the understanding of functional lateralization that extends beyond its immediate scope of investigation.

1.2 Research Hypotheses and Significance

I begin this study by hypothesizing a developmental scenario that can explain the existence of spatial frequency lateralization. This first hypothesis derives directly from a proposal by Hellige (1993) that is based on evidence that the visual system's capacity to transmit high spatial frequency information is poor at birth but improves rapidly over the next few months. The proposal suggests that, under such circumstances, an earlier developing right hemisphere could become relatively more proficient in the processing of low frequency information,

while a later developing left hemisphere could become relatively more proficient in the processing of high frequency information. My hypothesis posits the same scenario but goes beyond Hellige's proposal by specifying the visual system components and maturational processes that are involved, the type of hemispheric development that occurs, and the nature of the asymmetry that develops. In particular, I propose that differences in the time course of maturation of the two major visual pathways[1] interact with asynchronous hemispheric development to cause the development of a hard-wired asymmetry affecting the neural components that underlie spatial frequency processing. My proposal supplies the biological specificity that is required to transform the Hellige theory into a testable hypothesis.

Hard-wired asymmetry implies the existence of a fixed lateralization cross-over point such that the processing of frequencies below the point is right lateralized, while that of frequencies above the point is left lateralized. Such asymmetry is consistent with lateralization effects that depend on *absolute* frequency, but does not seem to be compatible with lateralization effects that depend on *relative* frequency[2]. My second hypothesis is aimed at reconciling hard-wired asymmetry with relative lateralization effects. Specifically, I propose

[1] That is, the magnocellular and parvocellular pathways (for more information, see Section 2.3).

[2] Lateralization based on absolute frequency depends on whether the test frequency is low or high relative to a point within the spectrum of spatial frequency sensitivity. Lateralization based on relative frequency depends on whether the test frequency is low or high relative to the other frequencies contained in the stimulus. Both types of lateralization have been observed in psychophysical experiments.

that the lateralization cross-over point changes with visual field location, shifting to lower frequencies as eccentricity increases, and that this arrangement, in conjunction with location-based spatial attention, can account for the relative frequency lateralization effect. As described later in the study, I base this proposal on the logical implications of my first hypothesis rather than deriving it from an existing theory. Nevertheless, it relates well to a theory proposed by Ivry and Robertson (1998) that similarly invokes a combination of attentional mechanisms and frequency-related asymmetry to account for the relative lateralization effect. Specifically, their theory suggests that an attentional process selects a task-appropriate range of frequencies for further processing; and that, within the selected range, low frequencies are amplified in the right hemisphere, while high frequencies are amplified in the left hemisphere. Ivry and Robertson develop this theory at the conceptual level without attempting to specify the biological nature of the hypothesized attentional and amplification processes. My hypothesis, in effect, represents a plausible implementation of their theory at the biological level.

My third and final hypothesis addresses the conflict between the evidence obtained in psychophysical investigations of spatial frequency lateralization and that obtained in electrophysiological investigations. The latter evidence points to temporal rather than spatial frequency as the significant factor in visual processing lateralization. Furthermore, it suggests a hemispheric bias in the treatment of output from the two major visual pathways that is at odds with the

asymmetry I propose to explain the psychophysical evidence. My hypothesis eliminates this conflict by taking the position that the electrophysiological data is explained by the impact of morphological and topological asymmetries on the measurements. My proposal implies that the lateralization apparent in the data is predominately an artifact produced by gross anatomical asymmetry rather than a reflection of true hemispheric differences in processing, and therefore provides information neither on lateralization as a function of particular frequency factors nor on hemispheric bias related to the visual pathways. The possibility that morphological asymmetry might underlie observed electrophysiological lateralization effects was raised in the Van Orden and House (1996) investigation of spatial frequency lateralization, but has generally not been given serious consideration in past research on this topic.

The research framed by these hypotheses constitutes the most comprehensive and biologically-explicit theoretical work on the neural basis of spatial frequency lateralization that has been done to-date. As such, it represents a significant addition to research on lateralization in visual processing. However, the greater significance of this research may lie in its support of a paradigm of asymmetric development that potentially accounts for lateralization on a much broader scale. In this paradigm, asynchronous development of homologous cortical regions results in asymmetry if three conditions apply: 1) multiple pathways supply distinctive input to these regions, 2) the input pathways differ from one another in their time course of maturation, 3) at least one input pathway

is still maturing during the time of the regions' development. The circumstance of these conditions is probably not limited to the visual system, but rather seems likely to occur throughout cortical development.

1.3 Approach

My approach in this investigation is to develop each hypothesis based on a reasoned argument that draws upon findings from a number of different areas of neuroscience research. Next, I reformulate the hypothesis as a computer model, thus ensuring that its underlying concepts and assumptions are made explicit. I then seek evidence in support of the hypothesis through simulation experiments that examine the model's capacity to account for relevant empirical data.

I begin the presentation of this work with a review of background information on spatial frequency processing and past research related to spatial frequency lateralization. I then present the research on each study hypothesis, successively and in the same basic format. This format includes a review of the relevant research, proposals, and empirical data together with the logical development of the hypothesis based on these elements; a specification of model principles and assumptions; a description of model design and dynamics; an analysis and interpretation of simulation results; and a discussion of findings and their implications. Because the research on the first two hypotheses is closely related and based on the same model, it is incorporated into a single chapter on the development of spatial frequency lateralization. The research on the third

hypothesis is presented in a chapter dealing with electrophysiological lateralization effects. The presentation ends with a chapter that summarizes the research, offers several theoretical predictions based on the results, and discusses implications of the study findings.

Chapter 2

Background

This chapter provides background information on the neural components of spatial frequency processing and a review of research related to spatial frequency processing lateralization. The background material begins with an introduction to frequency information in visual stimuli and visual system sensitivity to this information. Then visual pathways and spatial filters are discussed in the context of frequency sensitivity. Next, the review of related research explains the spatial frequency hypothesis and its relationship to various visual lateralization effects. This is followed by a discussion of spatial frequency lateralization experiments and visual lateralization modeling studies.

2.1 Frequency Components of a Visual Stimulus

According to the Fourier Theorem, any waveform can be described as the sum of sine waves of appropriate frequency, amplitude and phase. A visual stimulus can be thought of as a waveform that is defined in the spatial dimension as the variation in luminance across space and in the temporal dimension as the variation in luminance across time. Thus, a visual stimulus can be decomposed into and represented by sine wave components of various frequencies in both the

spatial and temporal dimensions (for detailed discussion, see Graham, 1989). The frequency of a spatial sine wave component is given in cycles per unit of distance, where the distance unit is usually degree of visual angle (cpd). The frequency of a temporal sine wave component is given in cycles per second (Hz). Experiments aimed at exploring visual system sensitivity to frequency typically employ stimuli having a single frequency component. In the spatial domain, such stimuli consist of simple sinusoidal gratings such as those shown in Figure 2.1. In the temporal domain, such stimuli consist of the sinusoidal modulation of luminance as a function of time known as flicker. Often the temporal fluctuation in luminance is imposed on a grating pattern, such that the light bars become dark as the dark bars become light, in a modulation pattern referred to as counterphase flicker.

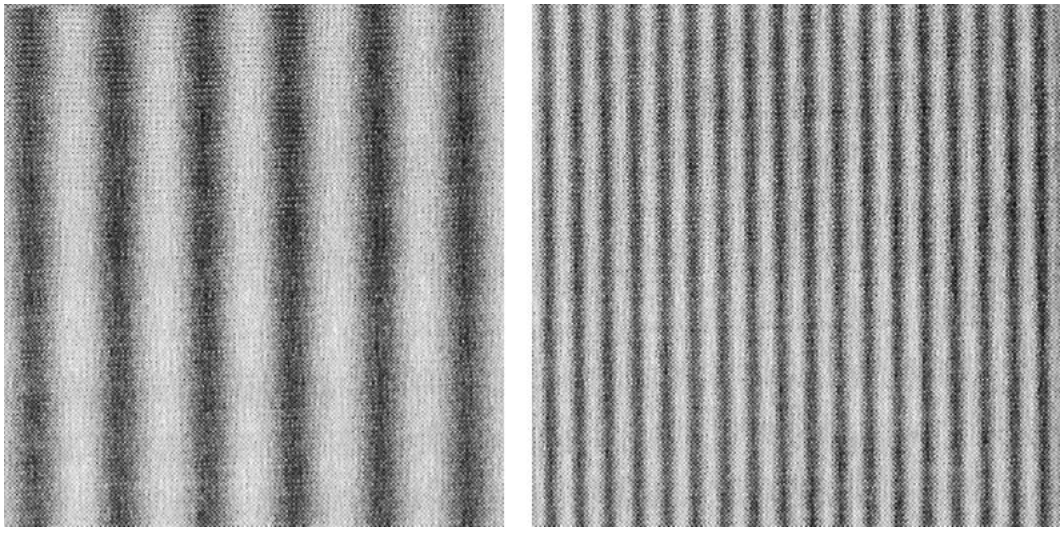

Figure 2.1: Two examples of sinusoidal gratings. The grating on the left is of relatively low spatial frequency, the grating on the right of relatively high frequency.

2.2 Visual System Sensitivity to Spatial and Temporal Frequency

The sensitivity of the visual system to spatial and temporal frequency is measured psychophysically by determining the minimum contrast in luminance (for a given average luminance) needed to detect a stimulus of a particular spatial and temporal frequency[3]. This information is represented by the contrast sensitivity function (CSF) which is defined as the reciprocal of the minimum contrast required for stimulus detection as a function of frequency. Spatial frequency sensitivity is a low-pass function for all but the lowest temporal frequencies where it becomes a band-pass function with a maximum near 5 cpd[4] (see Figure 2.2). On the other hand, the temporal frequency sensitivity is a low-pass function for all but the lowest spatial frequencies where it becomes a band-pass function with a peak near 8 Hz (see Figure 2.2). The combined spatiotemporal CSF is displayed in Figure 2.3.

[3] Luminance contrast is given by $(L_{max}-L_{min})/(L_{max}+L_{min})$ where L_{max} and L_{min} are the maximum and minimum values of luminance, respectively.

[4] A low-pass filter function is maximally sensitive to near-zero frequencies with declining sensitivity as frequency increases. A band-pass filter function is maximally sensitive to some range of intermediate frequencies with declining sensitivity to both higher and lower frequencies.

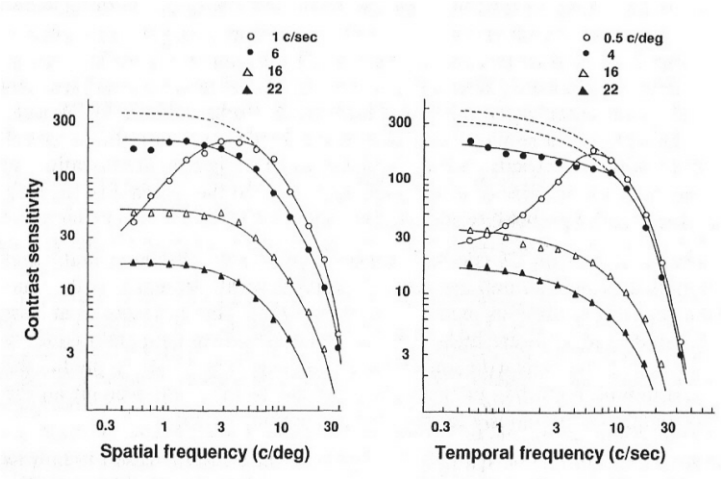

Figure 2.2: The contrast sensitivity functions for spatial frequency as measured at various temporal frequencies (left) and temporal frequency as measured at various spatial frequencies (right). (Reprinted from Robson, 1966, with permission.)

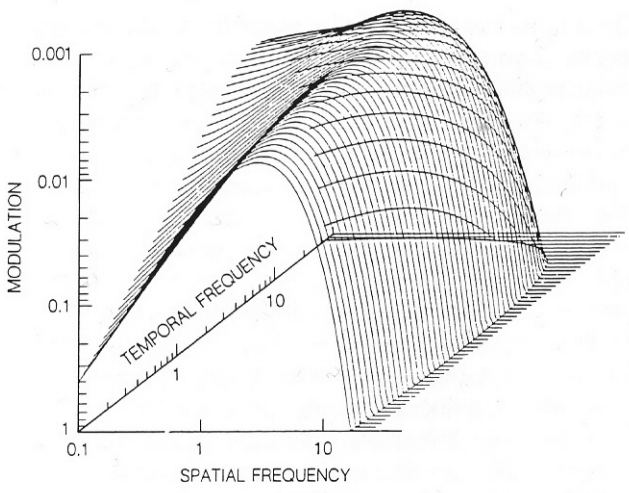

Figure 2.3: The combined spatiotemporal contrast sensitivity function (CSF) under photopic conditions. In this depiction of the CSF, the modulation axis shows actual contrast values rather than their reciprocals. (Reprinted from Kelly, 1979, with permission.)

2.3 The Visual Pathways and Frequency Sensitivity

Visual input is delivered to the visual cortex via two major pathways, the magnocellular and the parvocellular, that run in parallel from the retina through the lateral geniculate nucleus (LGN) of the thalamus to the primary visual cortex (V1) (for reviews see Livingstone & Hubel, 1988a; Merigan & Maunsell, 1993; Schiller & Logothetis, 1990; Shapley, 1990, 1992; Van Essen & DeYoe, 1995). The pathways are anatomically distinct through the primary afferent layer (layer 4) of V1 with the magnocellular pathway projecting mainly to layer 4Cα and the parvocellular mainly to 4Cβ (see Figure 2.4). Strict partitioning is not maintained beyond this point as an intermixing of the streams begins even in V1 (Allison, Melzer, Ding, Bonds, & Casagrande, 2000; Nealy & Maunsell, 1994; Sawarti & Callaway, 1996; Vidyasagar, Kulikowski, Lipnicki, & Dreher, 2002). However, the magnocellular pathway does provide the dominant input to the dorsal stream, responsible for object location tasks. Both pathways contribute substantially to the ventral stream, responsible for object identification tasks, with the parvocellular contribution being the stronger of the two. The relationship between the magnocellular and parvocellular pathways and the dorsal and ventral processing streams is illustrated in Figure 2.4.

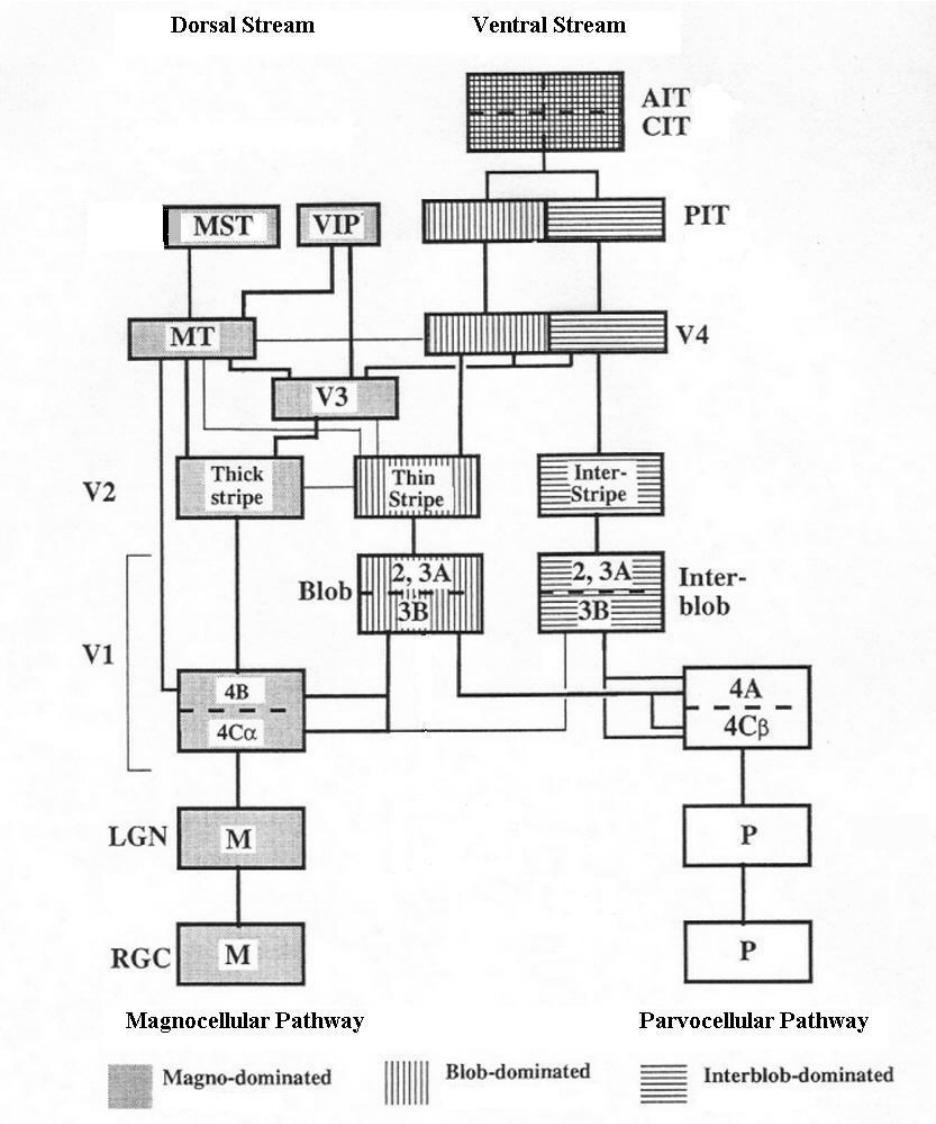

Figure 2.4: The magnocellular and parvocellular pathways originate in the M and P retinal ganglion cells (RGC), respectively. They remain distinct through the lateral geniculate nucleus (LGN) of the thalamus and terminate in separate layers of V1, the magnocellular in 4Cα and the parvocellular in 4Cβ. The magnocellular pathway provides the dominant input to the dorsal stream associated with the processing of motion and spatial relationships. The dorsal stream projects from layer 4B of V1 to the thick stripes of V2 and then on to the middle temporal area (MT), eventually reaching the medial superior temporal (MST) and ventral intraparietal (VIP) areas. Both pathways provide input to the ventral stream associated with the processing of color, texture, and form. The ventral stream comprises parallel projections from the blobs and interblobs of layer 2/3 in V1 to the thin stripes and interstripes of V2, respectively. The parallel projections continue through V4 and the posterior inferotemporal areas (PIT), eventually converging on the central and anterior inferotemporal areas (CIT and AIT). An intermixing of the streams results from a partial convergence, followed by a divergence, of the streams in V3, as well as from several cross-talk connections. (Adapted from Van Essen & DeYoe, 1995, with permission.)

The pathways are also physiologically distinct, differing in both processing speed and sensitivity to various features of the stimulus. Specifically, the magnocellular pathway is somewhat faster and more sensitive to absolute luminance than the parvocellular pathway. Furthermore, the magnocellular pathway is more sensitive to luminance contrast, while the parvocellular pathway is more sensitive to chromatic contrast. In addition, the pathways have overlapping but somewhat different sensitivities to both spatial and temporal frequency. The magnocellular pathway is most sensitive to low spatial frequencies and high temporal frequencies, while the parvocellular pathway is most sensitive to mid-to-high spatial frequencies and low temporal frequencies. This difference is reflected in the CSF for the individual pathways (see Figure 2.5) that was obtained from lesioning experiments on monkeys (Merigan, Byrne, & Maunsell, 1991; Merigan, Katz, & Maunsell, 1991).

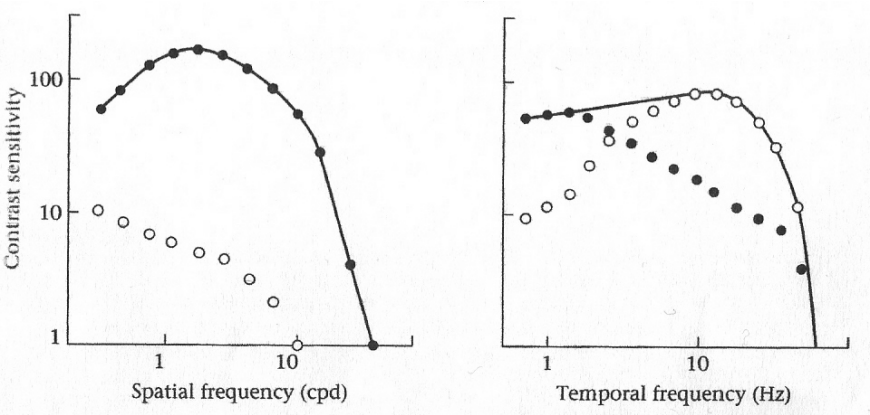

Figure 2.5: The contrast sensitivity functions for spatial (left) and temporal (right) frequency obtained in lesion studies using monkeys. Solid lines show the CSF obtained with both pathways intact; open circles, with only the magnocellular pathway intact; filled circles, with only the parvocellular pathway intact. Spatial contrast sensitivity was measured using a grating of zero temporal frequency. Temporal contrast sensitivity was measured at low spatial frequency. (From Merigan & Maunsell, 1993. Reprinted, with permission, from *The Annual Review of Neuroscience,* Volume 16 © 1993 by Annual Reviews, www.annualreviews.org.)

The magnocellular and parvocellular pathways are thought to provide the neural substrate for the two temporal processing channels that have been distinguished on the basis psychophysical experiments in humans (see Figure 2.6). The band-pass channel associated with the magnocellular pathway is characterized by a fast, transient response to the presentation of a visual stimulus. In contrast, the low-pass channel associated with the parvocellular pathway is characterized by a slower, sustained response.

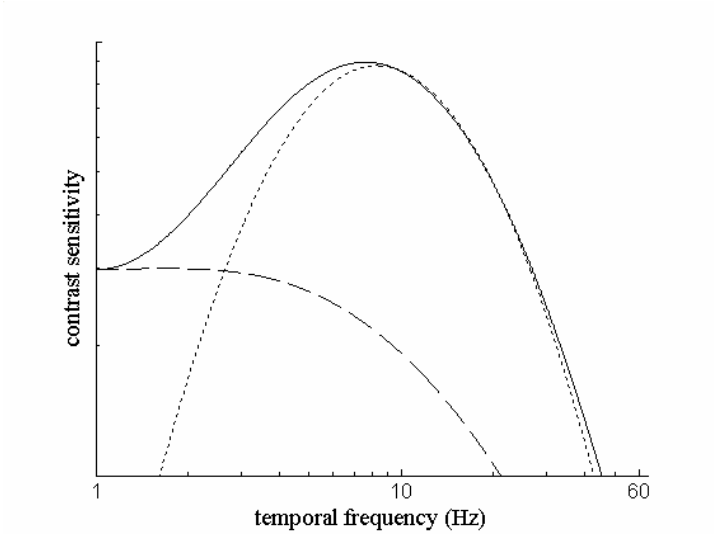

Figure 2.6: The temporal contrast sensitivity function (solid line) as the envelope of the transient channel sensitivity (dotted line) and the sustained channel sensitivity (dashed line). The curves shown are representative of sensitivities at low spatial frequency.

2.4 Spatial Filters

The receptive fields of V1 cells have an antagonistic center – surround organization that sums linearly to produce a transformation from the spatial to the frequency domain as shown in Figure 2.7 (for in-depth discussions of this topic, see De Valois & De Valois, 1988; Wilson, Levi, Maffei, Rovamo, & De Valois, 1990). Thus, the spatial organization of V1 cells allows them to act as filters that respond selectively to the spatial frequency content of a stimulus falling within their receptive fields.

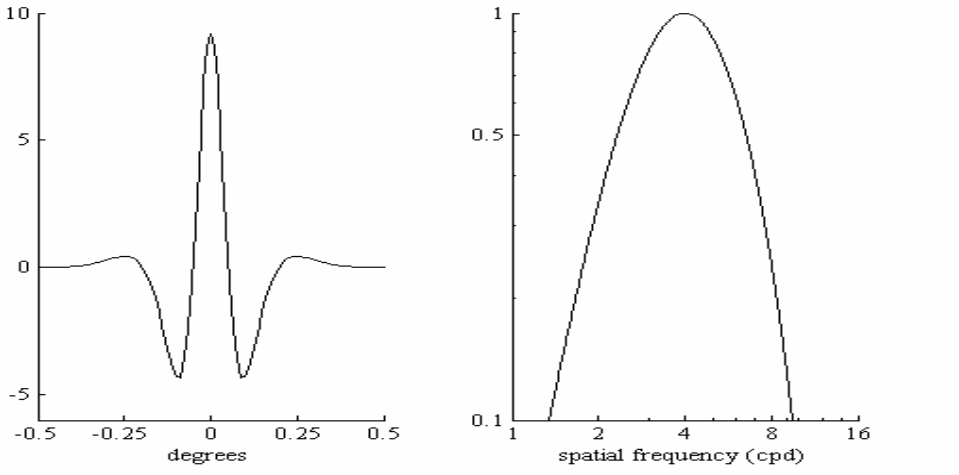

Figure 2.7: V1 cells transform information in the spatial domain into a representation in the frequency domain. The graph on the left shows a characteristic receptive field (RF) profile of a V1 cell, with response given as a function of spatial location. Responses below the 0 mark are antagonistic to those above the 0 mark, that is, they are of opposite signs. Assuming linear summation of the RF response, the cell should be maximally sensitive to a 4 cpd grating. This is confirmed by the cell's frequency sensitivity profile, shown on the right, obtained by computing the Fourier transform of the receptive field function.

The contrast sensitivity functions for individual cells differ from one another in peak frequency but are similar in bandwidth[5], with a tuning that is narrower than that of the CSF for the visual system as a whole (De Valois, Albrecht, & Thorell, 1982). Filters that are similar in peak frequency effectively constitute a channel that transmits frequency information within a restricted range. The collective activity of channels covering the range of peak frequencies found in V1 filters is thought to account for the spatial CSF as shown in Figure 2.8 (De Valois & De Valois, 1988). As suggested by the CSF, the distribution of

[5] Bandwidth refers to the difference between the high and the low frequency for which response drops to half maximum as measured in octaves. It is computed as $[\log(\omega_H)-\log(\omega_L)]/\log 2$ where ω_H and ω_L are the high and low half-amplitude frequencies, respectively.

filters across peak frequencies is non-uniform, with greater numbers falling in the middle of the frequency spectrum and fewer toward the high and low ends (De Valois et al., 1982).

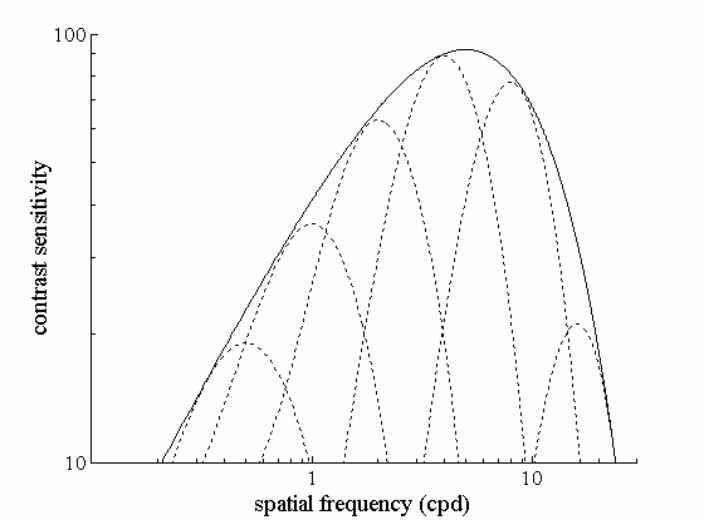

Figure 2.8: A depiction of the spatial CSF as the envelope of more narrowly tuned channels where each channel represents the collective activity of filters with similar preferred frequencies.

Each location in the visual field is processed by multiple spatial filters with overlapping receptive fields that represent roughly a six-octave range of peak frequencies. Because filter bandwidth is typically about one-and-a-half octaves (De Valois, et al., 1982), filters responding to the low frequency content of a local stimulus are differentiated from those responding to the high frequency content. Hence, the filters perform an approximate decomposition of the stimulus into its spatial frequency components and pass this information on for further processing.

The primary input to the V1 filters comes directly from the magnocellular and parvocellular pathways as shown in Figure 2.4. The frequency sensitivities of the pathways (see Figure 2.5) suggest that the contribution of the magnocellular pathway is greatest for filters responding best to low spatial frequencies and declines as peak frequency increases. Filters with peak frequencies above 10 cpd are likely to be driven almost exclusively by the parvocellular pathway.

2.5 Filter Variation with Retinal Eccentricity

Converging evidence supports the view that the distribution of spatial frequency filters by peak frequency tuning shifts toward lower frequencies with increasing retinal eccentricity. The receptive field size of V1 cortical cells increases as eccentricity increases (Dow, Snyder, Vautin, & Bauer, 1981; Hubel & Wiesel, 1974; Van Essen, Newsome, & Maunsell, 1984), suggesting the possibility of a shift in filter tuning to lower frequencies. Direct evidence of such a shift was found in studies that tested spatial frequency tuning in macaque V1 cells (De Valois et al., 1982; Schiller, Finlay, & Volman, 1976). The shift is readily apparent in the distributions of peak spatial frequencies observed at two different retinal eccentricities in the De Valois et al. (1982) study (see Figure 2.9).

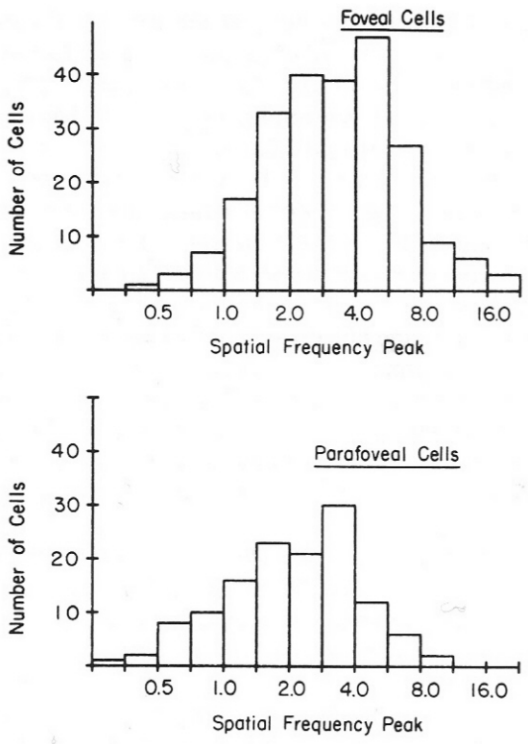

Figure 2.9: The distribution of peak spatial frequency of cells located in the foveal (0° to 1.5°) and parafoveal (3° to 5°) regions of the macaque monkey visual area V1. (Reprinted as adapted in De Valois and De Valois , 1988 from Figure 6 in De Valois et al., 1982, copyright 1982, with permission from Elsevier.)

Additional evidence of the frequency shift was obtained in a study that examined the patterns of deoxyglucose uptake produced in response to stimuli of various spatial frequencies across eccentricities that ranged from 0° to 8° (Tootell, Silverman, Hamilton, Switkes, & De Valois, 1988). The study found that the striate cortex of the macaque exhibits some degree of spatial frequency organization such that frequencies eliciting a response in a blob area are, on average, lower than the frequencies eliciting a response in the surrounding interblob area. However, the frequencies to which the two areas responded

changed systematically with retinal frequency. A frequency of 4.4 cpd elicited a robust response in blobs within the fovea, in interblobs at eccentricities of 4° to 6°, and in both at intermediate eccentricities. Thus, this frequency, from the middle of the spectrum, appears to be a low frequency relative to those represented in the fovea and a high frequency relative to those represented at eccentricities beyond 4°. Frequencies from the high end of the spectrum, 6.5-7 cpd, elicited a response in both blobs and interblobs or in blobs only, within the fovea. These frequencies elicited the greatest response in interblobs at eccentricities ranging from 3° to 8°, but with response diminishing with increasing eccentricity until it was virtually eliminated. In contrast, a frequency from the low end of the spectrum, 0.9 cpd, elicited a strong response in the blobs across the entire range of eccentricities. These results are consistent with more recent fMRI-based findings of a gradual shift in peak spatial frequency tuning to lower frequencies with increasing eccentricity throughout the retinotopic areas of the visual cortex including V1 (Sasaki et al., 2001).

A shift in filter tuning with increasing eccentricity should be reflected in the contrast sensitivity function (CSF). In fact, the CSF has been found to shift toward lower frequencies with increasing eccentricity (Kelly, 1984; Rovamo, Virsu, & Näsänen, 1978; Virsu & Rovamo, 1979). Experiments using a stimulus of fixed extent found that the (horizontal) shift in the CSF toward lower frequencies with increasing eccentricity is accompanied by general decrease (vertical shift) in sensitivity levels (Rovamo, Virsu, & Näsänen, 1978). This

decrease can be explained by the decrease in the area of V1 cortex representing a unit of visual field area with increasing eccentricity, referred to as cortical magnification (Dow, et al., 1981; Hubel & Wiesel, 1974; Tootell, Silverman, Switkes, & De Valois, 1982; Van Essen, et al., 1984). Because the number of cells per unit of cortical area is roughly constant throughout the primary visual cortex, the density of filters per unit of visual field area decreases with increasing eccentricity. This implies that the number of filters activated by a stimulus of fixed extent decreases with increasing eccentricity.

Both filter preferred spatial frequency and the number of filters per degree (linear density) as a function of eccentricity can be approximated by an equation of the form $X = X_0(1+E/E_2)^{-1}$ (Wilson et al., 1990). In this equation, X is the characteristic of interest, X_0 is its value at an eccentricity of 0°, E is eccentricity in degrees, and E_2 is the eccentricity for which $X = X_0/2$. Estimates of E_2 (Dow, et al., 1981; Hubel & Wiesel, 1974; Tootell et al., 1982; Van Essen, et al., 1984) suggest that the values for spatial frequency tuning and filter density differ, although Rovamo et al. (1978) found that CSF performance could be maintained as eccentricity increases by a simple magnification of the grating stimulus. Such magnification essentially uses a single value of E_2 to scale both the spatial dimensions of the stimulus and its spatial frequency components. Figure 2.10 shows how the CSF would scale with eccentricity based on a single E_2 value[6] of

[6] This value for E_2 is derived from a scaling function fitted by Kelly (1984) to data from Virsu and Rovamo (1979).

7.14°. The computed change in the CSF as a function of eccentricity closely resembles that observed in the Rovamo et al. (1978) experiments.

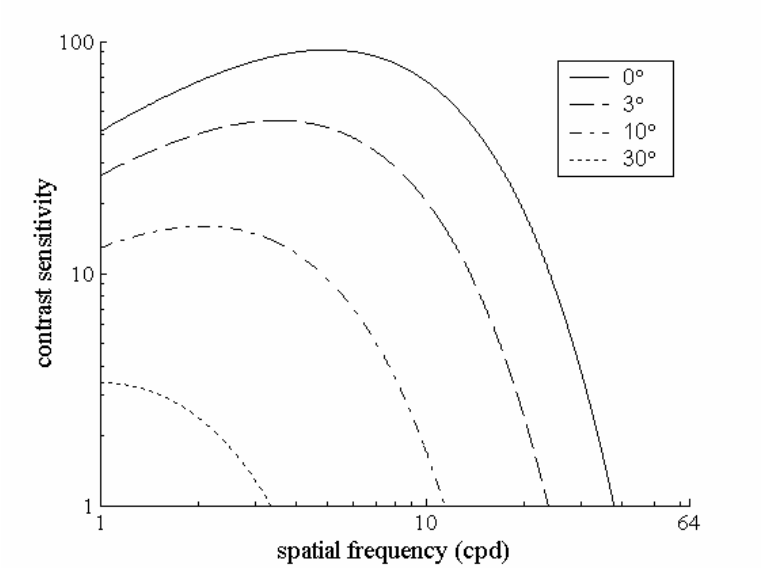

Figure 2.10: Contrast sensitivity function variation with retinal eccentricity computed for eccentricities of 0°, 3°, 10°, and 30° using the same factor to scale both frequency and sensitivity.

Several pieces of evidence suggest that contribution of the parvocellular pathway relative to that of the magnocellular pathway may diminish with increasing eccentricity. By combining available data on M and P cell densities and the representation of the visual field in the LGN, Connolly and Van Essen (1984) determined that the ratio of P cells to M cells decreases as eccentricity increases. Livingstone and Hubel (1988b) disputed this view on the basis of retrograde labeling experiments that did not reveal a change in the ratio of P to M cells across the visual field. However, a more recent retrograde labeling

experiment by Azzopardi, Jones, and Cowey (1999), which identified and addressed several methodological issues in the Livingstone and Hubel study, concluded that the P-to-M cell ratio does, indeed, decline with eccentricity, and that this ratio applies to the P and M afferents to V1, as well. They found that the decline could be described by a function of the form $y = 30.97e^{-.238\mathrm{E}} + 5.791e^{-.0003\mathrm{E}}$ where y is the P to M ratio at eccentricity E (in degrees) and the constants (based on the approach designated as Method 1 in their study) are derived via a least-squares fit to the data. The exact relationship between P and M cell afferents and spatial frequency filters is unknown, but it seems likely that the P pathway contributes less to filter activity relative to the M pathway as eccentricity increases.

2.6 The Spatial Frequency Hypothesis

Lateralization in visual processing based on the frequency content of the stimuli was first addressed by the spatial frequency hypothesis proposed by Sergent (1982). This hypothesis provides an overarching explanation for a variety of hemispheric asymmetries observed in psychophysical experiments on visuospatial processing. The hypothesis theorizes that, although the same visual input is transmitted to both cortical hemispheres, the right hemisphere is more efficient at processing the low spatial frequency components of the input while the left hemisphere is more efficient at processing the high spatial frequency input components. The hypothesis further proposes that the asymmetry arises in

processing that takes place beyond the "sensory level", meaning that the spatial frequency channels performing the sensory level processing are symmetric but the treatment of their outputs is not (Sergent 1982, 1987).

Since its proposal, the hypothesis has been invoked to explain the asymmetries observed in two areas of visual processing that are of particular interest in lateralization research: global versus local patterns and categorical versus coordinate spatial relationships (Hellige, 1993; Ivry & Robertson, 1998). In the global/local asymmetry, the right hemisphere exhibits superiority for processing the overall configuration of the stimulus, while the left hemisphere exhibits superiority for the processing of the details (Martin, 1979; Sergent, 1982; Van Kleek, 1989). In the coordinate-categorical asymmetry, the right hemisphere displays an advantage in the performance of distance-dependent spatial tasks (e.g., near or far judgments), while the left hemisphere displays an advantage in the performance of distance-independent spatial tasks (e.g., above or below judgments) (Hellige & Michimata, 1989; Kosslyn, Barett, Cave, Tang, & Gabrieli, 1989). In the former case, information on configuration is more likely to be conveyed by low spatial frequencies and information on details by high spatial frequencies; thus, the potential link between the global-local asymmetry and the spatial frequency hypothesis is readily apparent. In the latter case, coordinate tasks are thought to depend on coarse coding involving large receptive fields while categorical tasks depend on fine-grained coding involving small receptive fields (for more on this, see Section 2.7). Because large receptive fields are more

likely to be associated with the processing of low frequency information and small receptive fields with the processing of high frequency information (see Figure 2.7), the link to the spatial frequency hypothesis is implied.

The potential explanatory power of the spatial frequency hypothesis has led to a substantial amount of research being devoted to its verification (for reviews see Christman, 1997; Grabowska & Nowicka, 1996; Mecacci, 1993, 1997). Much of the research produced ambiguous results because either variation in spatial frequency was confounded with variation in other stimulus characteristics that could produce performance asymmetries, or the spatial frequency processing requirements of the experimental task were not known with certainty. Such problems were eliminated in studies in which input characteristics were carefully controlled, gratings of known spatial frequency content were used as stimuli, and the spatial frequency components needed to perform the task were well understood.

Among these studies, the psychophysical experiments examining visual field-spatial frequency interactions using tachistoscopic presentation[7] of stimuli over a range of spatial frequencies have provided the strongest evidence in support of the hypothesis. As predicted by the hypothesis, the studies that examined functions of sensory level processing, such as detection as a function of contrast (Fiorentini & Berardi, 1984; Kitterle, Christman, & Hellige, 1990; Peterzell, Harvey, & Hardyck, 1989), adaptation (Fiorentini & Berardi, 1984;

[7] Presentation restricted to either the right or the left visual field.

Rose, 1983), subthreshold summation (Fiorentini & Berardi, 1984), and visual persistence (Peterzell, Harvey, & Hardyck, 1989), found no significant visual field-spatial frequency interaction. However, studies that examined functions thought to involve post–sensory level processing, such as pattern identification (Christman, Kitterle, & Hellige, 1991; Kitterle, Christman, & Conesa, 1993; Kitterle et al., 1990; Kitterle, Hellige, & Christman, 1992, Proverbio, Zani, & Avella, 1997) and pattern discrimination (Kitterle & Selig, 1991; Niebauer & Christman, 1999), did find visual field-spatial frequency interactions consistent with the spatial frequency hypothesis.

Significant visual field-spatial frequency interactions were found in a series of studies that measured reaction time for pattern identification tasks (Christman et al., 1991; Kitterle et al., 1990, 1992, 1993). In these studies, an experimental stimulus (sinusoidal grating) consisted of a circular patch, 6.8° in diameter and centered along the horizontal meridian of the right or left visual field, with an inner edge eccentricity of either 3° (Christman et al., 1991; Kitterle et al., 1990, 1992) or 2° (Kitterle et al., 1993). The experiments required a choice identification of a stimulus based on a single characteristic such as the width of the grating. As predicted by the hypothesis, reaction time (RT) was faster for LVF/RH (left visual field/right hemisphere) presentation when the identification involved the processing of a low spatial frequency stimulus or the low frequency components of a compound stimulus. Also as predicted, reaction time was faster for RVF/LH (right visual field/left hemisphere) presentation when the

identification involved the processing of a high spatial frequency stimulus or the high frequency components of a compound stimulus. For example, Kitterle et al. (1990) found the identification of a 1 cpd sinusoidal grating was faster for LVF/RH presentation, while the identification of a 9 cpd sinusoidal grating was faster for RVF/LH presentation, as shown in Figure 2.11.

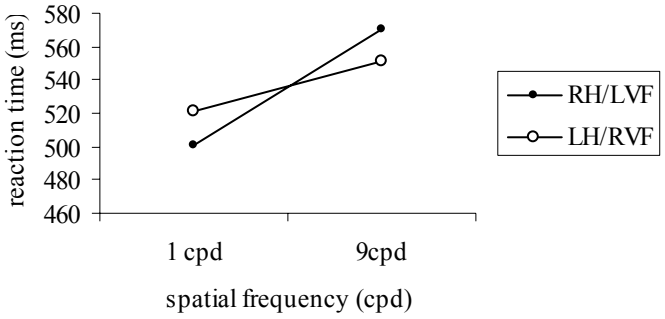

Figure 2.11: The absolute spatial frequency lateralization effect. Hemispheric performance (designated as RH/LVF or LH/RVF), as measured by reaction time, on the task of identifying sinusoidal grating stimuli as either 1 or 9 cpd. Reaction times are the means of data obtained in Experiment 4 of Kitterle et al., 1990.

Results consistent with the spatial frequency hypothesis were also obtained in a selective attention experiment in which subjects were asked to respond to the appearance of a sinusoidal grating of a particular frequency during random presentations of 1.5, 3 and 6 cpd gratings (Proverbio et al., 1997). Specifically, response to the 1.5 cpd target was faster for LVF/RH presentation and response to the 6 cpd target was faster for RVF/LH presentation. In addition to such basic findings, Kitterle et al. (1993) showed that the interference between

frequency components in a compound stimulus is consistent with the spatial frequency hypothesis, that is, interference of the low frequency component with the processing of the high frequency component is greater for LVF/RH presentation, while the reverse is found for RVF/LH presentation.

The studies that examined the post–sensory level processing function of pattern discrimination (Kitterle & Selig, 1991; Niebauer & Christman, 1999) found moderate support for the spatial frequency hypothesis. In these experiments, two sinusoidal stimuli separated by a constant difference (as measured in octaves) were successively presented and the second stimulus was determined to be of a lower or higher spatial frequency relative to the first stimulus. In contrast to the detection and identification tasks, discrimination task RT depends on the memory processing of the first stimulus as well as perceptual processing of the second stimulus and could be affected by interference between the first and second stimulus. The Kitterle & Selig (1991) experiments yielded a significant visual field-spatial frequency interaction, while the interaction was not significant for the Niebauer & Christman (1999) experiments but was generally consistent with the spatial frequency hypothesis.

The Christman et al. (1991) study produced results consistent with the spatial frequency hypothesis as applied to relative rather than absolute frequencies. In this study, subjects were asked to distinguish between two compound grating stimuli, one consisting of a base pair of sine-wave components and the other of three sine-wave components including the base pair. Two

experiments were conducted, the first using low spatial frequencies (.5 and 1 cpd) and the second using high spatial frequencies (4 and 8 cpd) for the base pair, with an identical third component (2cpd) in both experiments. As expected, the results showed that identification of the base pair stimulus was faster for LVF/RH presentation in the low frequency condition but was faster for RVF/LH in the high frequency condition (see Figure 2.12). The study also found that the addition of the third component slowed performance in both experiments. However, for the low frequency condition, the slow down was greater for the right hemisphere such that the identification of the three component stimulus took equally long in the two hemispheres. Conversely, for the high frequency condition, the slow down was greater for the left hemisphere such that identification of the three component stimulus was actually slower in the left than in the right hemisphere. Thus, the addition of an identical (2 cpd) component to the stimulus produced a shift in performance in favor of the right hemisphere when it was low in frequency relative to the base pair components, but in favor of the left hemisphere when it was high in frequency relative to the base pair components.

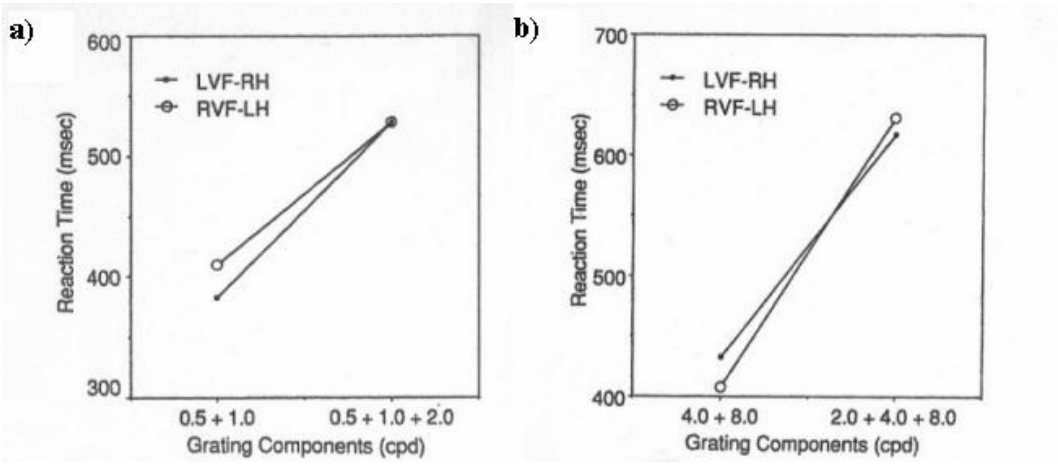

Figure 2.12: The relative spatial frequency lateralization effect. Hemispheric performance (designated as LVF-RH or RVF-LH) , as measured by reaction time, on the task of distinguishing between stimuli composed of either two or three sine-wave components for a) the low spatial frequency condition, and b) the high spatial frequency condition. (Reprinted from Christman et al., 1991, copyright 1991, with permission from Elsevier.)

It should be noted that the lateralization effects found in the psychophysical experiments of particular interest in this study, that is, those involving identification tasks based on spatial frequency (Christman, et al., 1991; Kitterle, et al., 1990, 1992, 1993) were significant, but generally small in magnitude. Typical differences in the reaction time for presentations to the right (*R*) and left (*L*) hemispheres were on the order of 20 milliseconds out of a total reaction time of about 500 milliseconds. When measured by a coefficient of asymmetry[8] computed as $\rho_{RT} = (RT^R - RT^L)/(RT^R + RT^L)$, lateralization is found to be approximately $\rho_{RT} = \pm 20/1000 = \pm 0.02$.

[8] The coefficient of asymmetry for an attribute designated as X is given by $\rho = (X^R - X^L)/(X^R + X^L)$, where X^R is the value of the attribute for the right hemisphere and X^L is the value of the attribute for the left hemisphere. The value of ρ can range from -1 to 1 with negative values indicating left lateralization and positive values indicating right lateralization (Lezak, 1995).

In contrast to the psychophysical experiments, electrophysiological studies examining visual evoked potential (VEP) as a function of the temporal and spatial frequency of a stimulus, do not provide much evidence in support of the spatial frequency hypothesis (Rebai, Bagot, & Viggiano, 1993; Rebai, Bernard, Lannou, & Jouen, 1998; Rebai, Lannou, Bernard, Bonnet, & Rochetti, 1997; Rebai, Mecacci, Bagot, & Bonnet, 1986, 1989). Instead they strongly support the view that asymmetry in the processing of a visual stimulus depends on both the temporal and spatial characteristics of the stimulus and cannot be explained by a simple dichotomy along the spatial dimension. In fact, they suggest that a strong dichotomy exists along the temporal dimension, with right hemisphere specialization for the processing of low temporal frequency stimuli and left hemisphere for high temporal frequency stimuli. They further suggest that the effect of spatial frequency on processing asymmetry depends on the temporal frequency of the stimulus. These experiments are discussed in more detail in Chapter 4, which specifically addresses the neural basis of the VEP results.

2.7 Related Modeling Studies

Several studies on lateralization in visual processing have used models to investigate specific hypotheses regarding the neural basis for experimentally observed effects (Baker, Chabris, & Kosslyn, 1999; Ivry & Robertson, 1998; Jacobs & Kosslyn, 1994; Kosslyn, Chabris, Marsolek, & Koenig, 1992). The studies by Kosslyn and colleagues examine asymmetry in receptive field size as

the basis of lateralization observed in psychophysical experiments on categorical-coordinate processing. The Ivry and Robertson study examines asymmetry in the treatment of spatial filter output as the basis of lateralization in spatial frequency, coordinate-categorical, and global-local processing.

The Kosslyn et al. study (1992) relates to experiments (Hellige & Michimata, 1989; Kosslyn, et al., 1989) that show an interaction between visual field and task for performance on choice tasks involving the presentation of identical two-element stimuli. These experiments showed that RT is faster for LVF/RH presentation when the stimulus is used in a coordinate task, but faster for RVF/LH presentation when it is used in categorical task. The study hypothesizes that coordinate processing requires precise representation of spatial location that could be provided by a coarse coding scheme. Since the effectiveness of coarse coding increases with increasing receptive field size, the superior performance of the right hemisphere on coordinate tasks might be explained by a greater utilization of input from visual neurons having relatively large receptive fields. Similarly, since small receptive fields more effectively delineate space into discrete sets of locations which could be used to specify categorical relations, left hemisphere superiority on categorical tasks might be explained by a greater utilization of input from visual neurons having relatively small receptive fields. The study simulation results show that when a multi-layered network is taught (using back-propagation) to perform a coordinate spatial task, the hidden units develop larger receptive fields than when it is taught to perform a categorical

spatial task. The results also show that networks with input units having large receptive fields perform better on learning the coordinate task (in terms of error rate) while those with input units having small receptive fields perform better on learning the categorical task.

The Jacobs and Kosslyn study (1994) extends the receptive field hypothesis to relate to lateralization observed in the processing of prototypes and exemplars (Marsolek, 1995). The Marsolek experiments show that, in a subject trained to classify patterns representing distortions (exemplars) of a set of prototypes according to their prototype base, the training patterns could be classified faster on LVF/RH presentation, but the previously unseen prototypes could be classified faster on RVF/LH presentation. The Jacobs and Kosslyn study suggests that prototype processing is a categorical task whereas exemplar processing, which requires precise spatial information, is a coordinate task. The study simulation results show that learning to identify the prototype category of a pattern is faster (in terms of learning epochs to reach accuracy goal) for networks having input units with relatively large receptive fields, while learning to identify its exemplar designation is faster for networks having input units with relatively small receptive fields. Additionally, in a simulation in which the receptive field sizes of the input units could adapt during task learning, relatively larger receptive field sizes develop for the exemplar task and relatively smaller sizes develop for the prototype task.

The Kosslyn studies interpret their simulation results as support for the hypothesis that receptive field size differences underlie the lateralization effects observed on categorical and coordinate spatial processing tasks (for significant dissent and rebuttal, see Baker et al., 1999; Cook, 1995; Cook, Fruh, & Landis, 1995; Kosslyn, Chabris, & Baker, 1995; Kosslyn, Chabris, Marsolek, Jacobs, & Koenig, 1995). They further interpret the results as a demonstration that hemispheric task specialization could lead to the development of a receptive field bias or, conversely, an existing receptive field bias could lead to the development of hemispheric specialization. Although their simulated lateralization effects result from structural differences in the network, they suggest that a receptive field size bias might be rooted in attentional rather than structural hemispheric differences.

The Ivry and Robertson study (1998) relates to the experiments investigating lateralization in spatial frequency (Christman, et al., 1991; Kitterle, et al., 1990, 1992, 1993), global-local (Martin, 1979; Van Kleek, 1989), and categorical-coordinate (Hellige & Michimata, 1989; Kosslyn, et al., 1989) processing mentioned earlier. The study hypothesizes that asymmetric processing of the output of spatial frequency filters underlies the lateralization effects observed in these experiments with the right hemisphere amplifying the output of low frequency filters and the left hemisphere amplifying the output of high frequency filters. Since low frequency filters have relatively large receptive fields and high frequency filters have relatively small receptive fields, this theory is

similar to Kosslyn's receptive field theory. However, the Ivry and Robertson theory is distinguished from the Kosslyn theory in that it can potentially account for relative as well as absolute frequency effects, while the Kosslyn theory, at least as implemented in the associated models, is limited to the latter.

The Ivry and Robertson theory is intended as a unified explanation of lateralization in the processing of frequency information in both the visual and auditory domains but, thus far, its modeling implementation has been limited to the visual domain. The theory, known as double filtering by frequency (DFF), posits a two-stage filtering process in which a band-pass filter, whose range is controlled by task-driven attentional mechanisms, passes select spatial frequency channel output on for further processing by a second filter. The first filter is proposed as the source of the relative frequency range determination. The second filter is proposed as the source of hemispheric asymmetry, with the right hemisphere performing low-pass filtering and the left performing high-pass filtering on the output of the first filter. Using DFF-based network models of the right and left hemispheres, the study simulations show superior right hemisphere performance (in terms of error rate) when learning to classify the lower of two frequencies and superior left hemisphere performance when learning to classify the higher. They also show a right hemisphere advantage in the learning of global patterns, coordinate tasks, and discriminations dependent on low frequency information, and a left hemisphere advantage on the learning of local patterns, categorical tasks, and discriminations dependent on high frequency information.

Although the DFF theory implies that the hypothesized hemispheric asymmetry involves some combination of structural and attentional differences, neither the neural bases of these differences nor the neural correlates of the double filtering processes are made explicit in the model of the theory.

The studies of visual processing lateralization discussed above attempt to link functional asymmetries to an assumed network asymmetry but do not attempt to link the development of the network asymmetry to specific biological factors. However, the link between the emergence of functional lateralization and biologically-motivated asymmetries that can affect network development has been investigated in neural network modeling studies involving supervised learning in phoneme generation task acquisition (Reggia, Goodall, & Shkuro, 1998), unsupervised learning in topographical map self-organization (Levitan & Reggia, 2000), and both supervised and unsupervised learning in letter identification task acquisition (Shevtsova & Reggia, 1999). The asymmetries examined in these studies include region size, excitability, and plasticity but not asynchronicity in hemispheric development.

Asynchronous hemispheric development has been considered as a contributing factor to lateralization development in a modeling study that combined it with differences in the timing of task learning to produce the emergence of lateralized task competency (Howard & Reggia, 2004). This study examined the effects of hemispheric asynchronicity in both the onset and the timing of the period of high plasticity on the acquisition of two dissimilar tasks

through supervised learning. The learning periods for the two tasks were offset such that one was delayed with respect to the other. All simulations were executed using a particular task order and then repeated using the reverse order.

The simulations of asynchronous onset of high plasticity assumed that at the start of first task learning, plasticity was high in one hemisphere and low in the other, but that concurrent with the start of second task learning, both hemispheres had reached a state of equally high plasticity. Under these conditions, the first task became strongly lateralized toward the hemisphere with the earlier onset of high plasticity. Furthermore, the second task became significantly, albeit less strongly, lateralized in the opposite direction despite the symmetry of hemispheric plasticity during its learning period. These results suggest that the lateralization of one task caused by an initial lag in the development of one hemisphere will not only persist after the development gap closes, but will also drive the lateralization of a second task learned subsequent to gap closure.

The simulations of asynchronous timing of high plasticity also assumed that plasticity was high in one hemisphere and low in the other at the start of first task learning, but that the plasticity levels reversed concurrent with the start of second task learning. Under these conditions, both the first and second tasks became strongly lateralized in the direction of the hemisphere with the higher plasticity during its *initial* period of learning, despite the reversal of the plasticity asymmetry that occurred during the first task learning period. The results suggest

that cognitive functions that follow different time courses of development can be strongly lateralized in opposite directions if asymmetry in plasticity for the regions that subserve them (even homologous regions) is oppositely directed during their respective times of initial development.

The Howard and Reggia (2004) study modeled a scenario in which the input from the external environment changed over time (as the second task was introduced) and learning was accomplished in a supervised mode. However, the findings imply that a change in input characteristics attributable solely to the maturation of the input systems to a particular region, when combined with asynchronous hemispheric development, has the potential to give rise to functional lateralization through Hebbian learning processes. The study did not attempt to model such a scenario explicitly.

To summarize, past modeling studies related to frequency lateralization have focused on demonstrating that asymmetry in the processing of spatial frequencies *can explain* a variety of visuospatial lateralization effects observed in psychophysical experiments. No modeling studies on this topic have focused on demonstrating that asymmetry in the processing of spatial frequencies *can be explained* in terms of specific biological asymmetries supported by empirical findings. Modeling studies related to asymmetric development have shown that biological asymmetry, including asynchronous hemispheric development, can give rise to the development of lateralized functionality. However, none of these has demonstrated that such asymmetry coupled with the particular conditions

extant in the developing visual system can produce lateralized spatial frequency processing. Finally, no modeling studies have attempted to explain the frequency lateralization effects observed in the electrophysiological experiments in terms of biological asymmetries, nor have any sought to resolve the apparent conflict between the psychophysical and the electrophysiological findings. The current study addresses these several important aspects of visual frequency processing lateralization that, thus far, have not been considered in the context of a computational modeling investigation.

Chapter 3

The Development of Lateralization in Spatial Frequency Processing

This chapter discusses a series of neural network modeling experiments designed to test two interrelated hypotheses on spatial frequency lateralization. The first hypothesis proposes that a specific set of conditions thought to exist during the first postnatal year can lead to the development of hard-wired asymmetry. The second hypothesis proposes that this asymmetry can account for both the absolute and the relative lateralization effects observed in the processing of spatial frequencies. The introductory section of this chapter summarizes the relevant developmental conditions. The next section describes the model used in the experiments. It begins with a statement of the assumptions that form the basis of the experimental design and an explanation of the principles underlying the experimental hypothesis. It then provides a complete description of the model input, architecture, and dynamics. This is followed by a section that presents the results of the simulation experiments. First, results obtained under a baseline set of model conditions are presented, demonstrating that the assumed conditions can produce the predicted lateralization. Next, the impact of the timing of hemispheric development on lateralization is explored by comparing results obtained under

varying developmental timing conditions with the baseline results. Then, the results of an experiment in which the values of model parameters are adjusted to reflect more accurately the empirically-observed distribution and bandwidths of V1 spatial frequency filters, are presented as further support of the experimental hypothesis. This is followed by the presentation of results that demonstrate the effect of the change in filter distribution with eccentricity on the lateralization function. Next, the simulation results are analyzed for evidence of hemispheric bias with respect to the magnocellular and parvocellular pathways. In addition, the results are used to construct a theoretical model of the neural basis for the relative frequency lateralization effect. The concluding section summarizes the model findings and discusses their implications.

3.1 Background

3.1.1 Asynchronous Hemisphere Maturation and Lateralization

The Hellige hypothesis (1993, 1995, 1996) on the development of spatial frequency lateralization is one of a number of hypotheses that propose a link between differences in the timing of maturation of the two hemispheres and the development of biological and functional asymmetries. Most of these proposals, including the Hellige theory, have argued for the earlier development of the right hemisphere (Best, 1988; Brown & Jaffe, 1975; Crowell, Jones, Kapuniai, & Nakagawa, 1973; de Schonen & Mathivet, 1989; Geschwind & Galaburda, 1987; Taylor, 1969; Turkewitz, 1988; but see also Corballis & Morgan; 1978; Corballis,

1991). And, indeed, the argument for a right-to-left developmental gradient is supported by evidence concerning morphological (Chi, Dooling, & Gilles, 1977; Dooling, Chi, & Gilles, 1983), biochemical (Bracco, Tiezzi, Ginanneschi, Campanella, & Amaducci, 1984), microanatomical (Scheibel, 1984), and regional cerebral blood flow (Chiron et al., 1997) asymmetries. The morphological evidence just cited suggests that the difference in the timing of development between the hemispheres is on the order of a week or two.

The Hellige hypothesis is a generalization of one advanced by de Schonen & Mathivet (1989) to explain the apparent right lateralization of face processing. Their hypothesis proposes that the co-occurrence of two conditions underlies development of lateralization in face processing: a) the earlier maturation of the right hemisphere and b) the increasing sensitivity of the visual system to high spatial frequencies as it develops postnatally. De Schonen and Mathivet argue that because the neonatal visual system is limited in sensitivity to the low end of the spatial frequency range, the earlier developing face recognition device in the right hemisphere becomes functional on the basis of low frequency input and, therefore, develops a specialization for low frequency input. They further argue that the face recognition device in the left hemisphere becomes functional on the basis of both low and high frequency input and, thus, does not develop the same specialization. To the extent that the efficient processing of low spatial frequency information by the face recognition device results in an advantage in facial pattern processing, the right hemisphere exhibits performance superiority.

Hellige theorizes that the scenario proposed by deShonen and Mathivet results in the development of a generalized hemispheric asymmetry related to the processing of spatial frequency information rather than an asymmetry specific to the processing of faces. This generalized asymmetry is described as a right hemisphere specialization for the processing of low frequency information and a left hemisphere specialization for the processing of high frequency information that affects all visual processing tasks. Hellige suggests that the developmental scenario may involve an interaction between the time course of visual development and the timing of "critical periods" of intense synaptic modification in the two hemispheres. A critical period hypothesis of this sort is consistent with evidence of intense synaptogenesis in the visual cortex in the second through eighth postnatal months (Huttenlocher, de Courten, Garey, & Van der Loos, 1982).

3.1.2 Visual System Development

The Hellige premise that sensitivity to high spatial frequencies is poor at birth, but develops rapidly during the first year, is corroborated by evidence from both psychophysical and electrophysiological studies (Gwiazda, Bauer, Thorn, & Held, 1997; Kelly, Borchert, & Teller, 1997; Norcia, Tyler, & Hamer, 1990; Peterzell, Werner, & Kaplan, 1995; for reviews of earlier studies, see Banks & Dannemiller, 1987; Dobson & Teller, 1978). These studies show that, as the visual system develops, the contrast sensitivity function (CSF) shifts toward

higher spatial frequencies and higher sensitivities but exhibits greater attenuation at low frequencies (see Figure 3.1). This results in an increase in sensitivity across the frequency spectrum that is relatively greater at the high end than at the low end, particularly between the second and the eighth month. However, if the differential change in sensitivity for low and high frequencies is to account for the development of lateralized spatial frequency processing, then it must be tied to a change in the response of the underlying frequency filters that is differentiated with respect to the peak frequency of the filter. That is, the increase in the response of a high frequency filter must be greater than the increase in the response of a low frequency filter during the time of hemispheric development.

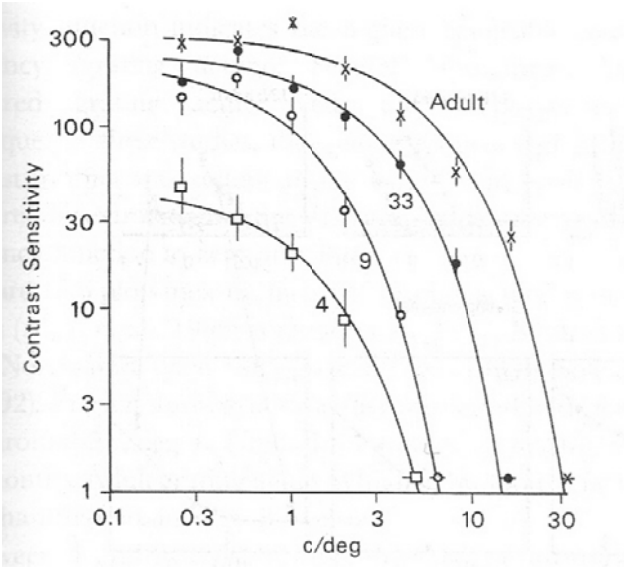

Figure 3.1: The development of the spatial contrast sensitivity function (CSF) for gratings phase-reversed at 6 Hz. Infant age in weeks is shown immediately below the associated graph. The CSF shifts toward higher frequency and higher sensitivity over the course of development, with a marked increase in low frequency sensitivity between the ages of 4 and 9 weeks and in high frequency sensitivity between the ages of 9 and 33 weeks. (Reprinted from Norcia, 2004, with permission. Figure based on data from Norcia et al., 1990.)

That the differential change in the CSF does not necessarily imply such a change in filter response is illustrated by the "shifting" model of filter development proposed by Wilson (1988). This model hypothesizes that spatial filters are initially tuned to a range of frequencies at the low end of the spectrum but, during the course of visual system development, are identically transformed by several changes that affect their sensitivity to spatial frequency (see also Movshon & Kiorpes, 1988). First, the migration of cones increases the cone packing density in the fovea causing a shift in filter sensitivity toward higher spatial frequencies. Second, the growth in the cone outer segment increases quantal catch resulting in greater filter sensitivity. Third, the development of lateral inhibition produces attenuation at low frequencies. The model proposes that these three factors can produce the qualitative changes observed in the CSF (see Figure 3.2) and uses anatomical data (Youdelis & Hendrickson, 1986) to show that the changes affecting the cones can quantitatively account for the observed increases in both acuity[9] and sensitivity (see also Peterzell & Kelly, 1997; Peterzell & Teller, 1996; Peterzell, Werner, & Kaplan, 1993, 1995). However, these three factors do not produce a greater increase in the sensitivity of high frequency filters in comparison with low frequency filters. Thus, the shifting filter model potentially explains the rapid increase in sensitivity to high spatial

[9] Acuity is defined as the highest detectable spatial frequency (for a given luminance).

frequencies, without providing a biological foundation for the Hellige hypothesis of lateralized development in spatial frequency processing.

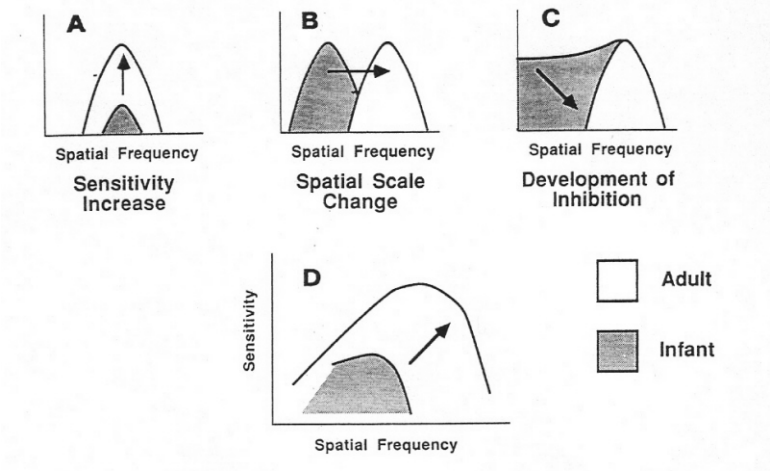

Figure 3.2: The diagram depicts the changes hypothesized to affect all spatial filters identically: A) an increase in sensitivity, B) a shift toward higher frequencies, and C) attenuation of sensitivity for low frequencies. The overall change in the CSF that results is shown in D. (Reprinted from Wilson, 1988, copyright 1988, with permission from Elsevier.)

However, the results of studies that investigated the development of temporal frequency processing suggest the existence of another factor affecting filter development that does provide a biological basis for lateralized development in spatial frequency processing (Dobkins & Teller, 1996; Hartmann & Banks, 1992; Rasengane, Allen, & Manny, 1997; Regal, 1981; Swanson & Birch, 1990). These studies found that the infant temporal contrast sensitivity function (tCSF) is considerably reduced in comparison to the adult tCSF, a finding that is consistent with the immaturity of the cone outer segment mentioned earlier. However, two findings suggest that the band-pass temporal channel matures rapidly in the first

two to four months (for a discussion of low-pass and band-pass temporal filters/channels, see Section 2.3). First, the critical flicker frequency (CFF), that is, the highest resolvable temporal frequency, matures rapidly approximating adult levels as early as 2 to 3 months (Dobkins & Teller, 1996; Regal, 1981; but see also, Hartmann & Banks, 1992; Rasengane et al., 1997). Second, the characteristic band-pass shape of the adult tCSF emerges by the third month with a peak near 4 Hz that quickly increases to reach the adult value of 8Hz at 4 months (Rasengane et al., 1997). Added to this is the finding that a reduction in sensitivity of the low-pass and band-pass temporal channels cannot explain the difference between the 4-month tCSF and the adult tCSF unless at least one of the channels changes in temporal scale during that time (Swanson & Birch, 1990). Together these results suggest that the band-pass temporal channel matures in advance of the low-pass temporal channel; this, in turn, implies that the magnocellular pathway matures in advance of the parvocellular pathway. Because the magnocellular pathway is most sensitive to low spatial frequencies and the parvocellular pathway to high spatial frequencies (see Section 2.3), differences in the timing of their development equate to differences in the timing of development of low and high spatial frequency filters as well. *Thus, the difference in the time course of magnocellular and parvocellular pathway development may provide a biological basis for the development of spatial frequency lateralization.*

The hypothesis of precocious maturation of the magnocellular pathway is supported by multiple lines of evidence (for review, see Fiorentini, 1992).

Psychophysical studies found differences in the maturations of various sensitivities that serve to distinguish the two pathways such as sensitivity to luminance (magnocellular) or color (parvocellular). For instance, luminance contrast sensitivity at low luminance reaches adult values earlier in development than luminance contrast sensitivity at high luminance (Fiorentini, Pirchio, & Spinelli, 1980). Furthermore, luminance contrast sensitivity develops earlier and along a different developmental trajectory than chromatic contrast sensitivity as shown in Figure 3.3 (Fiorentini, 1992).

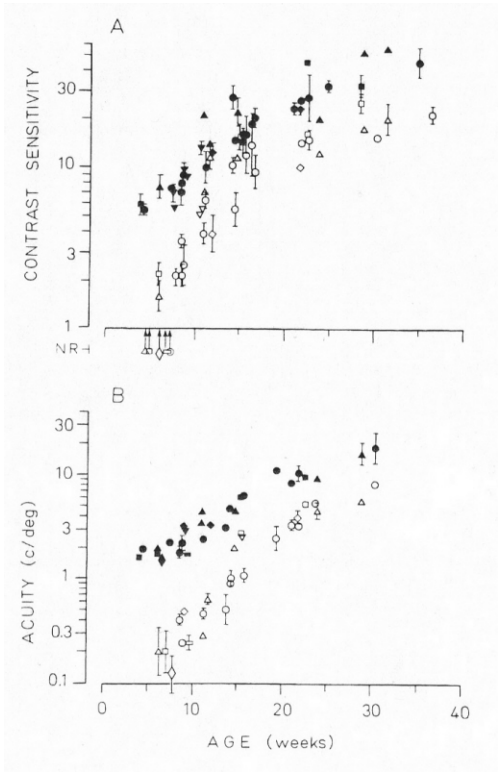

Figure 3.3: Development trajectories are shown for: A) contrast sensitivity for low spatial frequency and B) acuity, based on VEP response to isoluminant gratings (open symbols) or to isochromatic gratings (filled symbols). (Reprinted from Fiorentini, 1992, copyright 1992, with permission from Elsevier.)

In addition, the luminance tCSF displays an adult-like shape at 3 months while the chromatic tCSF does not begin to do so until 4 months (Dobkins, Anderson, & Lia, 1999). Anatomical investigations discovered that the period of plasticity during which the ocular segregation of inputs to V1 can be affected ends earlier for input layer 4Cα (magnocellular) than for input layer 4Cβ (parvocellular) (LeVay, Wiesel, & Hubel, 1980), and that horizontal connections in V1 layer 4B (magnocellular) appear to mature before those in layer 2/3 (parvocellular) (Burkhalter, 1993). An electrophysiological investigation found that the P1 component of the visual evoked potential response[10] to sinusoidal gratings of 0.5 and 2.5 cpd appears in the first and third month, respectively, and matures quickly, while the corresponding N1 component appears with a five month lag (Hammarrenger et al., 2003). In light of a previous study that concluded that the P1 component mainly reflects the activity of the magnocellular pathway, while the N1 component mainly reflects the activity of the parvocellular pathway (Ellemberg, Hammarrenger, Lepore, Roy, & Guillemot, 2001), this result was interpreted as evidence of earlier magnocellular pathway maturation. Finally, a physiological study (Hawken, Blakemore, & Morley, 1997) found that the response rates (spikes per second) of M-cells in the LGN of the macaque increases dramatically during the first two months after birth and then continues to increase more gradually through the eighth month. In contrast, P-cell response

[10] For information on the visual evoked potential response to patterned stimuli, see Chapter 4.

rates were found to increase steadily over the first eight months. These changes in the response rates of the magnocellular and parvocellular pathways, depicted in Figure 3.4, would result in the change in the relative activity of the low and high spatial frequency filters that is needed to drive lateralized development.

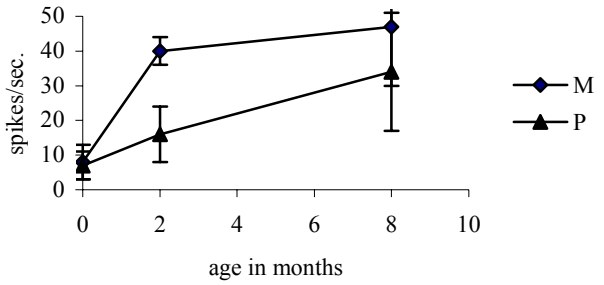

Figure 3.4: Mean response rates (± 1 SD) for M cells and P cells within the LGN of macaque monkeys as a function of age. The responses were obtained using high contrast stimuli of optimal spatial frequency. (Data from Hawken et al., 1997.)

3.2 The Model

3.2.1 Underlying Principles and Assumptions

The model described in this chapter is designed to examine the hypothesis that differences in the time course of maturation for the magnocellular and parvocellular pathways, in combination with asynchronous development of the right and left cortical hemispheres, can produce lateralized spatial frequency processing. The nature of this lateralization is a right hemisphere advantage associated with low spatial frequencies and a left hemisphere advantage associated with high spatial frequencies for the processing of a visual stimulus

that occurs beyond its initial processing in the primary visual cortex. This lateralization effect was observed in a number of psychophysical experiments that measured reaction times on identification tasks involving low and high spatial frequencies as discussed in Section 2.6 (Christman, et al., 1991; Kitterle, et al., 1990, 1992, 1993). The model presumes that such reaction time differences are attributable to differences in activation of underlying neural components, which it simulates directly.

The model incorporates several assumptions, all supported by existing experimental data, which are critical to the studied hypothesis:

1. Identical input is delivered to the primary visual cortex (V1) of the two hemispheres, and the activity in V1 of two hemispheres in response to the input is likewise identical (Fiorentini & Berardi, 1984; Kitterle et al., 1990; Peterzell et al., 1989; Rose, 1983).

2. Both the magnocellular and the parvocellular pathways undergo significant maturation during the first postnatal year that increases their activity in response to visual input (Hawken et al., 1997). The time course of this maturation is earlier and more accelerated for the magnocellular system (Burkhalter, 1993; Dobkins et al., 1999; Fiorentini, 1992; Hawken et al., 1997).

3. The development of the cortical areas processing visual input occurs asynchronously in the two hemispheres with the "critical period" of plasticity occurring earlier in the right hemisphere than the left (Bracco et al., 1984; Chi et al., 1977; Chiron et al., 1997; Dooling et al., 1983; Scheibel, 1984;).

4. Spatial frequency identification tasks are performed by the ventral stream to which both the magnocellular and parvocellular pathways make a substantial contribution (Livingstone & Hubel, 1988a; Merigan & Maunsell, 1993; Schiller & Logothetis, 1990; Shapley, 1990, 1992; Van Essen & DeYoe, 1995).

5. The ratio of the magnocellular to parvocellular contribution to the activity of the spatial frequency filters in layer 2/3 of V1 decreases as peak frequency increases (Merigan & Maunsell, 1993).

6. The development of one or more visual processing areas in the ventral stream beyond V1 overlaps the maturation of the visual pathways (Huttenlocher et al., 1982) and involves a competitive, activity-dependent learning process.

These assumptions imply that the contribution of the parvocellular pathway to V1 filter activity is greater for high frequency filters than for low, and that the parvocellular pathway is more mature at the time of left (in comparison to right) hemisphere development. Thus, high spatial frequency filters can be expected to compete more effectively for downstream connections in the left hemisphere resulting in the development of functional lateralization related to the processing of spatial frequencies. The model design described in the next section supposes that this competition begins with the connections to visual area V2, although it could begin at an area further along in the ventral stream assuming that some degree of spatial frequency selectivity is maintained throughout the stream.

3.2.2 The Basic Model Design and Dynamics

The model is a feed-forward, multi-layer neural network concerned only with the spatial frequency characteristics of visual input. The contrast and temporal frequency characteristics of the input are not explicitly modeled but are assumed to be such that system response as a function of spatial frequency is near maximum. This assumption is consistent with the characteristics of the stimuli employed in the psychophysical lateralization experiments of interest, which were of high contrast and contained a broad range of temporal frequencies. Similarly, the model filters are assumed to represent those V1 cells that respond maximally to the orientation and phase of the input grating stimulus, thus obviating the need to include these input characteristics in the model explicitly.

The architecture of the model is summarized schematically in Figure 3.5. The model features a right (*R*) and a left (*L*) hemisphere, each containing two layers representing areas associated with the initial processing of patterns in the ventral stream of the visual cortex: a filter layer corresponding to the blob/interblobs of V1 and a development layer corresponding to the thin stripe/interstripes of V2. As discussed in Chapter 2, visual input appears to be processed symmetrically through V1; therefore, sub-cortical structures are not included. The filter layer for each hemisphere represents two sets of filters located in distinct hypercolumns in V1 that respond identically to a grating stimulus and that converge on the same set of cells in V2. The filter sets of the right hemisphere process input from two locations within the left visual field, while those of the left hemisphere process input from mirror locations in the right visual field. The two retinotopic locations are specified as falling within the part of visual field stimulated in the psychophysical experiments of interest (Christman, et al., 1991; Kitterle, et al., 1990, 1992, 1993). In these experiments, a grating stimulus was presented as a circular patch of diameter 6.8° at a minimum eccentricity of 2 or 3° in order to limit the processing of the stimulus, as much as possible, to either the right or the left hemisphere. Although the corpus callosum connects the right and left visual fields on either side of the vertical meridian, these connections are confined to approximately 1° along the entire extent of the meridian in V1 in the macaque (Kennedy, Dehay, & Bullier, 1986). In V2 of the macaque, callosal connections increase in extent with distance from the horizontal

meridian, reaching up to 45° on either side of the vertical meridian at the extremes of the upper and lower visual fields (Abel, O'Brien, & Olavarria, 2000). Nevertheless, the connections are restricted to less than 2° along the horizontal meridian and do not extend into the visual field areas stimulated in the psychophysical experiments (Abel, et al., 2000). Based on these findings, the model assumes callosal connections are not present for the represented locations in V1 and V2.

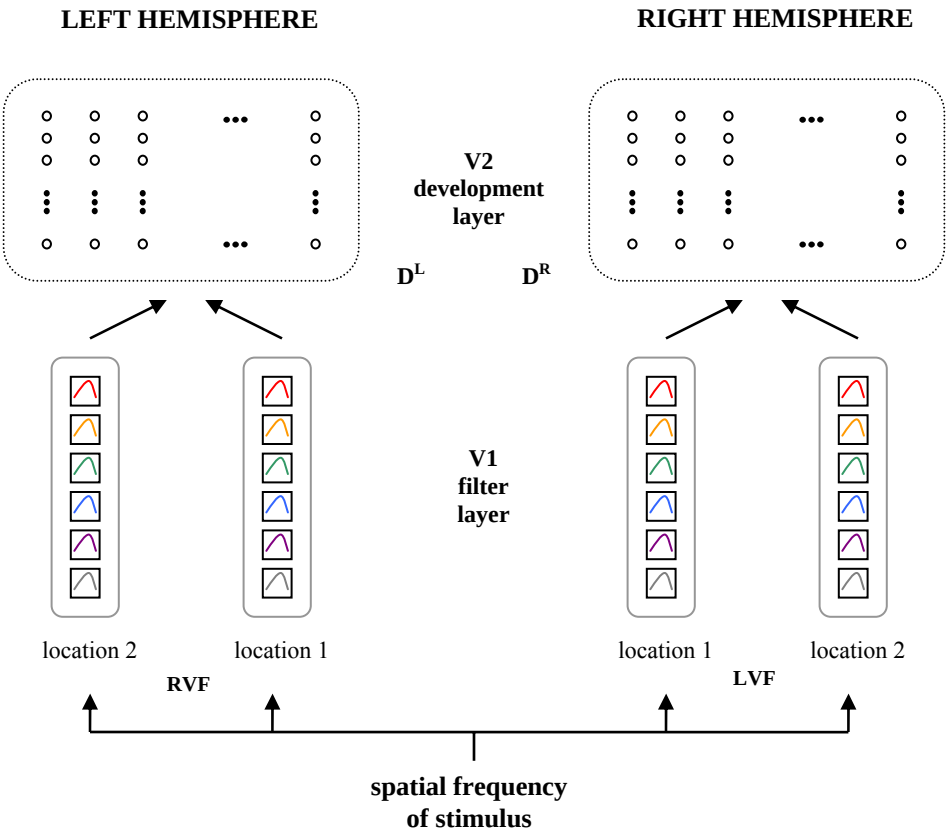

Figure 3.5: Model architecture. Visual input, in the form of a value representing the spatial frequency of a sinusoidal grating stimulus, is presented to filter sets in V1 of the right and left hemispheres. Each set comprises six filters that differ in their peak and range of frequency sensitivity (indicated by color). Two filter sets in the right hemisphere respond to input from two retinotopic locations in the left visual field (LVF), while two sets in the left hemisphere respond to input from mirror locations in the right visual field (RVF). Within each hemisphere, filter response is fed forward to V2 via weighted connections, converging on all units in development layer sets D^R and D^L. Lateralized V2 activation arises from the asymmetric development of these weighted connections.

The model, as specified by the equations and parameters that follow, is implemented in MATLAB 6 release 12. All simulation experiments are performed on a Dell Dimension 8200 with a 2.2 GHz Pentium 4 processor and 256 MB RAM under Windows XP.

Model inputs (set *I*) take the form of values corresponding to the spatial frequencies of various sinusoidal gratings given in cycles per degree (cpd). Filter response is then defined as a function of input frequency. The spatial frequency value for each input $i \in I$ is given in Table 3.1.

Table 3.1: Input Spatial Frequency Values

input *i*	ω (cpd)
1	0.5
2	1
3	2
4	4
5	8
6	16

A filter set (*F*) comprises six filters that individually respond to a restricted range of spatial frequencies but collectively cover the entire range of spatial frequency sensitivity. The response (at full maturity) of filter $j \in F$ to visual input of spatial frequency ω is given by a function of the form:

$$r_j(\omega) = \mathbf{[}A_j\{\sigma_{1j}\exp[-(\pi\sigma_{1j}\omega)^2] - B_j\sigma_{2j}\exp[-(\pi\sigma_{2j}\omega)^2] + C_j\sigma_3\exp[-(\pi\sigma_{3j}\omega)^2]\}\mathbf{]}_+ \quad (3.1)$$

where $[\ ]_+$ indicates the rectification operator defined as $[z]_+ = \max(z,0)$. This response function is the Fourier transform of the standard difference-of-Gaussians (DOG) function used to model a receptive field consisting of an excitatory center, an inhibitory surround, and a secondary excitatory lobe, as found in V1 spatial filters (Wilson et al., 1990). The filter's shape and peak frequency are determined by the constants B, C, σ_1, σ_2 and σ_3 and A is a normalization constant that sets the maximum response to 1. The values for the constants used in the simulations are calibrated such that the peak frequencies of the six filters are 0.5, 1, 2, 4, 8 and 16 cpd with a mean filter bandwidth of approximately one-and-a-half octaves. Thus, each input frequency elicits the maximum possible response from one of the six filters in a set. A typical filter is shown in Figure 3.6.

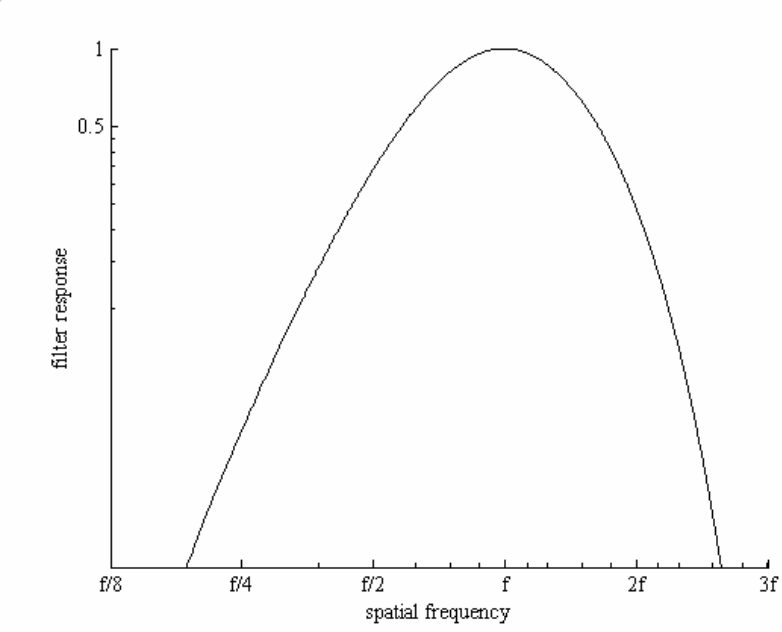

Figure 3.6: Filter response as a function of peak frequency *f*.

The development layer within a hemisphere (D^H with $H \in \{R, L\}$), consists of a 1000 unit set representing a retinotopic location that is a combination of locations 1 and 2. Each development layer unit is fully connected to the filter units within the filter sets for locations 1 and 2 via weighted connections. At the start of a development simulation, these connection weights are initialized to random values between 0 and 1, and then normalized such that the sum of the weights to a development unit from the filter units is 1. The same initial weights are used for corresponding filter-to-development unit connections in the right and left hemispheres; thus, the hemispheres start out in a symmetric state. Changes to the weights that potentially allow the hemispheres to develop asymmetrically are made after each presentation of an input. Although no lateral connections between development units are explicitly included in the model, lateral inhibition between all of the units within a set is implied by the model's learning rule (see Equation 3.10 and its explanation). The depiction of a development layer set as a two dimensional patch of cortical units in Figure 3.5 is meant to connote the (implicit) lateral connectivity between the units.

During a simulation, both hemispheres undergo a 10 month period of development. The timing of the developmental period, however, differs in the two hemispheres. The timing is determined by the values assigned to t_R and t_L, which represent the mid-points of the developmental periods in the right and left hemispheres (in postnatal months), respectively. A hemisphere's developmental

period is determined by a time-dependent plasticity function. Because the important factor with regard to asymmetric development is the difference in the timing of plasticity in the two hemispheres rather than the shape of the plasticity function, the plasticity function is assumed to take the form of a simple learning rate function. The learning rate function is given by $\eta^H(t) = 0.1$ if t_H-5 < t < t_H+5 and $\eta^H(t) = 0$ otherwise, where t_H is the mid-point of development for hemisphere $H \in \{R, L\}$ and 5 is half of the length of the 10 month development period.

A simulation proceeds from a start time to an end time in equal time steps. The start time corresponds to the earliest time of development in either hemisphere. Thus, given the assumption of earlier development in the right hemisphere ($t_R < t_L$), the simulation starts at time $t_R - 5$ (again, 5 corresponds to half of the hemisphere's 10 month development period). Similarly, the end time corresponds to the latest time of development in either hemisphere, that is, $t_L + 5$. Because the values for t_R and t_L used in the simulations are greater than 5 months, the developmental periods for both hemispheres fall within the postnatal timeframe. For example, the assumption of values $t_R = 7$ and $t_L = 8$ determines a developmental period that begins at age 2 months and ends at age 12 months in the right hemisphere, and that begins at age 3 months and ends at age 13 months in the left hemisphere. At each time step (epoch), the input set is reordered randomly and the complete set is presented to the filter layer in the new order. Weight changes are made after each input presentation. The simulations utilize a

time step of .0025 months; thus, a hemisphere's 10 month development period equates to 4,000 epochs.

In the filter layer, activation of unit $j \in F$ at time t in response to input of spatial frequency ω, is computed as the product of the filter's relative maturity μ_j at time t and its response function at full maturity, that is,

$$a_j(t,\omega) = \mu_j(t) r_j(\omega) \tag{3.2}$$

Relative filter maturity, μ_j, for filter $j \in F$ at time t is defined as the weighted sum of the relative maturity of the magnocellular (μ^M) and parvocellular (μ^P) pathways (at time t) as given by

$$\mu_j(t) = c_j^M \mu^M(t) + c_j^P \mu^P(t) \tag{3.3}$$

where the weights c_j^M and c_j^P represent the relative contributions of the two pathways to a filter's activity at full maturity. Values for these weights are chosen to be consistent with model assumption 5 (see Section 3.2.1) and are subject to the constraint $c_j^M + c_j^P = 1$, with $0 \le c_j^M \le 1$ and $0 \le c_j^P \le 1$. Thus, for example, if the magnocellular and parvocellular pathways are assumed to contribute equally to filter j when they reach maturity, then $c_j^M = c_j^P = 0.5$. Although empirical evidence indicates that a filter's response is not the simple sum of the responses that would be elicited if the two pathways were activated separately, it does suggest that it is greater than or equal to the response that would be elicited if only one pathway was activated (Allison et al., 2000; Nealy & Maunsell, 1994). This implies that filter response is a monotonically increasing function of the individual pathway

contributions, a characteristic that is captured by the linear function used in the model.

The relative maturities of the two pathway components, $\mu^M(t)$ and $\mu^P(t)$, are computed as:

$$\mu^M(\mathrm{t}) = m^M(\mathrm{t}) / (m^M(\mathrm{t}) + m^P(\mathrm{t})) \tag{3.4}$$

$$\mu^P(\mathrm{t}) = m^P(\mathrm{t}) / (m^M(\mathrm{t}) + m^P(\mathrm{t})) \tag{3.5}$$

where $m^M(t)$ and $m^P(t)$ represent the maturation levels of the pathway components as functions of time. In turn, the maturation levels are estimated by:

$$m^M(t) = .5 + \frac{1}{\sqrt{\pi}} \int_0^{.55(t-2)} e^{-x^2} dx \tag{3.6}$$

$$m^P(t) = .5 + \frac{1}{\sqrt{\pi}} \int_0^{.4(t-4)} e^{-x^2} dx \tag{3.7}$$

These functions compute indices of maturity between 0 and 1 (with 1 representing adult-like maturity) for $0 \leq t \leq 8$. For $t > 8$, the maturity index is set to 1 indicating that the pathway is assumed to have reached full maturity at 8 months. As shown in Figure 3.7, the functions reflect the rapid, early maturation of the magnocellular pathway and the later, slower maturation of the parvocellular pathway, consistent with the maturational data displayed in Figure 3.3 (Fiorentini, 1992) and Figure 3.4 (Hawken et al., 1997).

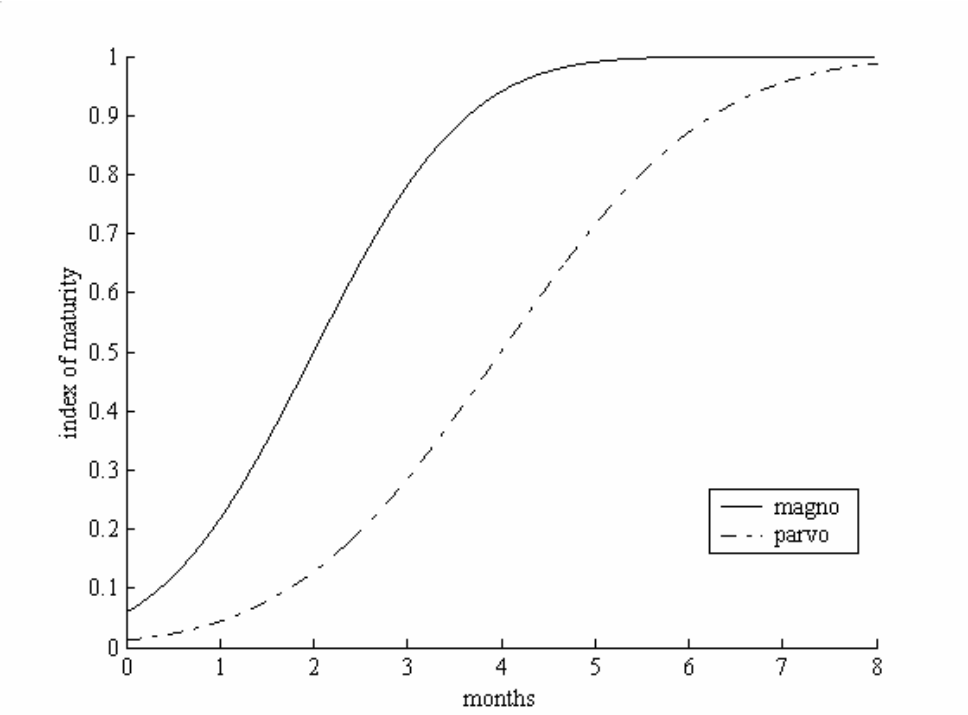

Figure 3.7: The estimated maturity indices for the magnocellular and parvocellular pathways, as given by m^M(t) and m^P(t), respectively, computed for postnatal months 0 to 8.

The corresponding relative maturity functions are shown in Figure 3.8. The use of relative maturity effectively normalizes filter activation levels that would otherwise rise with the increasing maturity of both visual pathways, resulting in a bias in cortical development toward the later developing hemisphere. Thus, the use of relative maturity implements the equivalent of homeostatic maintenance of activation levels in V1 during the course of visual system development (Turrigiano & Nelson, 2004). From the definitions of the relative pathway contributions, c_j^M and c_j^P, and the relative pathway maturities, $\mu^M(t)$ and $\mu^P(t)$, it is evident that relative filter maturity $\mu_j(t)$, as given by

Equation 3.3, is limited to values between 0 and 1 and is equal to 0.5 at full maturity ($t > 8$) for all $j \in F$.

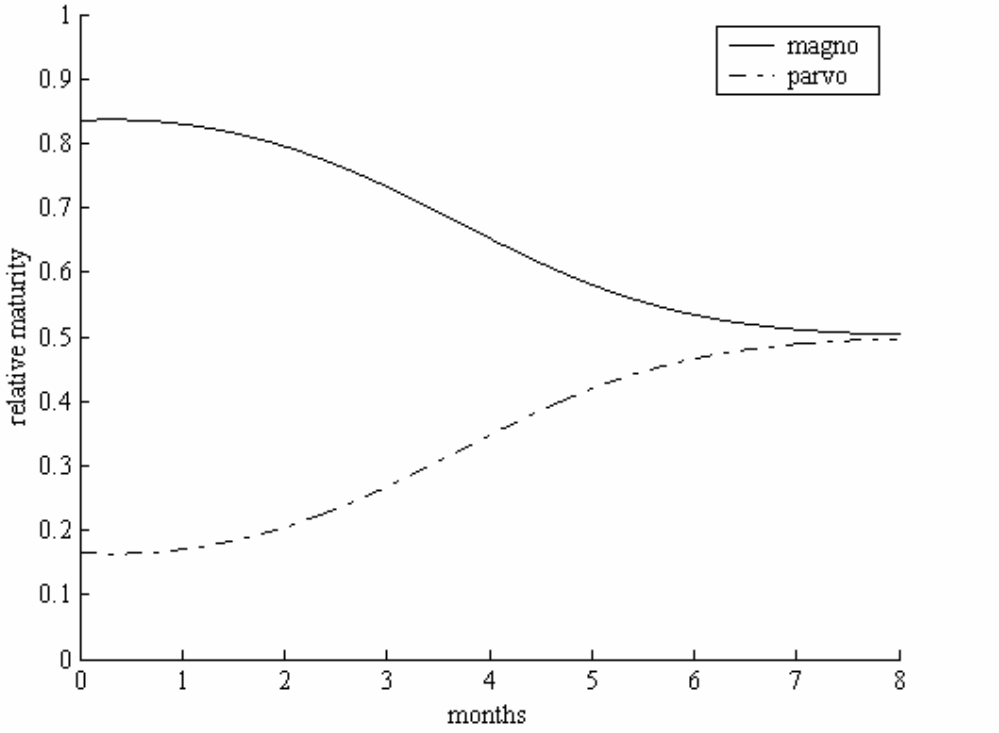

Figure 3.8: The relative maturity of the magnocellular and parvocellular pathways, as given by $\mu^M(t)$ and $\mu^P(t)$, respectively, computed for postnatal months 0 to 8. The earlier maturation of the magnocellular pathway is reflected in its initially greater relative maturity. The later maturation of the parvocellular pathway closes the maturity gap such that the relative maturity values for the two pathways converge.

In the development layer, activation of development unit *k* in hemisphere *H* is given by the total of the weighted sums of filter output from locations 1 and 2 in V1 of that hemisphere less the activation threshold, that is:

$$a_k^H = \sum_j^F w1_{kj}^H \; a_j + \sum_j^F w2_{kj}^H \; a_j \; - \theta \qquad (3.8)$$

where a_j is the activation of filter $j \in F$, $w1_{kj}^H$ and $w2_{kj}^H$ are the weights to unit $k \in D^H$ from filter j in the filter sets at locations 1 and 2, respectively, and θ is the activation threshold[11]. Because the model assumes that filter response to a particular stimulus at the two locations is identical, the weights from corresponding filters at the two locations can be added together as $w_{kj}^H = w1_{kj}^H + w2_{kj}^H$ and the sum used in the model computations. Thus, activation of unit k in the development layer of hemisphere H is computed as:

$$a_k^H = \sum_j^F w_{kj}^H \; a_j - \theta \tag{3.9}$$

The value for θ used in the simulations is 0.09, chosen to maximize the selectivity of development layer units while virtually assuring that each unit responds to at least one member of the stimulus set.

Weight adjustments are made based on a Hebbian learning rule following the presentation of each input. Specifically, the adjusted weight to the development unit k from filter j (summed across locations 1 and 2) in hemisphere H is given by

$$w_{kj}^H = w_{kj}^H + \eta^H \; a_j a_k^H \; / \sum_\ell^{D^H} a_\ell^H \tag{3.10}$$

[11] Boynton and Hegdé (2004) have demonstrated that results of a study on the selectivity of V2 neurons in the macaque (Ito & Komatsu, 2004) are at least partially explained by a simple model that accounts for V2 cell response as the sum of its response for one or more V1 components. Equation 3.8 deviates from this simple model only in its inclusion of a threshold non-linearity, θ. If θ is small compared with the largest V1 components, then equation 3.8 approximates the simple model.

where η^H is the learning rate for hemisphere H, a_j is the activity of filter $j \in F$ in response to the input, a_k^H is the activity of development unit $k \in D$ in hemisphere H, and $\sum_{\ell}^{D^H} a_\ell^H$ is the sum of all activity in the development layer of hemisphere H. This learning rule implements a weak competition for filter connections among development layer units such that the changes in weights on connections to a particular development unit depend on the activity of the unit relative to the total activity in the region. The rule implies the existence of lateral inhibitory connections between development layer units that effectively normalize the steady-state response of a development unit based on the overall response of the units in the surrounding region (Dayan & Abbott, 2001; Wilson & Wilkinson, 2004). Such normalization is found in V1, contributing to contrast gain control in filter response (Foley, 1994; Heeger, 1992) and is hypothesized to be a fundamental component of all cortical function (Heeger, 1992). The weight change is followed by weight normalization such that

$$w_{kj}^H = w_{kj}^H / \sum_j^F w_{kj}^H \ . \tag{3.11}$$

The weight normalization gives rise to competition among the filters resulting in a strengthening of connections from filters with relatively higher activity and a weakening of connections from filters with relatively lower activity.

3.2.3 Model Results Analysis

At the conclusion of a simulation, the lateralization of two attributes of interest is examined based on the computation of coefficients of asymmetry (for definition, see Footnote 8 in Section 2.6). The first attribute of interest is a structural metric that measures the strength of the projection from a filter to the development layer of a hemisphere. The structural metric is defined as the total of weights from filter unit $j \in F$ to the units in the development layer D for hemisphere H as given by:

$$W_j^H = \sum_{\ell}^{D^H} w_{\ell j}^H \tag{3.12}$$

Structural asymmetry as a function of filter peak frequency is then defined as

$$\rho_{struc}(f_j) = (W_j^R - W_j^L)/(W_j^R + W_j^L) \tag{3.13}$$

where f_j is the peak frequency of filter $j \in F$. The second attribute of interest is a functional metric that measures the activity that is produced in a hemisphere in response to a stimulus frequency. The functional metric is defined as the total activation of the development layer D in hemisphere H in response to input frequency $\omega_i, i \in I$, as given by

$$A_i^H = \sum_{\ell}^{D^H} a_{\ell}^H(\omega_i) \tag{3.14}$$

where $a_{\ell}^{H}(\omega_i)$ is the activation of development unit ℓ in hemisphere H in response to ω_i. Functional lateralization as a function of input frequency is then defined as

$$\rho_{func}(\omega_i) = (A_i^R - A_i^L)/(A_i^R + A_i^L) \tag{3.15}$$

where ω_i is the frequency of input $i \in I$. The structural asymmetry function reveals any hemispheric differences in the projections of spatial frequency filters (to V2) that depend on a filter's preferred frequency. The functional lateralization function reveals any hemispheric differences in activation that depend on the frequency of the input. The functional lateralization effects are the consequence of the underlying structural asymmetries.

3.3 Results

This section reports on several sets of experiments that are designed to examine the relationship between certain model parameters and lateralized development. Because differences in the initial values for the filter-to-development layer weights and the order of input presentation can affect the lateralization results, 20 simulations, differing only in the random values assigned to these parameters, were performed for each set of parameter values so that the significance of observed lateralization effects could be statistically evaluated. The structural asymmetry and functional lateralization results reported in both this and the remaining sections of this chapter are the mean values obtained over the 20

simulations. The graphs of these functions, shown for each set of experimental conditions, depict the mean values together with the 95% confidence intervals.

3.3.1 The Baseline Modeling Experiment

The purpose of the baseline modeling experiment is to examine the hypothesis that differences in the time course of development for the two visual pathways coupled with differences in the timing of development in the two cortical hemispheres can lead to lateralization in spatial frequency processing. For the baseline simulations, a specific scenario with respect to the timing of hemispheric development is assumed. In addition, the six V1 filters are assumed to have the same shape, albeit with different peak frequencies, and to be equally represented at a given retinotopic location. The effects of variations in these assumptions on model behavior are examined in subsequent sections.

For the baseline experiments, the mid-point of the period of hemispheric development is set to t_R = 7.7 months in the right hemisphere and t_L = 8.3 months in the left hemisphere. Thus, development in the left hemisphere is assumed to lag that in the right by 0.6 months. As mentioned previously, a 10 month developmental period is assumed, therefore, right hemisphere development occurs between 2.7 and 12.7 months in the right hemisphere and .between 3.3 and 13.3 months in the left hemisphere. The development periods are offset symmetrically about the 8 month point, which is the age at which the visual pathways, and therefore the filters, are assumed to reach full maturity.

The baseline experiments further assume that the response of filter j is given by Equation 3.1 using the parameter values shown in Table 3.2. The values for B, C, σ_1, σ_2 and σ_3 determine filters of identical shape having peak frequencies of 0.5, 1, 2, 4, 8, and 16 cpd and a bandwidth of ≈1.5 octaves[12], consistent with the findings on filter bandwidth discussed in Section 2.4 (De Valois, et al., 1982). The values for A are normalization constants that set the response of each filter to 1 at its peak frequency. The filter response as a function of peak frequency f, as determined by these parameters, is depicted in Figure 3.6 in Section 3.2.2.

Table 3.2: Filter Parameters for Uniform Filter Functions

filter j	*peak* (*cpd*)	*band width**	*A*	*B*	*C*	σ_1	σ_2	σ_3
1	0.5	1.49	4.64	0.894	0.333	0.432	1.056	1.416
2	1.0	1.49	9.28	0.894	0.333	0.216	0.528	0.708
3	2.0	1.49	18.56	0.894	0.333	0.108	0.264	0.354
4	4.0	1.49	37.12	0.894	0.333	0.059	0.132	0.177
5	8.0	1.49	74.24	0.894	0.333	0.030	0.066	0.088
6	16.0	1.49	148.48	0.894	0.333	0.015	0.033	0.044

* in octaves

[12] The values for parameters B, C, σ_1, σ_2 and σ_3 are based on those estimated by Wilson and Gelb (1984) to describe the response of a spatial frequency channel having a bandwidth of about 1.5 octaves with a peak frequency of 4 cpd. The estimated values are scaled to yield filters that differ only in peak frequency.

The pathway sensitivities discussed in Section 2.3 suggest the general characteristics, but not the precise values, of relative pathway contributions to filters of various spatial frequencies (designated in the model as c_j^M and c_j^P). Consequently, the baseline experiment examines the results produced by three different sets of relative contribution values (see Table 3.3). Each set is based on a simple linear pattern that is consistent with the assumption that the relative magnocellular contribution decreases, while the relative parvocellular contribution increases, with increasing frequency (Assumption 5 of Section 3.2.1). Each set also assumes that the magnocellular pathway does not contribute to the 16 cpd filter, consistent with the magnocellular pathway sensitivity to spatial frequency as discussed in Section 2.3. The sets differ in the overall ratio of the magnocellular-to-parvocellular contributions from low, to moderate, to high. The ratio is determined by the value that is chosen for the relative magnocellular contribution to the lowest frequency (0.5 cpd) filter, that is, by the maximum magnocellular contribution to a filter. The chosen values are 0.33 for the low (magnocellular contribution) set, 0.5 for the moderate set, and 1.0 for the high set as shown in Table 3.3.

Table 3.3: Relative Contributions of Magno (M) and Parvo (P) Pathways to Filter Activity

filter	*f* (cpd)	*low*		*moderate*		*high*	
		c^M	c^P	c^M	c^P	c^M	c^P
1	.50	.33	.67	.50	.50	1.0	0.0
2	1.0	.27	.73	.40	.60	.80	.20
3	2.0	.21	.79	.30	.70	.60	.40
4	4.0	.14	.86	.20	.80	.40	.60
5	8.0	.07	.93	.10	.90	.20	.80
6	16.0	0.0	1.0	0.0	1.0	0.0	1.0

An example set of timelines from a simulation based on the baseline parameter values previously specified, together with the moderate set of relative contribution values from Table 3.3, illustrates the development of structural asymmetry and functional lateralization. The factors underlying asymmetric development, that is, asynchronous periods of plasticity in the two hemispheres, and the changing relative maturity levels of the spatial frequency filters due to pathway maturation effects, are shown in Figure 3.9.

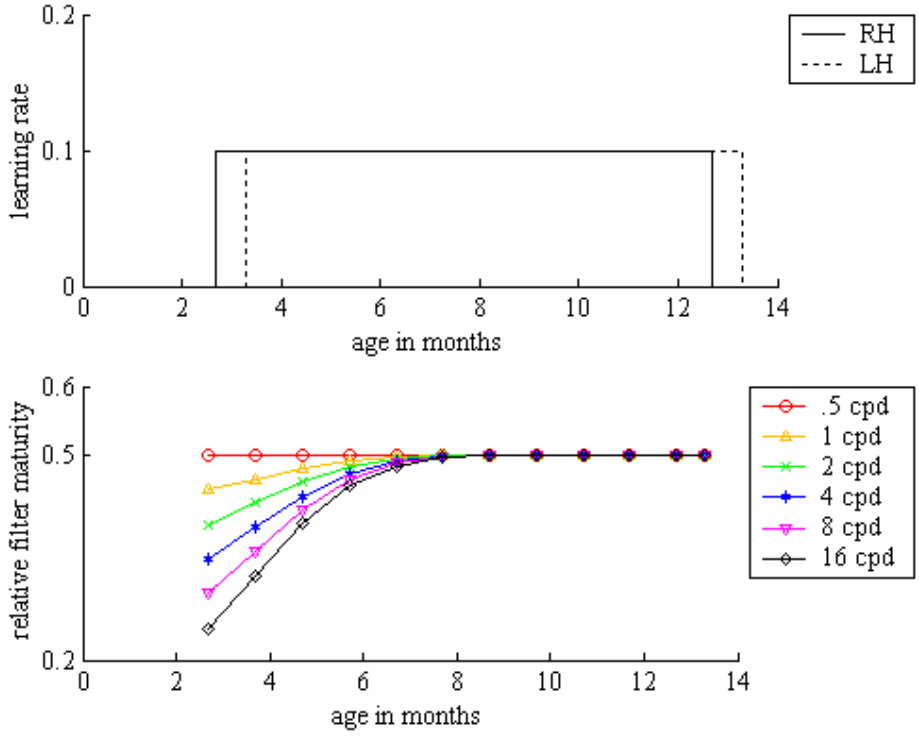

Figure 3.9: Factors underlying asymmetric development. The upper graph depicts the asynchronous periods of hemispheric plasticity in the right (RH) and left (LH) hemispheres as represented by the learning rate functions, $\eta^R(t)$ and $\eta^L(t)$. The functions are identical but offset in time by t_L-t_R = 8.3-7.7 = 0.6 months. The lower graph shows the changing relative maturities of the six spatial frequency filters, where the relative maturity of filter j is given by $\mu_j(t)$. Filters are equally mature at 8 months, the point of full maturity for the two visual pathways.

The change in the sum of the weights from each filter to the development layer that occurred over the course of development is shown in Figure 3.10 for both the right and the left hemispheres. The weights from each filter start out approximately equal, but diverge as development progresses.

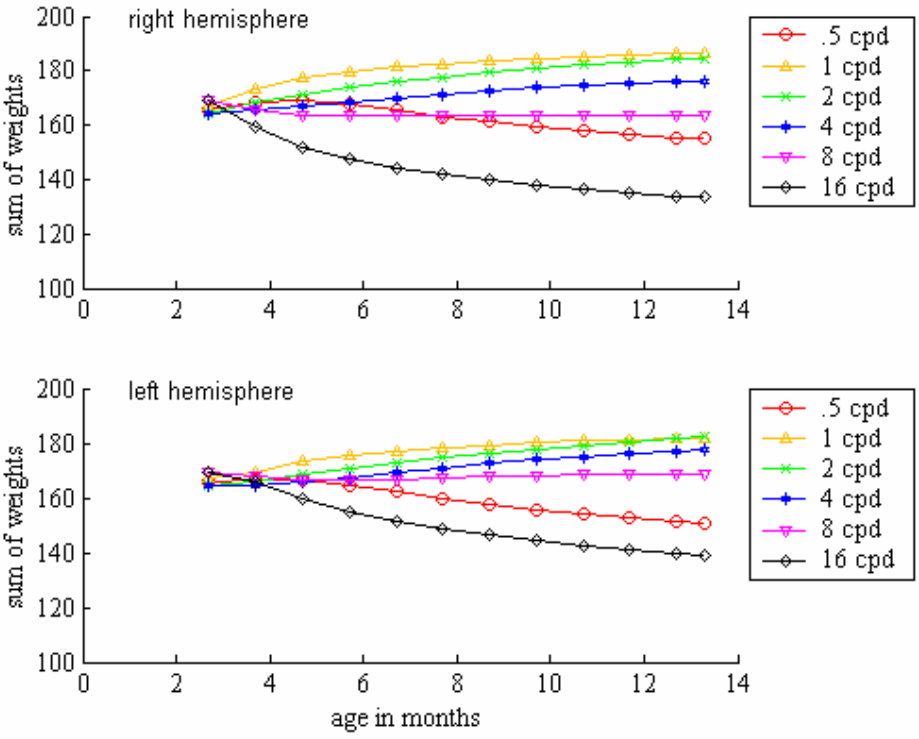

Figure 3.10: The change in the sum of the weights, W_j, from filter j to the development layer for each of the six spatial frequency filters. Weight development in the right hemisphere is shown in the upper graph, left hemisphere in the lower graph.

Although weight development for the two hemispheres is quite similar, weight asymmetry related to the spatial frequency of the filter emerges as shown in Figure 3.11. Consistent with the spatial frequency hypothesis, the weights from the low frequency filters develop rightward asymmetry, while the weights from the high frequency filters develop leftward asymmetry. The more pronounced changes in the asymmetry functions that appear at the beginning and the end of development are attributable to the asymmetric states of plasticity that occur at those times.

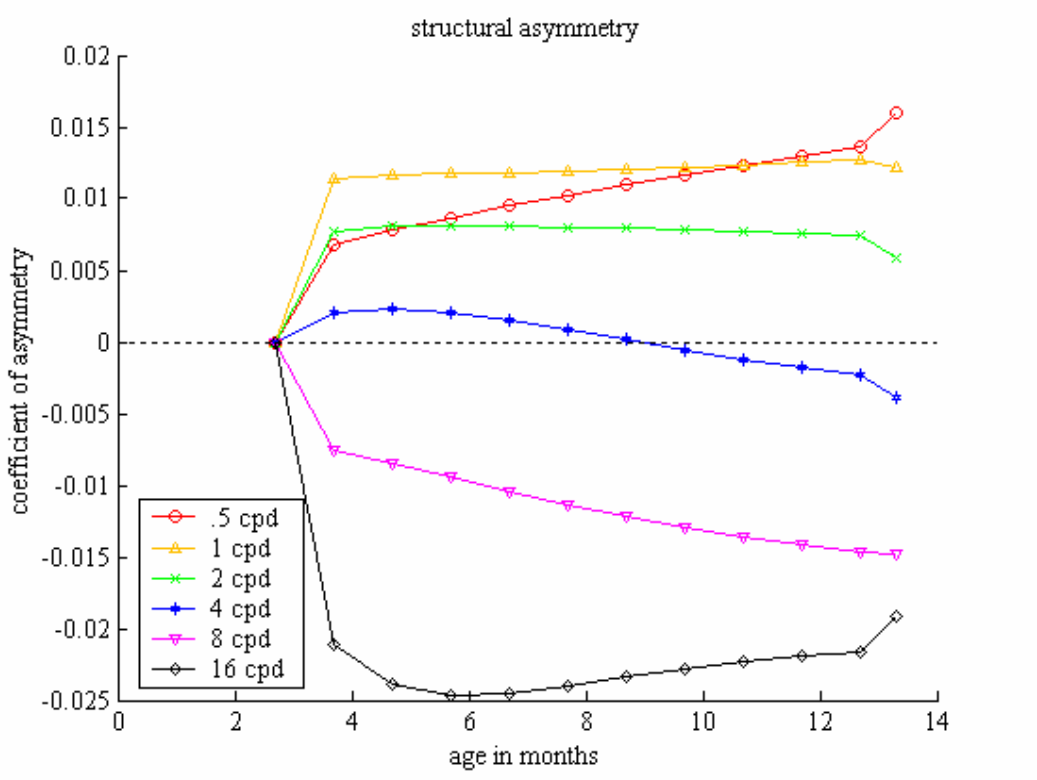

Figure 3.11: The development of structural asymmetry as measured by the coefficient of asymmetry, ρ_{struc}, computed for each of the six spatial frequency filters.

The change in the total development layer activation in response to each input frequency that occurred over the course of development is shown in Figure 3.12 for both the right and the left hemispheres. Activation increases for all input frequencies, but not equally.

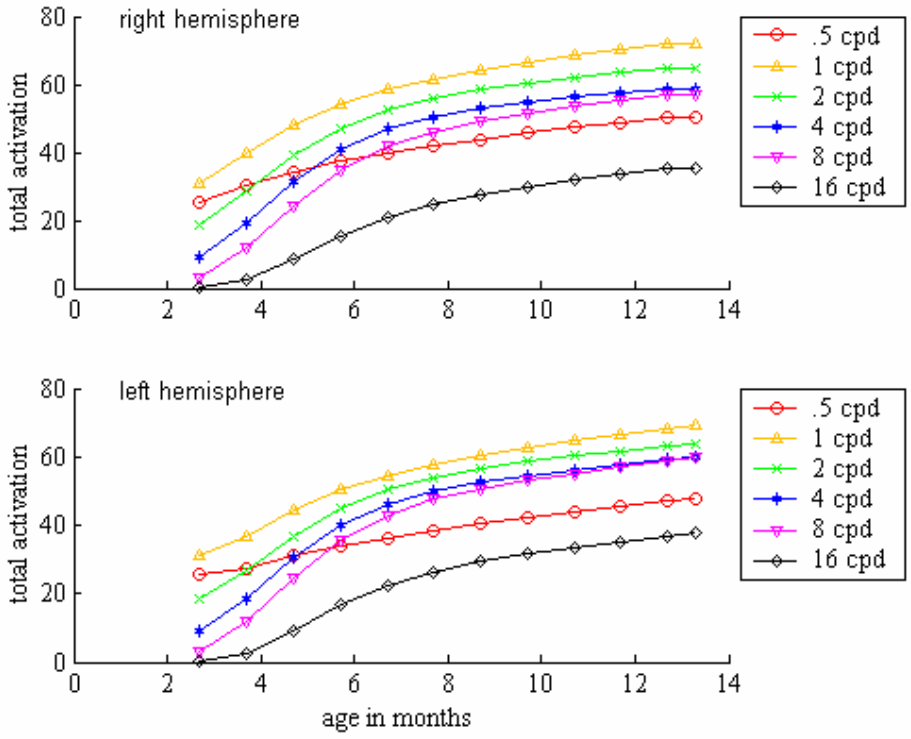

Figure 3.12: The change in the total development layer activation, A_i, in response to input i for each of the six input frequencies. Development layer activation in the right hemisphere is shown in the upper graph, left hemisphere in the lower graph.

Once again, the changes for the two hemispheres differ subtly but systematically, meaning that activation lateralization related to the spatial frequency of the input emerges (see Figure 3.13). Consistent with the spatial frequency hypothesis, the activation resulting from the low frequency input is right lateralized, while the activation resulting from the high frequency input is left lateralized. The more pronounced changes in lateralization that appear at the beginning and the end of development are again attributable to the asymmetric states of plasticity that occur at those times. The early plasticity of the right hemisphere causes an initial right

lateralization of activation in response to all input frequencies. As the left hemisphere begins to develop, right lateralization decreases to the extent that, in the case of high spatial frequency inputs, the direction of lateralization reverses.

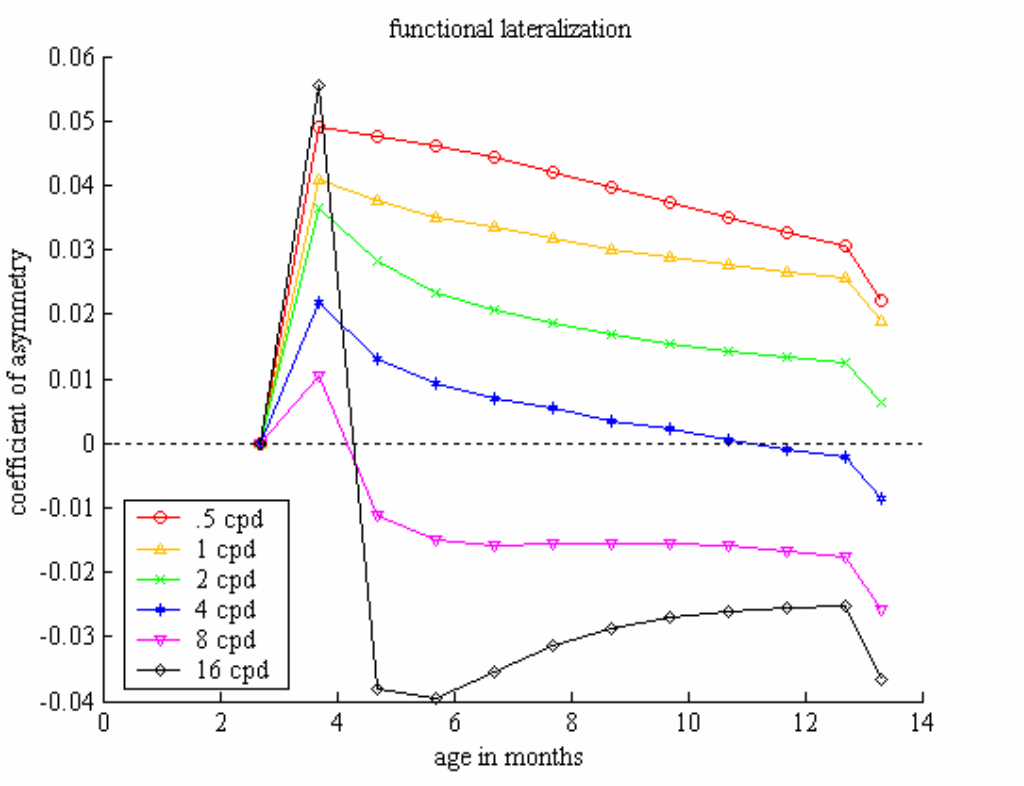

Figure 3.13: The development of functional lateralization as measured by the coefficient of asymmetry, ρ_{func}, computed for each of the six input frequencies.

The baseline experiment, as mentioned earlier, consists of simulations based on each of the three sets of pathway contribution values specified in Table 3.3 as *low*, *moderate* and *high*. These three conditions produce consistent results that support the experimental hypothesis, that is, right lateralization develops for

low spatial frequencies and left lateralization develops for high frequencies. The structural asymmetry results (see Figure 3.14) indicate that the connections from the lower frequency filters to the development layer become relatively stronger in the right hemisphere while the connections from the higher frequency filters to the development layer become relatively stronger in the left hemisphere. The functional lateralization results (see Figure 3.15) indicate that development layer activation in response to low spatial frequency input becomes relatively stronger in the right hemisphere while activation in response to higher frequency input becomes relatively stronger in the left hemisphere. For both structural asymmetry and functional lateralization, the crossover point is approximately 3 cpd for all three of the component contribution conditions.

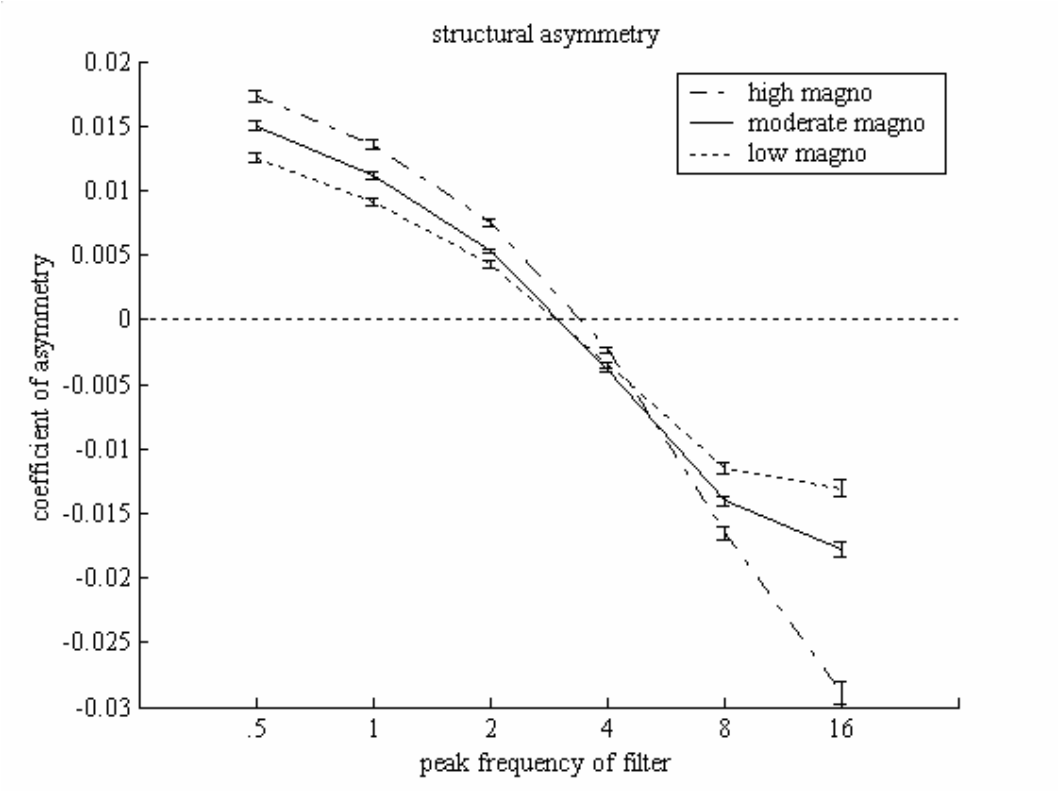

Figure 3.14: The graphs show the structural asymmetry that developed for each of three variations in the ratio of the overall magnocellular-to-parvocellular contribution to filter activity (low, moderate, and high). Each point in a graph represents the asymmetry in the weight of the connections from the filter of the specified peak frequency to the development layer computed as the coefficient of asymmetry ρ_{struc}. Depicted are the mean values together with the 95% confidence limits (error bars), with positive (negative) values indicating rightward (leftward) asymmetry.

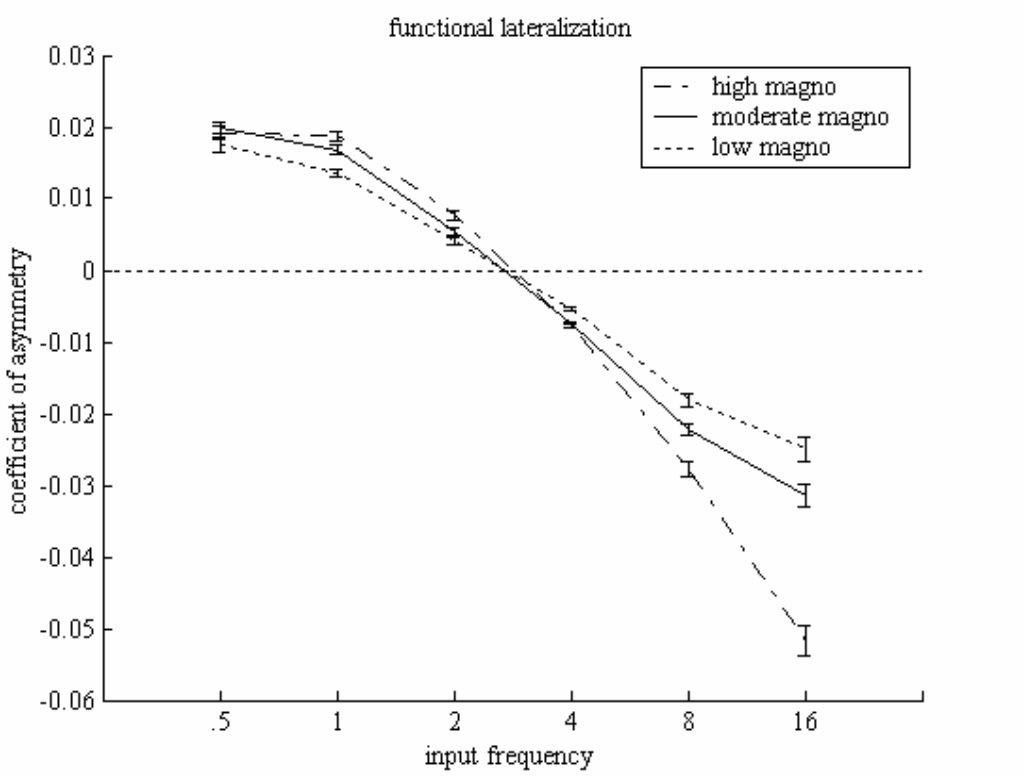

Figure 3.15: The graphs show the functional lateralization that developed for each of three variations in the ratio of the overall magnocellular-to-parvocellular contribution to filter activity (low, moderate, and high). Each point represents the lateralization observed in the total activation of the development layer in response to input of the specified frequency computed as the coefficient of asymmetry ρ_{func}. Depicted are the mean values together with the 95% confidence limits (error bars), with positive (negative) values indicating rightward (leftward) asymmetry.

Like the lateralization effects that were observed in the psychophysical experiments described in Section 2.6, the structural asymmetry and functional lateralization effects produced in the simulation experiments are small, but significant. As mentioned earlier, the reaction time lateralization effects, as measured by the coefficient of asymmetry, were found to be on the order of ±0.02

in the psychophysical experiments. For the simulation experiments, the maximum absolute values for coefficient of asymmetry were approximately 0.03 for structural asymmetry and 0.05 for functional lateralization.

The lateralization effects produced under each of the three pathway contribution assumptions appear quite similar, particularly with respect to the functional lateralization cross-over point, which is virtually identical for the three conditions. This suggests that the systematic decrease in the relative contribution of the magnocellular pathway to filter activity as a function of the peak frequency of the filter is more important than the actual relative contribution values in determining the characteristics of the lateralization that develops. Both structural asymmetry and functional lateralization effects do appear to increase somewhat as the magnocellular-to-parvocellular contribution ratio increases from low to moderate to high. However, a single factor analysis of variance applied to the results obtained under the three conditions did not find the differences to be significant for either structural asymmetry [$F(2,15) = 1.0$, $p < .4$, $\alpha = .05$] or functional lateralization [$F(2,15) = 0.72$, $p < .5$, $\alpha = .05$]. Because the choice of relative contribution values was found to have little impact on the lateralization effects, only one set of values, namely those designated as 'moderate' in Table 3.3, are used in the experiments that follow.

3.3.2 The Effects of the Timing of Development on Lateralization

The baseline experiment served to demonstrate that differences in the time course of maturation for the two visual pathways coupled with differences in the timing of cortical plasticity in the two hemispheres could lead to the development of lateralization in spatial frequency processing. The next set of experiments investigates the sensitivity of the lateralization effects to variations in the timing of hemispheric development. Two variations in the timing of development are examined: first, in the timing of the hemispheric developmental periods relative to visual pathway development and second, the timing of development of the left hemisphere development relative to that of the right.

The effect of the timing of the hemispheric developmental periods relative to visual pathway development was examined by moving the timing forward in one month increments while keeping a constant one month difference between the hemispheres. Given that the difference in the relative maturity of the magnocellular and parvocellular pathways decreases monotonically (after the age of 0.5 months), earlier hemispheric development can be expected to produce greater lateralization.

Six simulations were performed with t_R = 6, 7, 8, 9, 10, 11 and t_L = 7, 8, 9, 10, 11, 12 respectively. The simulation results indicate that, in general, greater structural asymmetry and functional lateralization result from earlier hemispheric development (see Figures 3.16 and 3.17). The highest degree of asymmetry and lateralization is clearly associated with the earliest hemispheric development and

is virtually eliminated in the case of late development. A single factor analysis of variance applied to the results of the six simulations found the effect of the timing of hemispheric development to be highly significant in the case of both structural asymmetry [$F(5,30) = 8.66$, $p < .00004$, $\alpha = .05$] and functional lateralization [$F(5,30) = 6.46$, $p < .00035$, $\alpha = .05$].

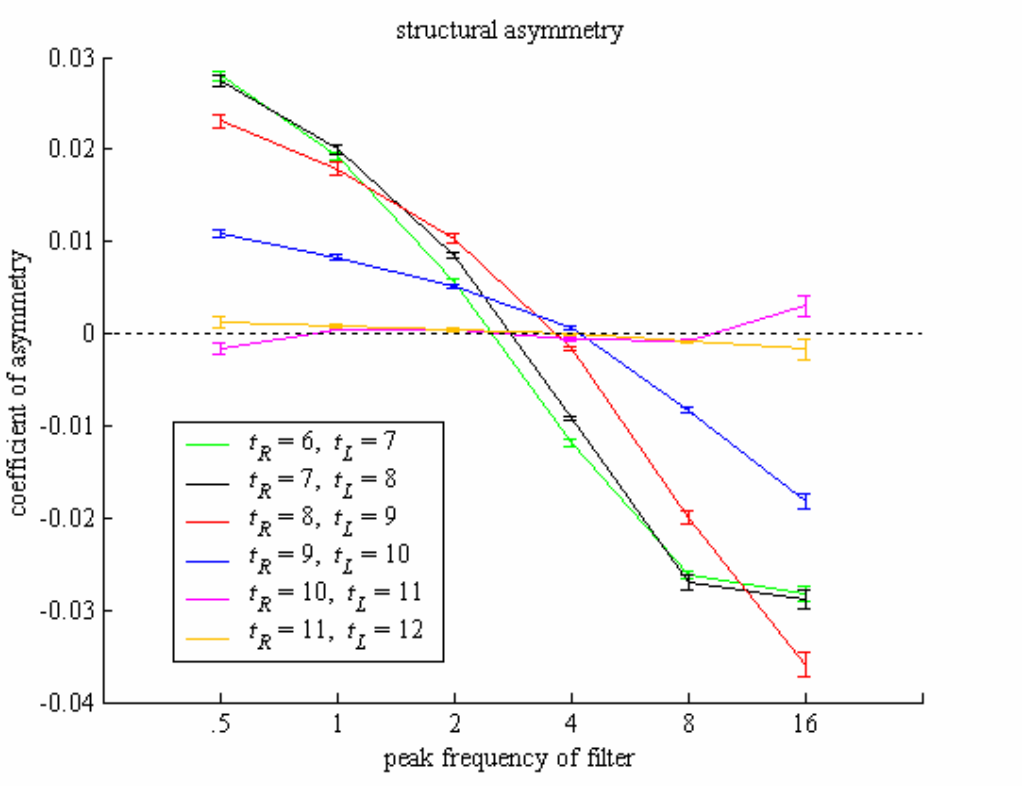

Figure 3.16: The effect on structural asymmetry of varying the overall timing of the developmental periods while maintaining a 1 month difference between the hemispheres. The values for t_R and t_L correspond to the respective mid-points for the developmental periods in the right and left hemispheres.

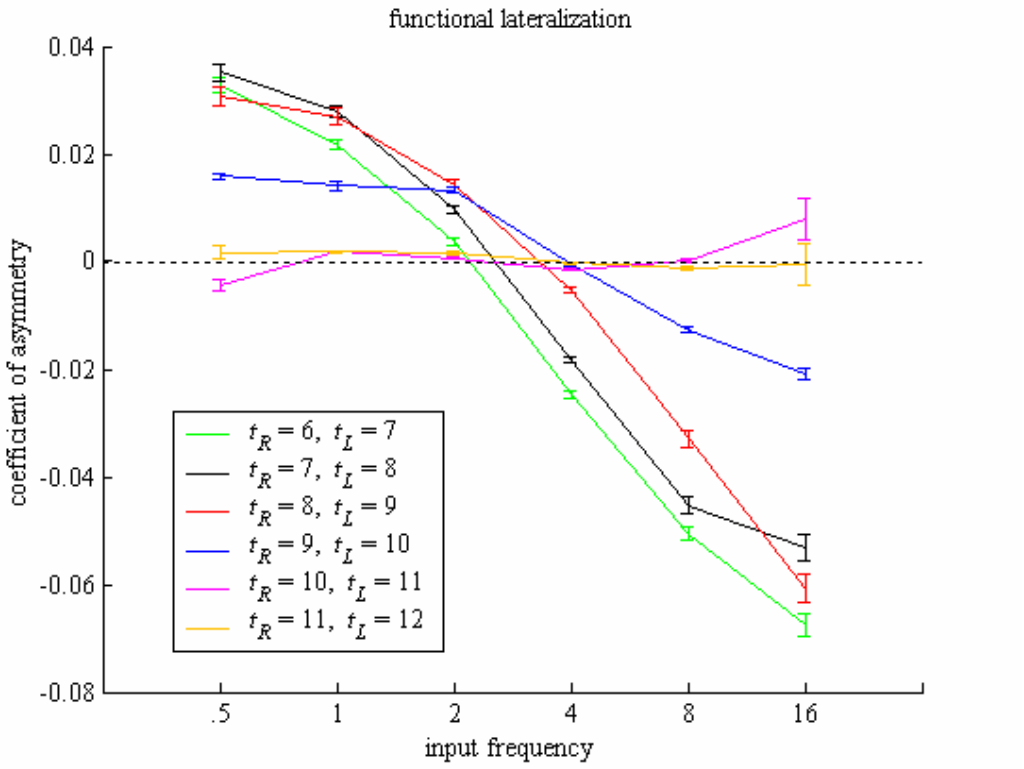

Figure 3.17: The effect on functional lateralization of varying the overall timing of the developmental periods while maintaining a 1 month difference between the hemispheres. The values for t_R and t_L correspond to the respective mid-points for the developmental periods in the right and left hemispheres.

The next set of simulations examines the effect of variation in the magnitude of the difference in the timing of development between the two hemispheres. Because the relative maturity functions are monotonic, it is expected that the greater the difference, the greater the lateralization produced. Three simulations were performed with developmental midpoints of t_R = 7.5, 7.7, and 7.85, and t_L = 8.5, 8.3, 8.15, respectively. Thus, a constant mean midpoint of 8 months was maintained for all simulations while the timing difference decreased

from 1 to .6 to .3 months. The results of these simulations support the contention that the magnitude of lateralization varies with the magnitude of the difference in the timing of hemispheric development (see Figures 3.18 and 3.19). A single factor analysis of variance applied to the results of the three simulations found the effect of the difference in the timing of development on structural asymmetry to be statistically significant [$F(2,15) = 6.23$, $p < .011$, $\alpha = .05$], as was the effect on functional lateralization [$F(2,15) = 5.25$, $p < .019$, $\alpha = .05$].

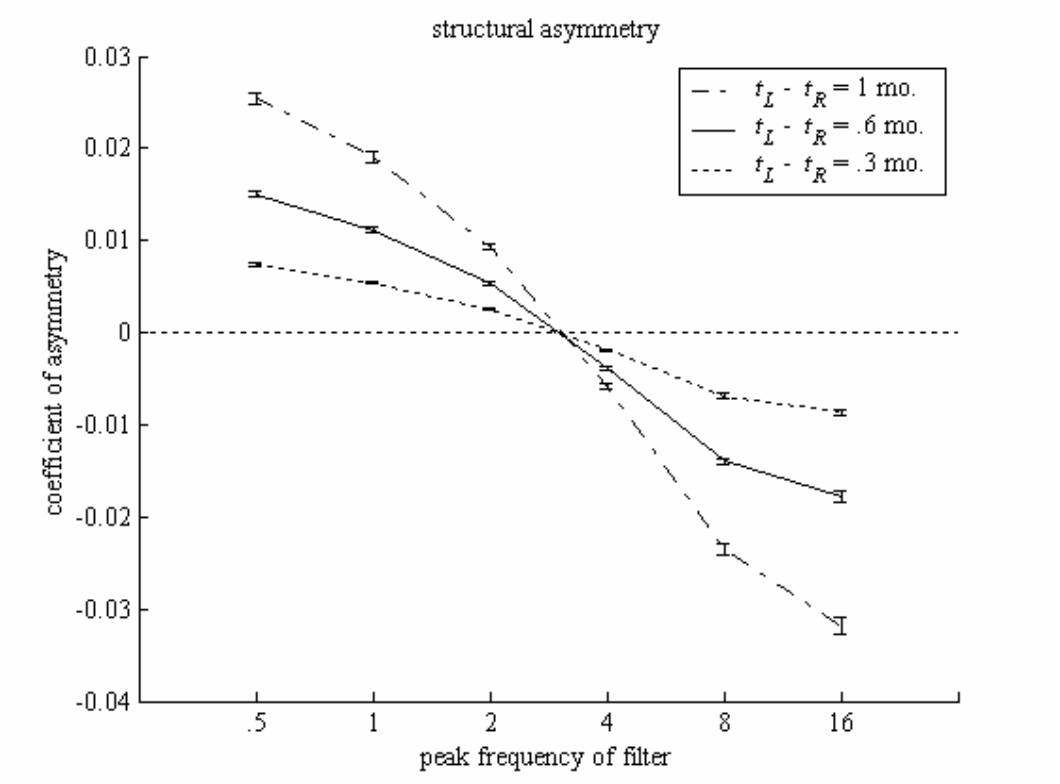

Figure 3.18: The effect on structural asymmetry of varying the difference in the timing of hemispheric development as specified by the value of t_L - t_R, where t_R and t_L are the midpoints of the development periods for the right and left hemispheres, respectively.

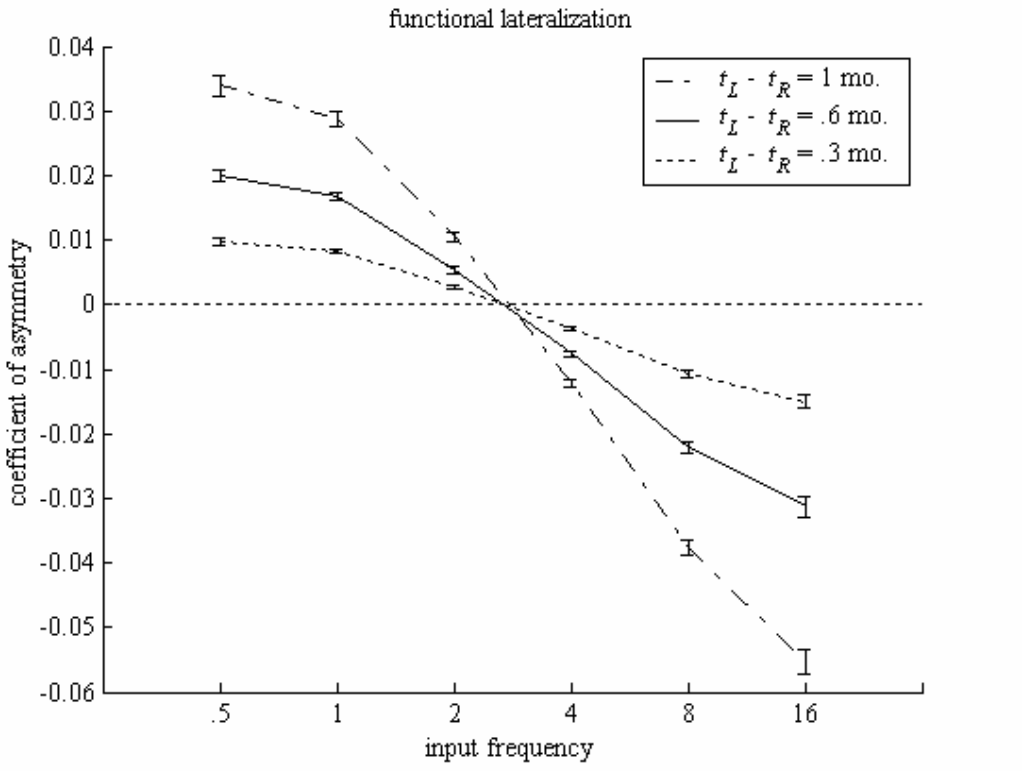

Figure 3.19: The effect on functional lateralization of varying the difference in the timing of hemispheric development as specified by the value of t_L - t_R, where t_R and t_L are the midpoints of the development periods for the right and left hemispheres, respectively.

3.3.3 The Effect of Non-Uniform Filter Functions

The previous simulations assumed response functions for the six filters that differed only in their peak frequency. Physiological data from the macaque, however, indicates that the filter response function changes with peak frequency such that the bandwidth narrows as the peak frequency increases (De Valois et al., 1982). In fact, bandwidths were observed to decrease from ~ 2.2 octaves for filters with peak frequency < .7 cpd, to ~ 1.2 octaves for filters with peak frequency > 11.0 cpd (see Figure 3.20).

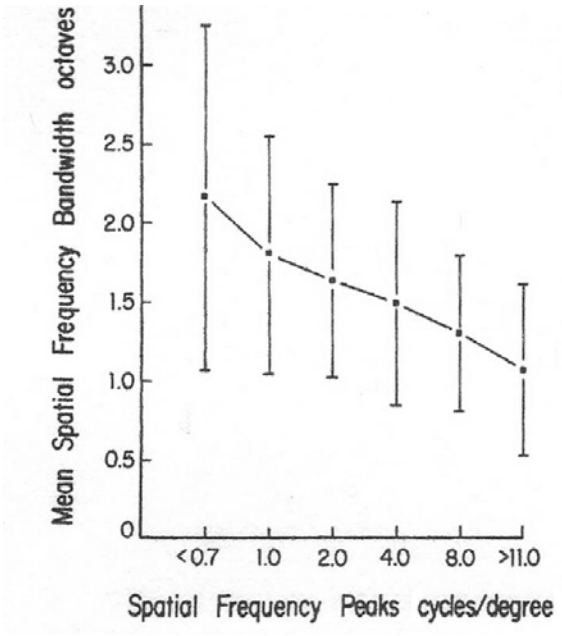

Figure 3.20: Mean bandwidth of macaque V1 cells as a function of their peak spatial frequency (±1 SD). (Adapted from De Valois et al., 1982, copyright 1982, with permission from Elsevier.)

In order to examine the impact of filter function assumptions on asymmetry and lateralization effects, the next experiment compares two simulations, both based on the timing values of t_R = 6.5 and t_L = 7. The first utilizes the same uniform filter functions used in the simulations thus far (based on the parameter values given in Table 3.2). The second uses filter functions calibrated to be consistent with the empirical findings just discussed. The set of function parameter values applied to Equation 3.1 to produce the six filters[13] is given in Table 3.4, together with the filter bandwidths. A graph of the six filters determined by these parameters is shown in Figure 3.21.

[13]The parameter values for filter 4 are identical to those used for the uniform filter set. For filter 5, the filter function is defined by Equation 3.1 for input frequency $\omega > 1$. If $0 \leq \omega \leq 1$, $r(\omega)=0$. For filter 6, the filter function is defined by Equation 3.1 for input frequency $\omega > 5$. If $0 \leq \omega \leq 5$, $r(\omega)=0$.

Table 3.4: Filter Parameters for the Non-Uniform Filter Functions

filter	*peak* (*cpd*)	*band width**	*A*	*B*	*C*	σ_1	σ_2	σ_3
1	0.5	2.17	4.444	0.333	0.0	0.333	1.000	0.0
2	1.0	1.92	8.789	0.520	0.111	0.195	0.508	0.720
3	2.0	1.64	17.81	0.707	0.222	0.108	0.262	0.377
4	4.0	1.49	37.12	0.894	0.333	0.059	0.132	0.177
5	8.0	1.35	88.77	1.106	0.429	0.034	0.064	0.084
6	16.0	1.18	246.3	1.317	0.525	0.020	0.031	0.041

* in octaves

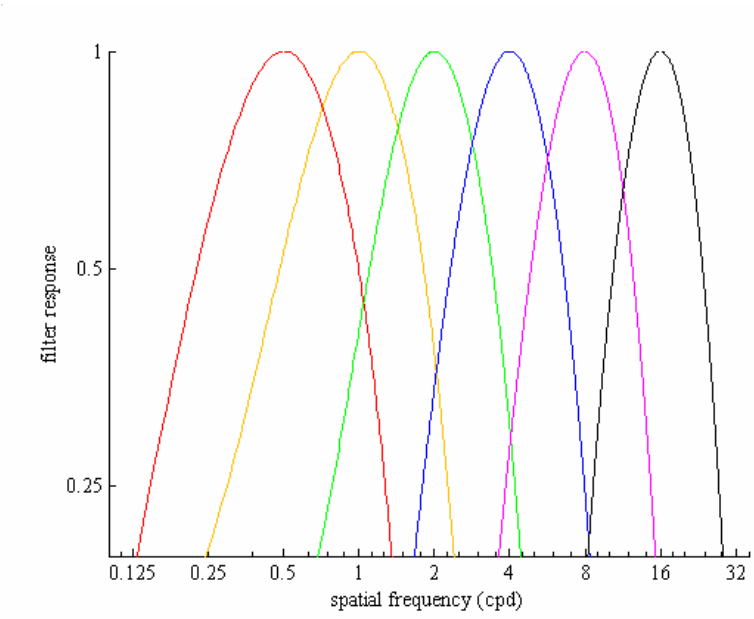

Figure 3.21: Response functions for the six filters showing the narrowing of filter bandwidth as the peak frequency increases.

The results of the two simulations are presented for comparison in Figures 3.22 and 3.23. As is evident, the assumption of the more veridical filter functions does not affect the results qualitatively, that is, low spatial frequencies continue to exhibit rightward asymmetry and high spatial frequencies leftward asymmetry. Quantitatively, the results are similar as well although the assumption of non-uniform filters produces some differences at the frequency extremes, particularly in the case of functional lateralization at high spatial frequency.

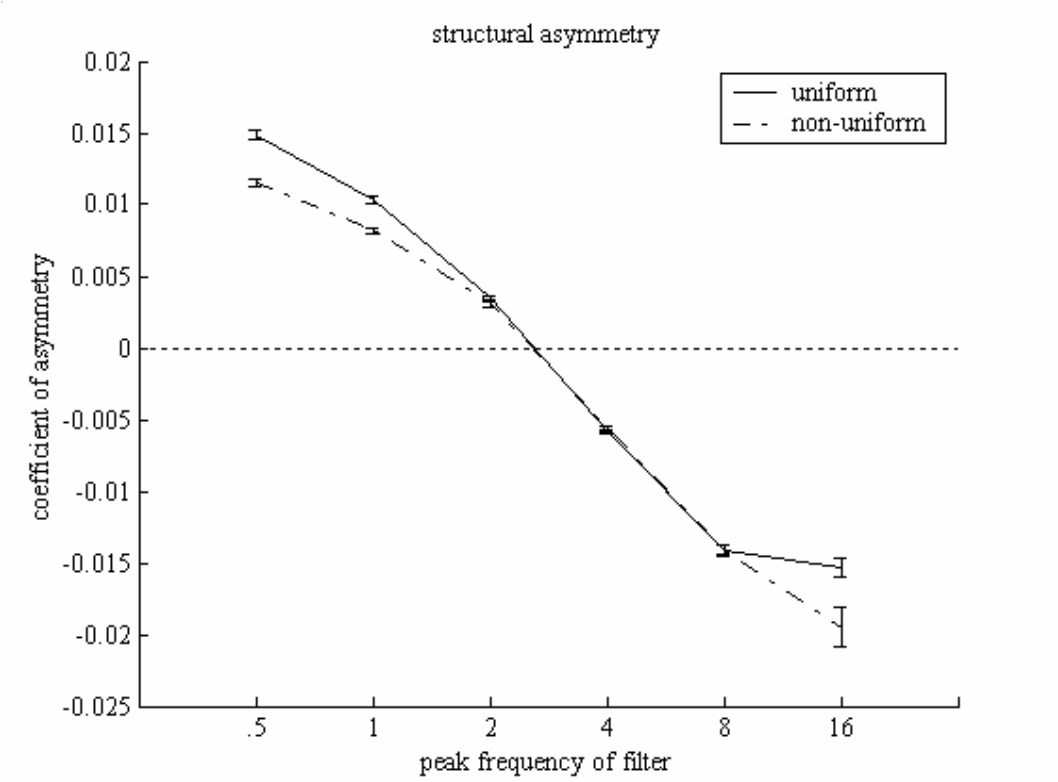

Figure 3.22: A comparison of asymmetry in the weight of the connections from filters to the development layer assuming either filter response functions that are uniform in shape or non-uniform functions for which bandwidth and peak frequency are inversely related.

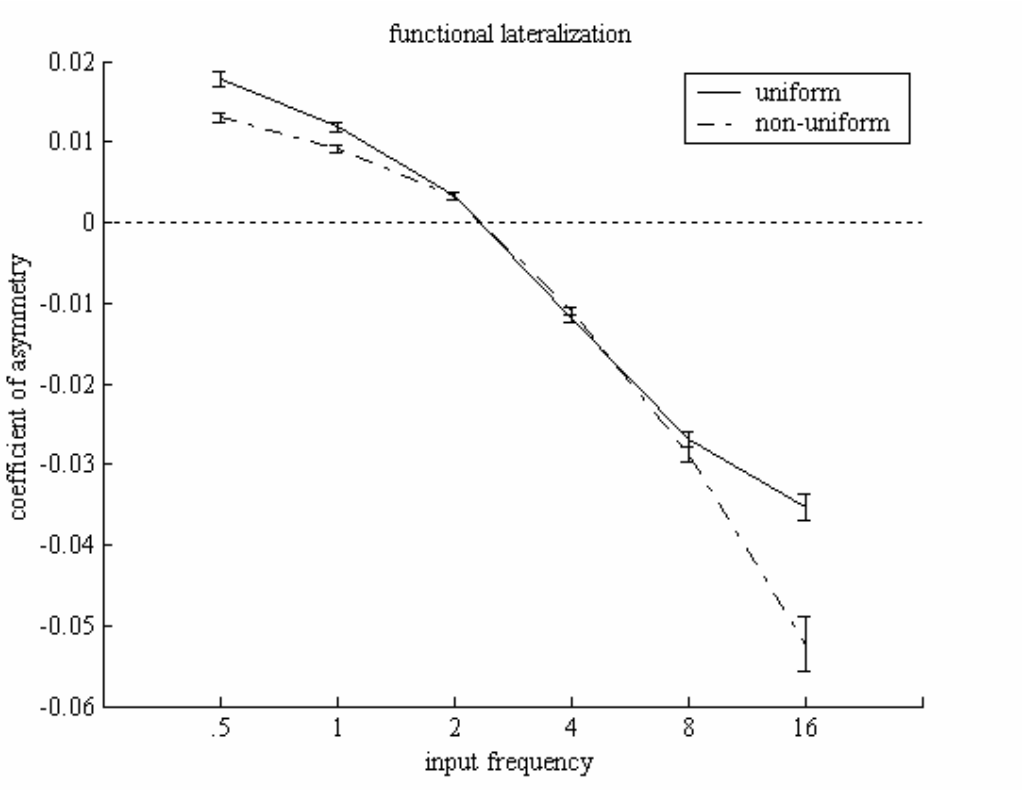

Figure 3.23: A comparison of lateralization in development layer activation in response to input of a particular frequency assuming filter response functions that are either uniform in shape or non-uniform with bandwidth and peak frequency inversely related.

3.3.4 The Effect of Unequal Filter Representation

The simulations discussed thus far assumed that filters, distinguished by their peak frequencies, are distributed equally at a given location in V1. Hence, each of the six filters was represented in a filter set by one unit. However, the distribution of peak frequencies found in samples of macaque V1 cells is non-uniform, with greater numbers falling in the middle of the frequency spectrum

and fewer toward the high and low ends (De Valois et al., 1982). The next set of simulations examines the effect of such a distribution on the development of asymmetry in spatial frequency processing by allocating more than one unit to the mid-spectrum filters in the filter set. The number of units allocated for each of the six filters is given in Table 3.5. The numbers are in approximate proportion to the distribution observed empirically (see Figure 3.24). Other simulation parameters are the same as those used in the simulations based on non-uniform filters including the timing parameters, $t_R = 6.5$ and $t_L = 7$.

Table 3.5: Distribution of Filters in Filter Set

filter	*peak freq* (cpd)	*number of units*
1	.50	1
2	1.0	3
3	2.0	6
4	4.0	6
5	8.0	3
6	16.0	1

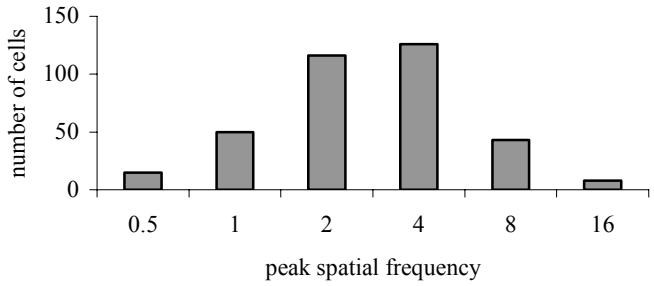

Figure 3.24: The distribution of peak spatial frequencies found in a sample of 358 macaque V1 cells (228 foveal, 130 parafoveal). The individual foveal and parafoveal distributions are shown in Figure 2.9. (Based on data from De Valois & De Valois, 1988.)

As can be seen in Figures 3.25 and 3.26, the assumption of this more empirically-motivated filter distribution does not alter the basic pattern of lateralization observed in the baseline experiment. The association of right lateralization with low spatial frequencies and left lateralization with high spatial frequencies persists. However, maximum lateralization is no longer associated exclusively with frequency extremes. In fact, no significant functional lateralization is associated with input frequency 16 cpd. This outcome suggests that psychophysical experiments may not produce the most robust lateralization effects at frequency extremes but rather at mid-low and mid-high frequencies such as 1 and 8 cpd.

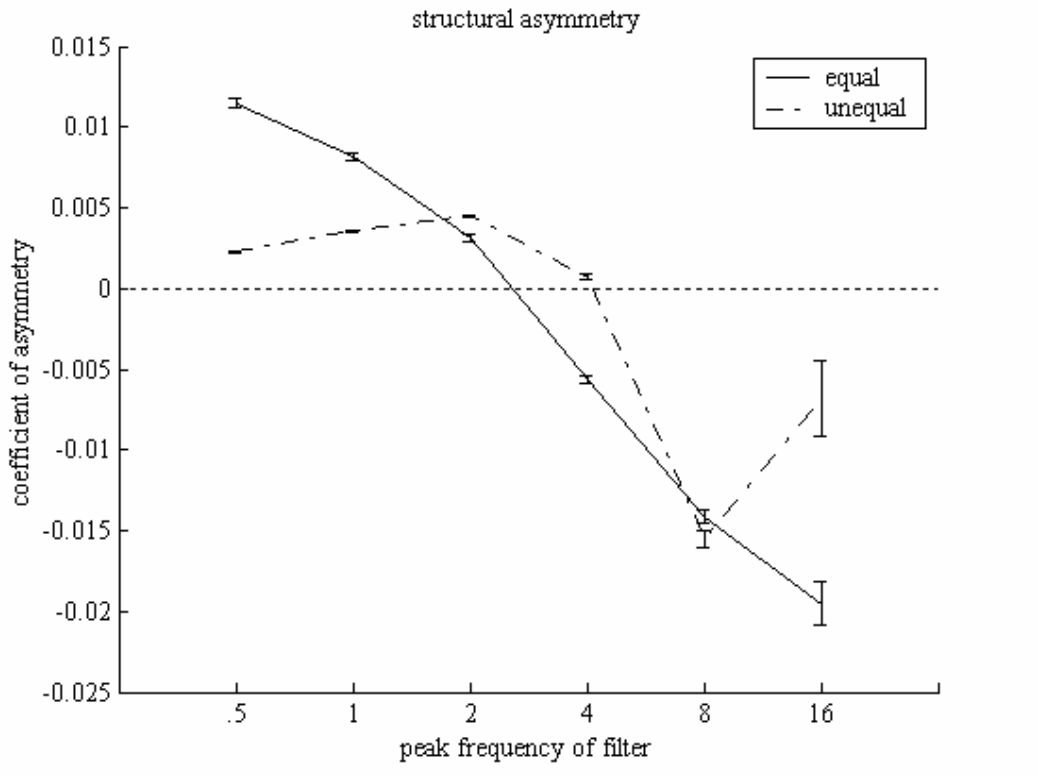

Figure 3.25: A comparison of asymmetry in the weight of the connections from filters to the development layer assuming that filters of varying peak frequencies are distributed in either equal or unequal numbers. In the latter case, it is assumed that filters in the middle of the spectrum are represented in greater numbers than those at the low and high ends.

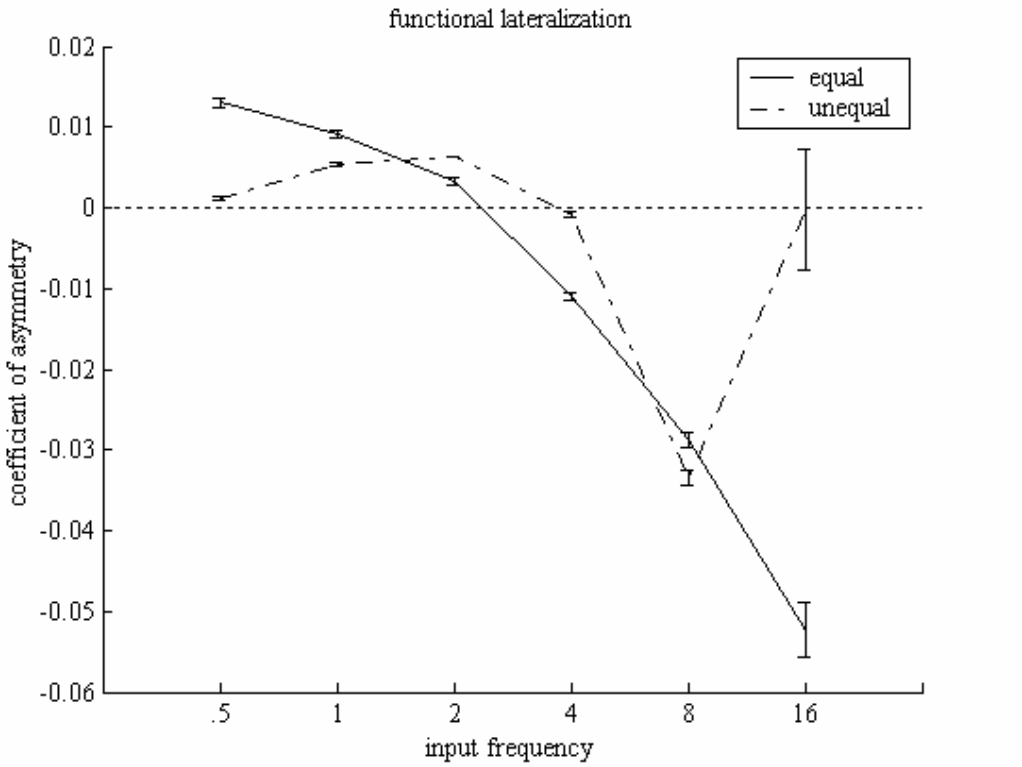

Figure 3.26: A comparison of lateralization in development layer activation in response to input of a particular frequency assuming that filters of varying peak frequencies are distributed in either equal or unequal numbers. In the latter case, it is assumed that filters in the middle of the spectrum are represented in greater numbers than those at the low and high ends.

An example of the time course of functional lateralization development for the input frequencies that exhibited significant lateralization in the simulations based on the unequal filter distribution (0.5, 1, 2, 4, and 8 cpd) is shown in Figure 3.27. These results indicate that strong lateralization effects develop between the second and sixth month that diminish as development continues beyond this point. Thus, if hemispheric development is concentrated within postnatal months 2 to 6, it should produce stronger lateralization than if it extends over a longer period.

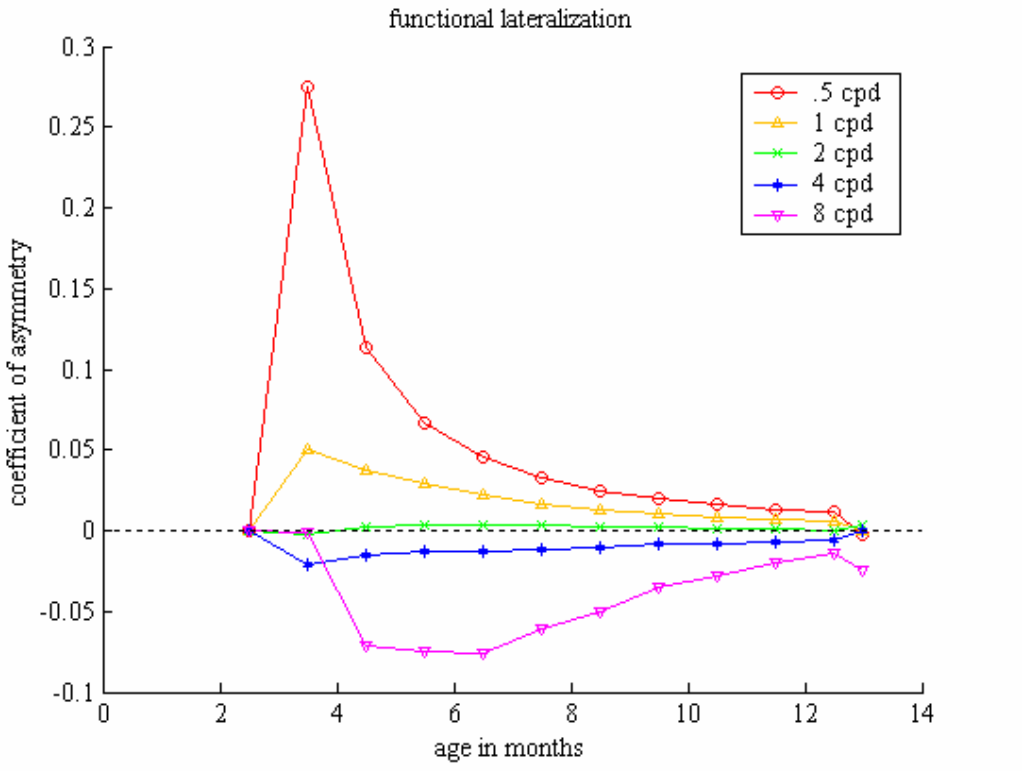

Figure 3.27: The development of functional lateralization under the assumption of the unequal filter distribution shown in Table 3.5. Lateralization is measured by the coefficient of asymmetry, ρ_{func}, computed for input frequencies 0.5, 1, 2, 4, and 8 cpd. Maximal lateralization develops between postnatal months 2 and 6, and then diminishes as development continues.

It is worth noting that the model produces a distribution of peak frequencies in V2 that is shifted lower in comparison with V1 peak frequencies (see Figure 3.28). This is consistent with findings (in the macaque) of a mean peak spatial frequency of 1.4 cpd for V2 cells (Levitt, Kiper, & Movshon, 1994) as compared to a mean peak spatial frequency of 3.5 cpd for V1 cells (De Valois et al., 1982). It is also in agreement with the evidence of a shift in peak frequency sensitivity to lower frequencies at the V1/V2 border obtained in fMRI imaging

experiments (Sasaki et al., 20001). Furthermore, selectivity as measured by the mean value of the stimulus selectivity index[14] is 0.57 for V2 units and 0.72 for V1 units, indicating that the average bandwidth of V2 units exceeds that of V1 units. This is consistent with the findings of studies that suggest V2 cells, with a mean bandwidth of approximately 2.4 octaves (Levitt et al., 1994), are more broadly tuned than V1 cells, with a mean bandwidth of approximately 1.5 octaves (De Valois et al., 1982). The agreement between the model and the empirical findings in these areas argues in favor of the validity of the model's basic design.

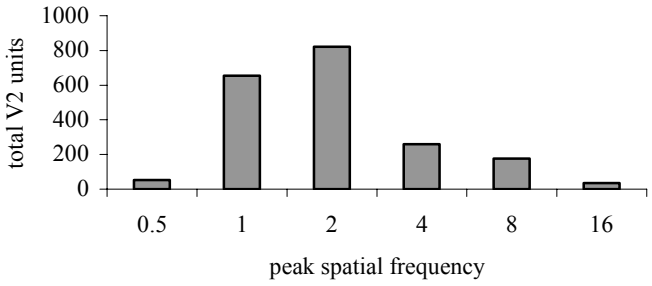

Figure 3.28: The distribution of peak frequencies for V2 units (combined right and left hemispheres) predicted by the model.

3.3.5 Spatial Frequency Lateralization Variation with Eccentricity

The results of the development simulations presented in the previous section indicate that the distribution of spatial frequency filters affects the lateralization function. Thus, the change in filter distribution as a function of

[14] The stimulus selectivity index for a unit is computed as $1-(\alpha_{mean}/\alpha_{peak})$ where α_{mean} is the average activation of the unit for all input frequencies and α_{peak} is the activation of the unit for its most effective frequency (Hedgé & Van Essen, 2003).

eccentricity (see Section 2.5) can be expected to cause eccentricity-dependent differences in the lateralization that develops. The experiments presented in this section examine the relationship between spatial frequency lateralization and eccentricity.

The experiment examines lateralization as a function of eccentricity by performing separate simulations of development at three eccentricities designated as foveal, parafoveal, and extrafoveal. Variation in eccentricity is represented in the model as variation in the relative filter distribution; therefore, three different sets of relative filter distributions values are used in the simulations. The foveal and parafoveal relative filter distributions are based on the peak frequency distributions found in the macaque at eccentricities of 0° to 1.5° and 3° to 5°, respectively (De Valois & De Valois, 1988), as shown in Figure 2.9. The extrafoveal distribution is derived by shifting the macaque distribution found at 3° to 5° toward lower frequencies by one-half octave. In accordance with the information discussed in Section 2.5, a half octave shift downward in filter frequency from that found at 3° to 5° (i.e., ~ 4°) eccentricity should approximate the distribution at eccentricity E, where $(1+4/E_2)^{-1} = 2^{½}(1+E/E_2)^{-1}$ and E_2 is the spatial frequency scaling parameter. Estimates for E_2 include 3.4° (Rovamo & Virsu, 1979), 5.7° (Kelly, 1984, based on data from Virsu & Rovamo, 1979), 6.0° (Dow et al., 1981), and 7.1° (Kelly, 1984) yielding estimates for E of 7.0°, 8.0°, 8.1°, and 8.6°. The relative filter distributions computed for the three

eccentricities are shown in Figure 3.29. These relative distributions are approximated using a set of twenty filters as specified in Table 3.6.

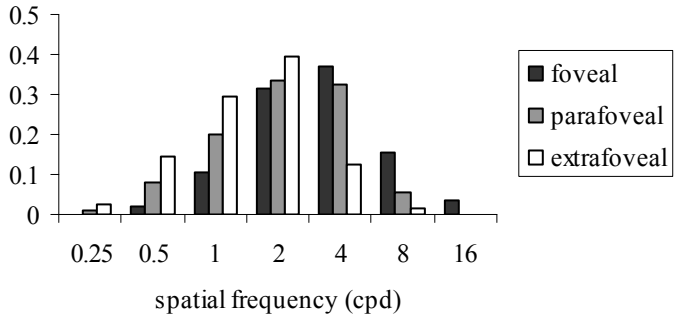

Figure 3.29: Estimated relative distributions for spatial frequency filters at three eccentricities, foveal (0° to 1.5°), parafoveal (3° to 5°), and extrafoveal (7° to 8.6°), based on data from DeValois & DeValois (1988).

Table 3.6: Distribution of Filters in Filter Set as a Function of Eccentricity

filter	*peak freq* (cpd)	*foveal units*	*parafoveal units*	*extrafoveal units*
1	.50	1	2	3
2	1.0	2	4	6
3	2.0	6	7	8
4	4.0	7	6	3
5	8.0	3	1	0
6	16.0	1	0	0

In the absence of evidence that the increase in receptive field size with increasing eccentricity differentially affects the magnocellular and parvocellular systems, it is reasonable to assume that the relative contributions of the two pathways to the spatial filters track with the shift in filters to lower frequencies. Thus, the contribution ratios would shift about a half octave lower as eccentricity increases from the foveal region to the parafoveal region, and again from the parafoveal region to the extrafoveal region. However, the decrease in the P to M cell ratio with eccentricity (see Section 2.5) suggests that the parvocellular contribution to filter activity at the parafoveal eccentricity is approximately half that at the foveal eccentricity. Similarly, the parvocellular contribution at the extrafoveal eccentricity is approximately one third that at the foveal eccentricity. If the relative contributions of the magnocellular and parvocellular pathways to filter activity used in the earlier simulations are assumed for the foveal region, then the shift coupled with the decrease in parvocellular contribution with increasing eccentricity yields the estimates for filter contributions in the parafoveal and extrafoveal regions shown in Table 3.7. These filter contribution estimates are used in the simulations.

Table 3.7: Relative Contributions of Magno (M) and Parvo (P) Pathways to Filter Activity as a Function of Eccentricity

filter	*f* (cpd)	*foveal*		*parafoveal*		*extrafoveal*	
		c^M	c^P	c^M	c^P	c^M	c^P
1	.50	.50	.50	.63	.37	.67	.33
2	1.0	.40	.60	.52	.48	.57	.43
3	2.0	.30	.70	.40	.60	.43	.57
4	4.0	.20	.80	.26	.74	.25	.75
5	8.0	.10	.90	.09	.91	-	-
6	16.0	0.	1.0	-	-	-	-

The simulations were run using input frequencies of .25, .5, 1, 2, 4, 8, and 16 cpd. The functional lateralization that developed at each eccentricity for the range of frequencies used in the Christman et al. (1991) experiment is shown in Figure 3.30. Parafoveal and extrafoveal ranges are restricted to .5 through 4 cpd because activation levels at 8 cpd were too low at these eccentricities to provide meaningful lateralization results. The simulation results indicate that spatial frequencies in the range of .5 to approximately 1.5 are consistently right-lateralized, while those in the range of approximately 2.5 to 8 are consistently left-lateralized across the three eccentricities. On the other hand, frequencies in the range of 1.5 to 2.5 cpd appear to shift from right to left lateralization as

eccentricity increases. This change in the lateralization of frequencies near 2 cpd suggests that the relative frequency effect observed in Christman et al. (1991) might be explained in terms of the allocation of spatial attention to more or less eccentric regions of the stimulus. This possibility is examined in Section 3.4.2

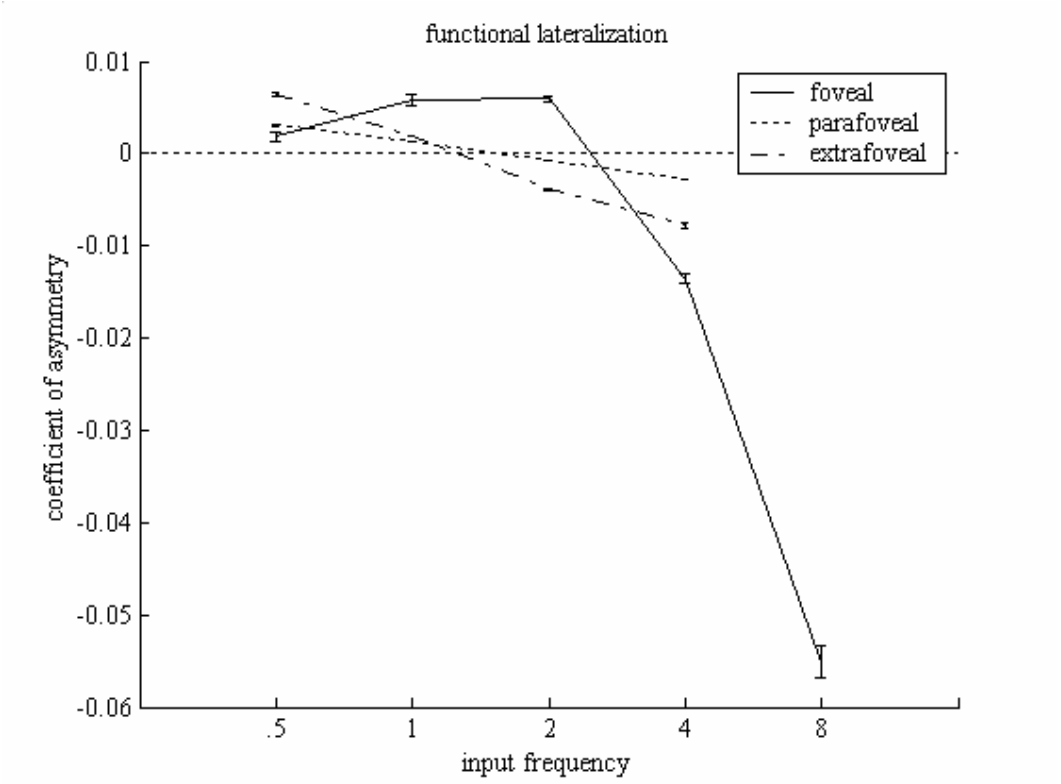

Figure 3.30: The variation of functional lateralization with eccentricity. Foveal represents approximately 0° to 1.5°, parafoveal 3° to 5°, and extrafoveal 7° to 8.6°.

Although not shown in Figure 3.30, simulation results for the foveal condition exhibited left lateralization for an input frequency of .25 cpd and right lateralization for an input frequency of 16 cpd. This result suggests that the

downward trend in lateralization predicted at the low and high frequency extremes could culminate in a reversal of lateralization direction.

3.4 Additional Analysis and Interpretation of Simulation Results

3.4.1 Hemispheric-Visual Pathway Bias

As mentioned in the discussion of the baseline results (Section 3.3.1), the pattern of structural asymmetry that emerges in these simulations suggests that the right hemisphere may develop a bias toward the output of the magnocellular pathway, while the left hemisphere develops a bias toward the output of the parvocellular pathway. This possibility can be examined by computing the contribution of visual pathway $X \in \{M, P\}$ to the total of the connection weights from the filter layer to the development layer in hemisphere $H \in \{R, L\}$ as:

$$W^{XH} = \sum_{j}^{F} c_j^X W_j^H \tag{3.16}$$

where W_j^H is given by Equation 3.12. A coefficient of asymmetry based on this metric can then be computed for both the magnocellular and parvocellular pathways.

The results, which are based on the simulations for the unequal filter distribution presented in Section 3.3.4, indicate that the expected biases are present (see Figure 3.31). However, they are small in comparison to the structural asymmetries associated with the low and high frequency filters (see Figure 3.25). This is understandable given that both the magnocellular and the parvocellular

pathways contribute to both low and high frequency filters, albeit unequally. Thus, although differences in the maturation of the two visual pathways drive the asymmetric development, the resulting asymmetry exhibits more of a hemispheric bias toward the outputs of the low and the high frequency filters than toward the outputs of a particular visual pathway.

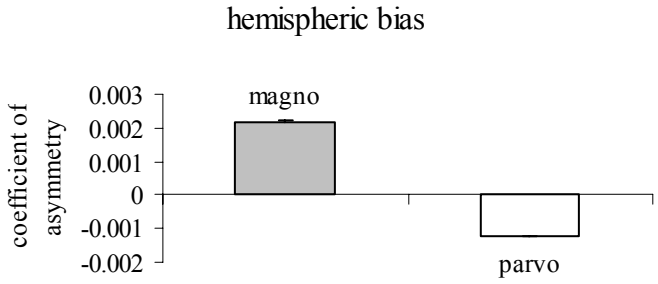

Figure 3.31: Total weights from the filter layer to the development layer exhibit a right hemisphere bias toward the output of the magnocellular system and a left hemisphere bias toward the output of the parvocellular system (based on the simulations for the unequal filter distributions discussed in Section 3.3.4).

3.4.2 The Neural Basis of the Relative Frequency Lateralization Effect

The results of the Christman et al. (1991) experiments suggest that the processing of the 2 cpd frequency is right lateralized in the high frequency condition and left lateralized in the low frequency condition. The simulations of lateralized development as a function of eccentricity (see Section 3.3.5) predict that the direction of processing lateralization for spatial frequencies around 2 cpd shifts from right at central eccentricities to left at eccentricities beyond about 5°.

Thus, the predicted eccentricity-dependent shift in lateralization has the potential to explain the observed relative frequency effect if eccentricity somehow factors into the processing of the stimulus in a way that depends on frequency condition.

In the Christman et al. (1991) experiments, the stimuli were presented at the same eccentricity for both frequency conditions. Therefore, the eccentricity-dependent effect could arise only if a) 2 cpd lateralization shifts within the range of eccentricity covered by the stimulus, and b) attention causes the processing of the stimulus to be dominated by a region of lesser eccentricity in the high frequency condition, and of greater eccentricity in the low frequency condition[15]. The stimulus used in the experiments extended from 3° to 9.8° along the horizontal meridian. Thus, it seems possible that the first of these two circumstances occurred, that is, the lateralization function resembled the foveal pattern for the innermost region and the extrafoveal pattern for the outermost region. The contention that the latter circumstance occurred as well is supported by empirical findings on attention as described below.

Substantial evidence supports the view that covert attention can be directed toward a selected location in visual space, enhancing the processing of information within the attended region while suppressing the processing of information in unattended locations (for reviews, see Cave & Bichot, 1999; Desimone & Duncan, 1995; Kastner & Ungerleider, 2000; Mangun, 1995; Posner & Peterson, 1990). Based on such evidence, spatial attention has been

[15] This assumes that there were no differences in eye fixation between frequency conditions in the Christman experiments.

hypothesized to operate like a spotlight (Posner, Snyder, & Davidson, 1980) or a zoom lens (Eriksen & St. James, 1986; Eriksen & Yeh, 1985) that can be directed anywhere within the visual field and adjusted in size to suit the requirements of the task. Such models propose that limited attentional resources can be spread over a large region or concentrated on a small region of the visual field, with improvement in the processing of information within the region of concentration coming at the cost of diminished processing effectiveness outside of that region.

Neuroimaging studies using fMRI have found physiological correlates of spatial attention throughout the retinotopically-mapped visual processing areas including V1 (Brefcznski & DeYoe, 1999; Martinez et al., 1999; Sasaki et al., 2001; Somers, Dale, Seiffert, & Tootell, 1999; Tootell et al., 1998). The exact nature of attentional modulation is unknown, but the results of the study that collected ERP data in conjunction with fMRI data (Martinez, et al., 1999) indicate that the initial sensory input to V1 from the LGN is unaffected. The studies are consistent in concluding that attentional modulation increases as a function of level in the visual hierarchy with strong effects observed in V4 and weak effects in V1.

Studies based on single cell recording experiments in macaques also found that attentional modulation increases at each level in the visual hierarchy (Luck, Chelazzi, Hillyard, & Desimone, 1997; Moran & Desimone, 1985; Reynolds, Chelazzi, & Desimone, 1999), with the Reynolds study, in particular, providing insight as to the underlying cause. Specifically, this study found that attentional

modulation in the case of one attended and one unattended stimulus is greater when the location of the unattended stimulus falls within a cell's receptive field than outside of it. Because receptive field size increases with hierarchical level (Smith, Singh, Williams, & Greenlee, 2001), the simultaneous presence of stimuli in attended and unattended locations, and consequently the degree of attentional modulation, is likely to increase with hierarchical level. The Reynolds study also found that when two stimuli are both located within a cell's receptive field, the response is intermediate to the responses evoked by the stimuli presented individually. However, when attention is directed toward the location of one of the stimuli, cell response becomes more like its response to that individual stimulus (Moran & Desimone, 1985; Luck et al., 1997; Reynolds et al., 1999). These results are theoretically explained by the 'biased-competition' model (Duncan & Desimone, 1995; Reynolds et al., 1999). This model hypothesizes that the two populations of neurons activated by the two stimuli within the receptive field of the responding cell compete for representation by the cell, and that attention to location biases the competition in favor of the population representing that location.

The biased-competition model can be combined with information on receptive field size and areal cortical magnification to produce a theoretical model of the neural basis of the relative frequency lateralization effect observed in the Christman et al. (1991) experiments as follows. At an eccentricity of 5°, V4 cells have receptive field sizes of about 6° (in diameter) and V2 cells of about 2° to 4°

(Katsner & Ungerleider, 2000). Thus, a stimulus of diameter 6.8°, extending from eccentricity 3° to 9.8° along the horizontal meridian, should be contained within the receptive fields of some population of V4 cells. These V4 cells receive their input from V2 cells that can be divided into two equal populations based on the eccentricity of their receptive fields. One population represents the less eccentric (inner) region, the other the more eccentric (outer) region of the stimulus. Equality in the two V2 cell populations implies that the area of the outer region will exceed that of the inner region by roughly a factor of 3 due to the cortical magnification factor. Attention is then allocated to either the inner or the outer region (or spread to include the outer region at the expense of the inner region) causing the response of the V4 cells to become more reflective of the V2 population representing the attended location. Because the response to the 2 cpd frequency is right lateralized in the V2 population responding to the inner region and left lateralized in the V2 population responding to the outer region, the lateralization of the V4 response changes with the allocation of attention.

The model of the basis of the relative frequency effect just described is depicted in Figure 3.32, which illustrates the allocation of attention to the inner region of the stimulus within the receptive field of a V4 cell. Because V4 cell receptive fields are generally restricted to the upper or lower visual field, only the part of the stimulus falling in the upper visual field is shown. The model is consistent with the findings of psychophysical studies that examined attentional resolution (Nakayama & Mackeben, 1989; Intriligator & Cavanaugh, 2001).

These studies found that attentional resolution is much less than visual resolution, and like visual resolution, degrades with eccentricity but at a faster rate (Intriligator & Cavanaugh, 2001). Nevertheless, estimates of attentional resolution based on the Intriligator and Cavanaugh findings range from about .5° at an eccentricity of 3° to about 2° at an eccentricity of 9.8°, suggesting that attention can be focused on an inner region approximately 2° in size or an outer region approximately 4° in size as required by the model.

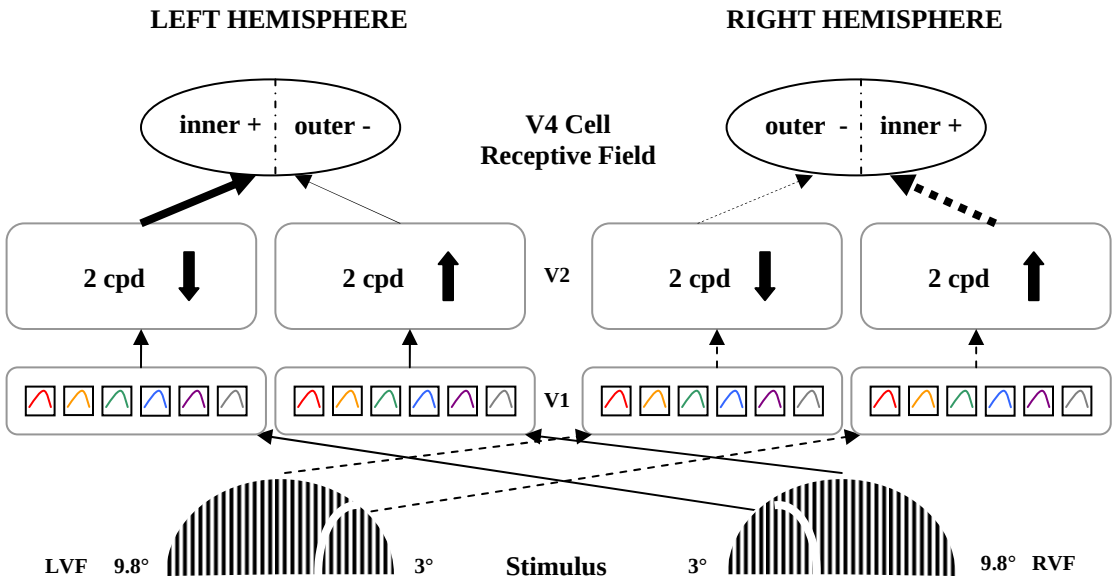

Figure 3.32: A theoretical model of the relative frequency lateralization effect. The stimulus is presented in either the upper left or the upper right visual fields. The LVF presentation is projected through the right hemisphere as designated by the dashed arrows, the RVF presentation through the left hemisphere as designated by the solid arrows. Inner and outer regions of the stimulus have equal representation in the V1 filters and the V2 processing units. Lateralization of the V2 response to the 2 cpd frequency differs for inner and outer regions as shown by the arrow indicators. In this depiction, attention is allocated to the inner region as indicated by the heavier arrows connecting the V2 inner region cell population to the V4 cell. Attention biases the response of the V4 cell in favor of the inner region as denoted by the + and the - in the parts of the receptive fields that are associated with the inner and outer regions, respectively.

The discussion, thus far, supports the assertion that attention could be focused on the inner region for the high frequency condition and the outer region for the low frequency condition in the Christman et al. (1991) experiments, but does not address why it would be. The proposed allocation of attentional resources can be explained in terms of task performance optimization. Assuming the V1 filter-to-V2 cell ratio remains constant across the visual field, the change in the relative distribution of filters with increasing eccentricity (see Figure 3.24) implies that more of the filters associated with the outer region will respond to low frequencies, while more of the filters associated with the inner region will respond to high frequencies. Thus, task performance should be enhanced by allocating attentional resources to the inner region in the high frequency condition and to the outer region in the low frequency condition.

Evidence that spatial attention can be adjusted to produce optimal performance on a task is found in experiments involving the identification of global and local targets (Kinchla, Solis-Machias, & Hoffmann, 1983; Robertson, Egly, Lamb, & Kerth, 1993) and in the detection of low contrast sinusoidal gratings (Davis, 1981; Davis & Graham, 1981). In the former experiments, targets appeared either at the global or at the local level, with a fixed probability assigned to each level for the duration of an experiment. When the probability of a global target was higher than that of a local target, identification of global targets was speeded up but identification of local targets was slowed down. When the

probability levels were reversed, the effects on performance were similarly reversed. In the latter experiments, gratings of various frequencies between 1 and 16 cpd appeared in one of two time intervals and were presented either in fixed blocks, in which one frequency appeared with 100% probability, or in mixed blocks, in which one frequency appeared with 95% probability (with the subject's prior knowledge). Performance on the selection of the correct time interval was maintained in the mixed block condition (relative to the corresponding fixed block condition) for the high probability frequency, but was impaired for the low probability frequencies. In the Christman et al. (1991) experiments, each frequency condition was maintained over a block of trials such that the probability that a response to a stimulus containing particular frequencies would be required was 100% within the block. Thus, in theory, spatial attention would be adjusted to optimize performance for each frequency condition.

3.5 Discussion

The results of these modeling experiments support the study hypothesis that differences in the time course of maturation of the magnocellular and parvocellular pathways, interacting with the asynchronous development of cortical areas involved in the learning of visual patterns, can produce lateralization in the processing of spatial frequencies. The lateralization effect expected in the case of earlier right hemisphere development, that is, a right hemisphere advantage in the processing of low spatial frequencies and a left

hemisphere advantage in the processing of high spatial frequencies, developed under every condition tested, including a variety of pathway contribution, developmental timing, and filter bandwidth and distribution conditions. The magnitude of the lateralization depended on the timing of hemispheric development but appeared to be less sensitive to the overall timing than to the difference in timing between the two hemispheres. The collective results of the timing condition tests strongly suggest that hemispheric differences in the timing of the critical period for development will lead to spatial frequency lateralization provided the critical periods occur during the time of rapid change in the relative maturity of the two visual pathways. The results also suggest that the lateralization effect generally increases as a function of a frequency's distance from the lateralization crossover point; however, the results obtained under the most biologically-valid conditions indicate that the effect may be reduced, or possibly reversed, at the low and high frequency extremes.

The functional lateralization observed in the simulation experiments was produced by the development of structural asymmetries in the strength of the connections from the various spatial frequency filters in V1 to the processing units in V2. The structural asymmetries incorporated a right hemisphere bias toward the output of the magnocellular pathway as well as a left hemisphere bias toward the output of the parvocellular pathway. However, the visual pathway-based asymmetry was small in comparison to the filter-based asymmetry despite being driven by visual pathway differences.

The results of this study provide support for the theories that propose a relationship between asynchronous development of the hemispheres and functional lateralization (Best, 1988; de Schonen & Mathivet, 1989; Hellige, 1993; Turkewitz, 1988). The potential validity of these theories was previously demonstrated in a modeling study that investigated the lateralization effects related to the timing of task learning and its interaction with the state of hemispheric plasticity (Howard & Reggia, 2004). In that study, differences in the timing of task learning periods, coupled with differences in the timing of plasticity for the two hemispheres was shown to produce oppositely directed lateralization for two distinct tasks. The timing of the task learning periods was controlled by changing the stimuli presented to the network over time. Thus, change external to the system, that is, in the stimuli presented by the environment, elicited the lateralized development. This study extends the earlier work by demonstrating that changes internal to the system that affect the input to asynchronously developing cortical areas can produce lateralized development in the absence of any change in the external stimuli.

The study results provide particularly strong support for the hypothesis of spatial frequency lateralization put forth by Hellige (1993). This hypothesis proposes that the combination of earlier right hemisphere development, coinciding with the impoverished state of visual input extant in the early post-natal months, and later left hemisphere development, coinciding with the availability of more comprehensive visual input, leads to the development of

lateralization in the processing of spatial frequencies. The study simulations bolster the plausibility of this theory by demonstrating that a specific scenario consistent with both the assumptions of the theory and current findings on the neurobiology of the visual system and its development produces the expected lateralization.

As previously mentioned, the study results indicate that the magnitude of lateralization initially increases as a function of distance from the lateralization crossover point, but then decreases toward the frequency extremes such that it is greatly reduced or reversed in direction. These findings imply that experiments investigating task-dependent lateralization in visual pattern processing may find no significant lateralization, or lateralization that is inconsistent with the spatial frequency hypothesis, if task performance is exceedingly dependent on the processing of very low or very high spatial frequencies. They also suggest a neural basis for the left lateralization that has been observed in experiments that examined flicker fusion thresholds (Parsons, Majumder, & Chadler, 1967), simultaneity judgments (Nicholls, 1994), and gap detection (Nicholls, 1994). Each of these investigations of asymmetry in temporal processing used flashing lights or screens as stimuli for which the power in the spatial dimension may have been concentrated at the low frequency extreme.

The study findings support the existence of a right hemisphere – magnocellular pathway bias and a left hemisphere – parvocellular pathway bias. However, the results suggest that such biases are small in comparison to filter-

based biases. This implies that for tasks that depend primarily on the processing of low or high frequency information, hemispheric differences in task performance may be evident, while hemispheric differences in the change in task performance resulting from manipulations affecting a particular visual pathway, may be too small to detect. Such a situation could account for the results obtained in the Roth and Hellige (1998) study. That study found that a coordinate task and a categorical task were differentially processed by the two hemispheres and, furthermore, were differentially impacted by manipulations of magnocellular and parvocellular processing. However, when the impact of a particular pathway manipulation on a particular task was compared across hemispheres, no difference was found.

This study models the development of asymmetry in the connections from V1 to V2. Established asymmetry in these connections could provide the basis for further asymmetric development in later developing connections within the visual hierarchy. These might include long-range connections within visual areas as well as feed-forward connections between areas. If so, lateralization effects could grow stronger and functionality more divergent with increasing level in the visual hierarchy.

The simulation results demonstrate that the spatial frequency lateralization function changes with increasing eccentricity, with the cross-over point moving to lower frequencies. Consequently, the direction of lateralization for frequencies near the cross-over point is predicted to change from right to left with increasing

eccentricity, consistent with the second study hypothesis. This result, together with relevant findings on spatial attention, permit the construction of a theoretical model that specifies the visual system structures and attentional operations involved in producing the relative frequency lateralization effect. The model supports the proposal that spatial attention in combination with eccentricity-dependent lateralization differences can produce lateralization effects that are consistent with the spatial frequency hypothesis as applied to both absolute and relative frequencies.

The proposal embodied in this theoretical model is consistent with the Double Filtering by Frequency (DFF) theory of lateralization (Ivry & Robertson, 1998; Robertson & Ivry, 2000) in attributing relative frequency lateralization to attentional effects, and can be viewed as an interpretation of the DFF theory in terms of the biology of the visual system (see Section 2.7). In this interpretation, spatial attention functions as the first filter, effectively selecting and amplifying the task-relevant range of frequencies, and the eccentricity-dependent hard-wired asymmetry functions as the second filter, effectively amplifying the relatively low frequencies in the right hemisphere and the relatively high frequencies in the left hemisphere. However, the DFF theory, as described by Ivry and Robertson and as implemented in their model, seems to suggest that attention can amplify the output of filters responding to a selected range of frequencies independently of visual space location, and that asymmetric hemispheric amplification is produced by dynamic asymmetric adjustments to the strength of feed-forward connections

from the selected filters. In contrast, the study proposal suggests that attention amplifies the output of filters responding to a selected location in visual space, and that asymmetric hemispheric amplification is produced by static asymmetries in the feed-forward connections from the filters responding to visual input at the selected location.

The hypothesis that attention amplifies the output of filters responding to a selected location in space rather than the output of filters responding to a selected range of frequencies is supported by an fMRI investigation of local and global attention (Sasaki et al., 2001). In this study, figures subtending a visual angle of 29.4° composed of smaller symbols subtending 2.4° were presented centrally. The subjects maintained fixation on the center of the figure while discriminating either the global feature or the local feature of the stimulus in separate blocks of trials. Attention to the local feature resulted in greater activity within the representation of the central 1.2° throughout the various retinotopic maps. In contrast, attention to the global feature produced greater activity in the representations of more peripheral eccentricities extending to about 15°. These results suggest that local and global attention effects are mediated by the allocation of spatial attention to locations of optimal size and eccentricity for task performance.

A notable alternative to the theory on the relative frequency lateralization effect developed in this investigation is the hypothesis that the effect arises from asymmetric channel interference (Christman, 1997). This hypothesis proposes that, for compound stimuli, low frequency interference with high frequency

processing is greater in the right hemisphere, while high frequency interference with the processing of low frequencies is greater in the left hemisphere, in accordance with the spatial frequency hypothesis and the results of the Kitterle et al. (1993) study. Thus, the processing of a particular frequency in a compound stimulus such as the ones used in the Christman et al. (1991) study could be differentially affected depending on its spectral position relative to the other frequencies in the stimulus. However, channel interference would affect not only the processing of an added component but that of the base components as well, a complication that does not appear to be considered by this hypothesis. In any case, the channel interference hypothesis is consistent with the hard-wired asymmetry proposed in this study as the basis of spatial frequency lateralization. Furthermore, the study proposal on the basis of the relative frequency effect and the channel interference hypothesis are not mutually exclusive. It is possible that both spatial attention and channel interference are involved in producing the relative frequency lateralization effect.

Another possible explanation for the relative frequency effect observed in the Christman et al. (1991) study depends on neither attention nor channel interference but simply on the proposed hard-wired asymmetries. The explanation proceeds as follows. The low frequency base components not only activate 0.5 and 1 cpd filters but also produce some activation in 2 cpd filters. Similarly, the high frequency base components not only activate the 4 and 8 cpd components but also produce some activation in 2 cpd filters. Because the added 2 cpd

component activates not only the 2 cpd filters but also the 1 and 4 cpd filters, the most effective information on which to base the identification of the three component stimulus may be provided by the 1 cpd filters in the high frequency condition, and the 4 cpd filters in the low frequency condition. If the processing of 1 cpd frequency information is right lateralized and the processing of 4 cpd frequency information is left lateralized, as found in the simulation experiments, then the addition of the 2 cpd component could produce oppositely directed lateralization effects for the low and high frequency conditions.

The alternative explanations for the relative frequency lateralization effect just discussed imply that attentional processes may not be involved at all. Additional evidence on the involvement of attention could be provided by a repetition of the Christman et al. (1991) experiment with a condition that mixed the presentation of low and high frequencies within a block. It would be interesting to see what lateralization effects are produced under such a mixed frequency condition.

The significance of the research presented in this chapter is attributable mainly to its simulation of an empirically-observed functional lateralization using a model grounded in the relevant neurobiology. The explicit, albeit substantially simplified, representation of the elements of visual system development and processing proposed to underlie the lateralized development enhances the credibility of the study results. These results demonstrate that lateralization in spatial frequency processing can arise from an interaction between developmental

events affecting the initial processing of a visual stimulus and the (even slightly) asynchronous development of cortical areas receiving the output of the initial processing. The success of this demonstration evokes the intriguing possibility that lateralization effects observed in other sensory systems might be linked to similar developmental events specific to those systems. Furthermore, it advances the notion that the developmental paradigm exemplified by the model, that is, multiple neural systems with differing maturational time courses supplying input to asynchronously developing cortical areas, might underlie, or significantly contribute to, the development of a variety of lateralization phenomena. This notion is further supported by evidence that asynchronous maturation of homologous regions occurs repeatedly throughout the course of cortical development during the first twenty years (Thatcher, 1992; Thatcher, Walker, & Giudice, 1987).

Chapter 4

The Basis of Electrophysiological Frequency Lateralization Effects

The modeling experiments of the previous chapter predicted the development of hard-wired asymmetry that can account for the results of psychophysical experiments in which low spatial frequencies were processed faster by the right hemisphere and high spatial frequencies were processed faster by the left hemisphere. Analysis of the hard-wired asymmetry revealed a right hemisphere bias toward the output of the magnocellular pathway and a left hemisphere bias toward the output of the parvocellular pathway. Because the magnocellular pathway is sensitive to high temporal frequencies and the parvocellular pathway to low temporal frequencies, such a bias would be consistent with right lateralization in the processing of high temporal frequencies and left lateralization in the processing of low temporal frequencies. However, electrophysiological experiments that investigated lateralization as a function of temporal, as well as spatial, frequency found the opposite lateralization effect (Rebai et al., 1986, 1989). Specifically, the processing of low temporal frequencies appeared to be right lateralized while that of high temporal frequencies appeared to be left lateralized. Furthermore, temporal frequency

rather than spatial frequency appeared to be the dominant factor underlying lateralization effects. Thus, the findings of the electrophysiological experiments seem to be at odds with the existence of the hard-wired asymmetry predicted by the development model. The research reported in the present chapter offers a resolution to this apparent conflict.

This chapter develops the hypothesis that the frequency lateralization effects observed in the visual evoked potential (VEP) data obtained in the experiments of Rebai and colleagues (1986, 1989, 1993, 1997, 1998) are caused primarily by hemispheric asymmetry in the anatomy, rather than in the processing, of the visual cortex. The potential validity of the hypothesis is examined using a computational model of the VEP wave generated in response to a grating stimulus of a particular spatial and temporal frequency. The first section of the chapter provides background on the VEP and reviews the findings of the Rebai experiments. In addition, findings concerning anatomical asymmetry in the visual cortex and the location of VEP sources are presented and discussed. The next section describes the design of the VEP computational model and the analytical methods that are used in the investigation of the study hypothesis. This is followed by a section that presents the results of specific model implementations. First, the model is used to demonstrate the potential relationship between anatomical asymmetry effects and lateralization in VEP component latency and amplitude measurements. Next, the effects of variation in model parameter values are examined and values are identified that yield results similar

to those observed empirically. Finally, asymmetry in the model parameter values is used to represent conditions consistent with the study hypothesis, and the model results are compared with experimental data. The concluding section of the chapter summarizes the study findings and discusses additional experimental findings that are explained by or that support the study conclusions.

4.1 Background

4.1.1 The Visual Evoked Potential

A visual evoked potential (VEP) is the electric potential generated by the flow of current across the neural membrane in response to a visual event (for in-depth discussions on the evoked potential, see Kutas & Dale, 1997; Rugg & Coles, 1995; Zani & Proverbio, 2003). In the cortex, current flow in the apical dendrites of a pyramidal cell in response to a stimulus creates a small electrical dipole. Because patches of cortical tissue contain spatially-aligned and synchronously activated cells, the potential fields generated by the individual dipoles within a patch summate to create fluctuations in electrical potential large enough to be measured at the scalp. The combined effect can be approximated by a single equivalent dipole located in the middle of the patch.

An equivalent dipole generates a change in potential in response to the presentation (or phase reversal) of a particular stimulus that has a characteristic time-course with the peak amplitude occurring reliably close to a specific latency. Because the propagation of electric potential field is effectively instantaneous, the

time-course of the change in potential generated by a dipole is invariant across electrode locations. In contrast, the magnitude and direction of the change in potential varies with the dipole's distance and orientation relative to electrode position. Consequently, the contribution of a dipole source to the total electric field potential varies by electrode location. The evoked potentials generated by responding dipoles add linearly to produce a change in the electrical potential as a function of time (as measured at a particular location) that appears as a *transient* wave having prominent positive and negative peaks. These peaks, referred to as VEP components, are usually designated by polarity (P for positive, N for negative) and either order in the wave (e.g., P1 for first positive, N1 for first negative, etc.) or latency (e.g., P100 for a positive peak occurring about 100 ms after stimulus presentation). In contrast to the transient wave produced by a single presentation or phase reversal of a stimulus, repeated presentations or phase reversals generate a *steady-state* VEP wave having a frequency equal to the presentation or reversal rate[16]. For steady-state waves, individual wave components are discernible only at low temporal frequencies.

VEP waves generated in response to a particular visual stimulus have distinctive component sequences at specific electrode locations. Those generated at occipital-parietal electrode locations in response to patterned stimuli are

[16] The reversal rate is twice the temporal frequency of a phase-reversed stimulus.

characterized by a dominant N1-P1-N2 wave complex[17] (Blumhardt, Barrett, Halliday, & Kriss, 1989; Jeffreys & Axford, 1972; Onofrj, Fulgente, Thomas, & Curatola, 1995). The latency and amplitude of these components vary with subject, location of measurement, and stimulus characteristics such as size, visual field location, spatial frequency, and presentation mode (pattern onset or pattern reversal). For pattern reversal stimuli, peak latencies are typically in the range of 70-100 ms for N1, 90-130 ms for P1, 140-180 ms for N2 (Blumhardt et al., 1989; Onofrj et al., 1995). The N1 component is most evident at ventro-medial occipital sites (Martínez, Di Russo, Anllo-Vento, & Hillyard, 2001), while the P1 component is most prominent at lateral occipital sites (Baas, Kenemans, & Mangun, 2002; Kenemans, Baas, Mangun, Lijffjt, & Verbaten, 2000; Martínez et al., 2001; Proverbio, Zani, & Avella, 1996; Zani & Proverbio, 1995). The N2 component is quite evident at all occipital-parietal locations (Di Russo, Martinez, Sereno, Pitzalis, & Hillyard, 2001).

4.1.2 The Rebai Experiments

The electrophysiological investigations of lateralization in frequency processing considered in this chapter (Rebai et al., 1986, 1989, 1993, 1997, 1998) are summarized below. As in the psychophysical experiments, the stimuli used in these experiments consist of sinusoidal gratings of specified spatial frequency.

[17] A number of different and, sometimes, conflicting labels are used to refer to these components throughout the literature. For example, N1 and N2 are sometimes referred to as C1 and N1, respectively.

Each of these investigations compares VEP measurements made at mirror locations over lateral occipital sites in the two hemispheres[18] for evidence of hemispheric asymmetry in frequency processing (see Figure 4.1). In each case, the interpretation of results assumes that lateralization effects are attributable solely to actual hemispheric differences in processing. Hence, shorter latencies or larger amplitudes in the VEP measurements for a hemisphere are interpreted as evidence of superior performance in the neural processing of the visual stimulus.

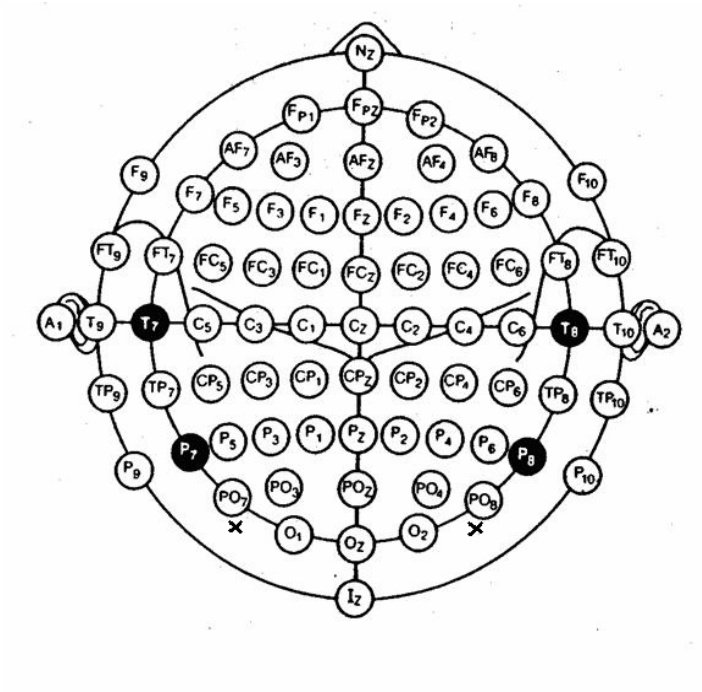

Figure 4.1: A montage of the standard electrode positions based on Sharbrough et al., 1991. The **X** marks shown a bit below and slightly medial to the PO_7 and PO_8 positions indicate the approximate location of the electrodes in the Rebai experiments.

[18] The electrodes yielding lateralized results were placed 5cm from the midline position located 2.5 cm (2 cm in the 1986 study) above the inion. These placements correspond most closely to standard sites PO_7 and PO_8 (Sharbrough et al., 1991). Although the earlier Rebai et al. (1986, 1989, 1993) studies characterize this electrode placement as located over the temporal region of the cortex, it is more accurately described as located over the lateral region of the occipital lobe near the parietal-occipital border (Homan, Herman, & Purdy, 1987).

Rebai et al. (1986) examined the lateralization effects of temporal frequency for a single spatial frequency, namely 3 cpd (cycles per degree). Using sinusoidal gratings phase-reversed over a range of temporal frequencies (4 to 18 Hz) as input and presented in the central visual field (6.25° by 5°), this study measured the steady-state potential in a group of right-handed subjects. A Fourier analysis of the steady-state VEP wave generated at each temporal frequency was performed to find the amplitude of the second harmonic[19] component. These amplitudes were normalized across the frequency range for each subject and then averaged to produce a mean temporal frequency amplitude function for each hemisphere.

As shown in Figure 4.2, the mean data indicated that the amplitude of the second harmonic had a tendency to be greater in the right hemisphere (RH) for low temporal frequencies (< 7 Hz) and was significantly greater in the left hemisphere (LH) for high temporal frequencies (> 7 Hz). Furthermore, the amplitude functions were in the shape of an inverted U with peaks at 6 Hz in the right hemisphere and 8 Hz in the left hemisphere. Thus, this investigation found a lateralization effect tied to the temporal frequency of the stimulus, with right lateralization observed at low temporal frequencies, and left lateralization observed at high temporal frequencies.

[19] For a phase-reversed stimulus, the fundamental frequency is equal to the temporal frequency f and the second harmonic of the fundamental frequency is equal to the reversal rate $2f$. The largest amplitude is found at the second harmonic.

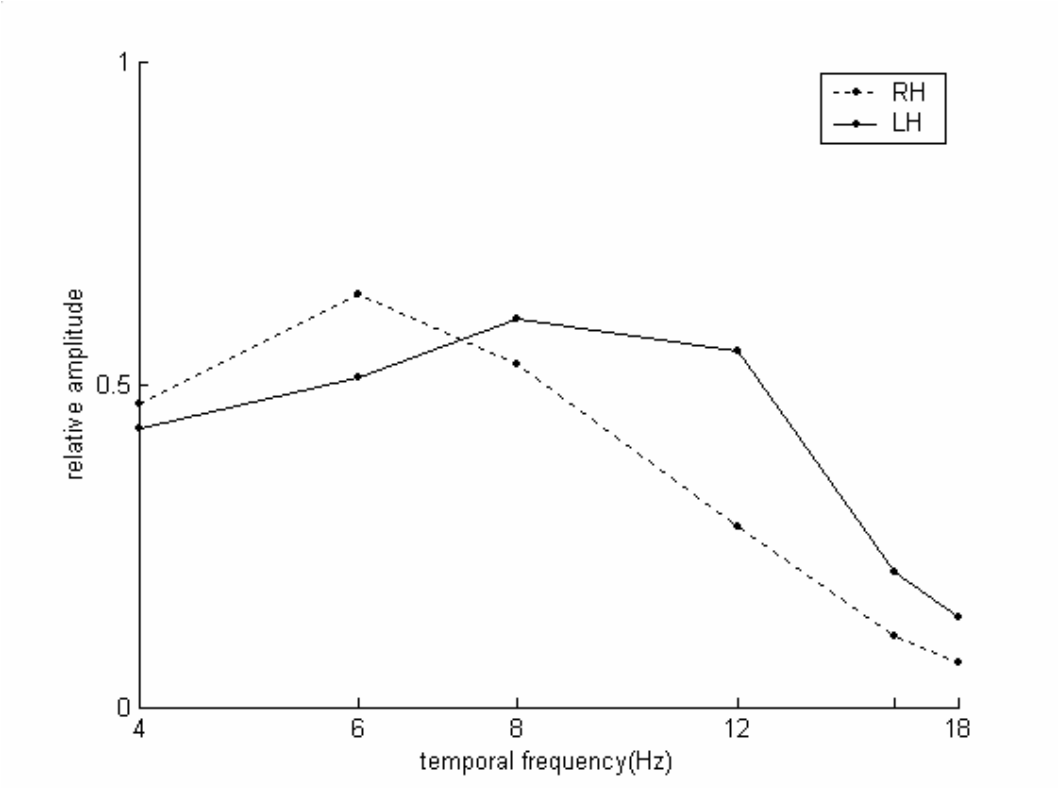

Figure 4.2: The temporal frequency amplitude functions based on the mean of individual normalized amplitude functions as measured in the right (RH) and left (LH) hemispheres. (Data from Rebai et al., 1986.)

Rebai et al. (1989) examined lateralization as a function of spatial frequency for both low (4 Hz) and high (12 Hz) temporal frequency phase-reversed gratings in groups of both right-handed and left-handed subjects. The input stimuli covered a range of spatial frequencies (.5 to 16 cpd), and were presented in the central visual field (6.25° by 5°). For spatial frequencies in the range of 3 to12 cpd, the right-handed group exhibited the same lateralization pattern observed in the earlier investigation. Specifically, the amplitude of the second harmonic component in the spectrum of the steady-state wave was

significantly larger in the right hemisphere at the low (4 Hz) temporal frequency and significantly larger in the left hemisphere at the high (12 Hz) temporal frequency (see Figure 4.3).

For the left-handed group, a different pattern of lateralization was observed characterized by a significant interaction between spatial and temporal frequency. At the low (4Hz) temporal frequency, mean amplitudes were greater in the right hemisphere for spatial frequencies less than 7cpd and greater in the left hemisphere for frequencies greater than 7 cpd. For the high (12 Hz) temporal frequency, the lateralization pattern appeared to be reversed, at least for high spatial frequencies, but was far less evident (see Figure 4.3).

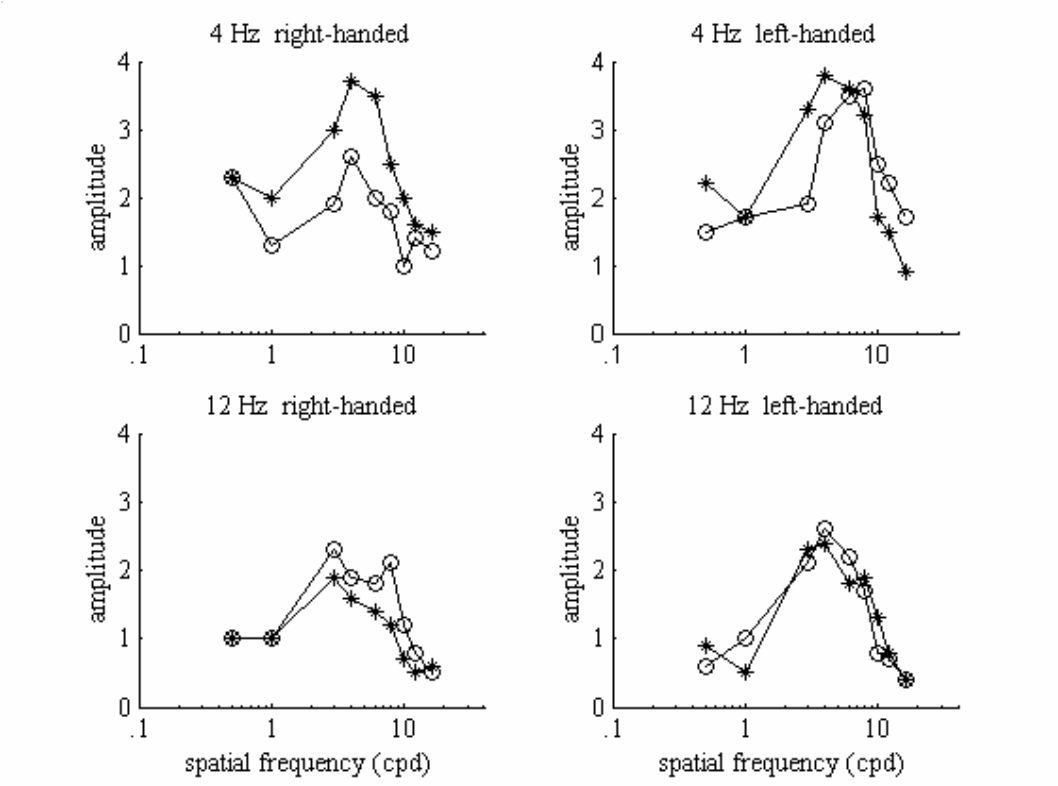

Figure 4.3: The amplitude of the second harmonic of the VEP wave generated in response to stimuli of temporal frequencies 4 and 12 Hz for spatial frequencies of 0.5, 1, 3, 4, 6, 8, 10, 12, and 16 cpd. The data points represent the mean of individual amplitude functions as measured in the right (RH) and left (LH) hemispheres in a group of right-handed and a group of left-handed subjects. (Copied from Rebai et al., 1989, copyright 1989, with permission from Elsevier.)

This study concludes that a) there is hemispheric processing asymmetry related to the spatial and temporal frequency of the input, most likely associated with the integration of sensory information, and b) temporal frequency rather than spatial frequency is the key factor underlying the asymmetry. The study notes that, in right-handers, right hemisphere response is very sensitive to spatial and temporal frequency while left hemisphere response is comparatively steady across all frequencies. Furthermore, the study speculates that, in right-handers, the

greater right hemisphere response to the low temporal frequency reflects a greater sensitivity to the outputs of the sustained (parvocellular) visual system, while the greater left hemisphere response to the high temporal frequency reflects a greater sensitivity to the outputs of the transient (magnocellular) visual system.

Further support for this hypothesis of RH-parvocellular, LH-magnocellular sensitivity in right-handers was obtained in Rebai et al. (1993). Using sinusoidal gratings, this investigation compared VEP amplitudes across spatial frequencies obtained for ON-OFF presentation (ONSET phase only) to those obtained for phase-reversal presentation at a low temporal frequency (1Hz). The ON-OFF mode of stimulation (also known as pattern onset mode) includes a purely spatial component that the reversal mode does not, and therefore was expected to evoke a greater contribution from the sustained visual system. Consistent with the hypothesis of superior right hemisphere sensitivity to sustained system output, right hemisphere VEP amplitudes observed for the ON-OFF mode were significantly greater than those observed for the reversal mode at medium-to-high spatial frequencies (> 2 cpd), while left hemisphere VEP amplitudes were not significantly different for the two modes of stimulation. As was observed in the earlier investigations, the right hemisphere exhibited a high degree of sensitivity to the spatial and temporal frequency of the stimulus, whereas the left hemisphere response was relatively stable across all frequencies.

Using the same experimental methods, Rebai et al. (1998) confirmed the findings on VEP amplitudes for ON-OFF stimuli while also showing that the

latency of the first positive VEP component was shorter in the right hemisphere for medium-to-high spatial frequencies. The latency results were interpreted as being consistent with the amplitude data as the more sensitive hemisphere was expected to have the faster and stronger response to the stimulus. Thus, the results of this investigation were interpreted as supporting the RH-parvocellular, LH-magnocellular hypothesis and the theory of right hemisphere specialization for the low level processing of spatial frequency information in right-handers.

The results of Rebai et al. (1989) suggested the existence of a relationship between handedness and VEP lateralization effects. This relationship was further explored in Rebai et al. (1997). This investigation used essentially the same experimental methods as Rebai et al. (1993) but employed square rather than sinusoidal gratings (2, 4, 6, 8, and 10 cpd) and limited stimulation to the ON-OFF mode. The experiments were performed on four sets of subjects grouped on the basis of two factors: subject handedness (right or left) and familial left-handedness (present or absent). Each of the four sets exhibited a unique pattern of lateralization. The hemispheric asymmetry observed for the combined group of right-handers was consistent with Rebai et al. (1989). Specifically, the right hemisphere exhibited sensitivity to spatial frequency with an amplitude curve resembling the contrast sensitivity function (see Section 2.2), while amplitudes in the left hemisphere displayed relatively little variation as a function of spatial frequency. Lateralization was significant in the medium-to-high spatial frequency range (> 2 cpd). Asymmetry was not significant in the combined group of left-

handers, however, a large difference in amplitude in favor of the right hemisphere was observed at the low frequency (2 cpd), consistent with Rebai et al. (1989). In addition, for the left-handers with familial left-handedness, both the right and left hemispheres exhibited sensitivity to spatial frequency similar to the pattern observed for left-handers in Rebai et al. (1989).

4.1.3 Anatomical Asymmetry in the Visual Cortex

The implicit assumption on which the electrophysiological experiments just discussed are based is that the two hemispheres are essentially symmetric in their anatomy such that the set of active dipoles contributing to the VEP comprises bilateral dipole pairs that mirror one another in both location and orientation. This assumption is necessary to the interpretation of asymmetries in VEP measurements made at mirror electrode locations as actual hemispheric differences in processing efficiency. However, research on anatomical asymmetries has identified both morphological and topological differences in the occipital lobes that could conceivably result in significant asymmetries in dipole pairs in the visual cortex, especially near the occipital poles. Furthermore, some patterns of morphological asymmetry have been found to correlate with handedness.

The most salient morphological asymmetry is the protrusion of one of the occipital poles termed occipital petalia (see Figure 4.4). This condition often occurs in conjunction with a more medial positioning of the protruding pole. Both

computed tomography and MRI studies have found that left occipital petalia occurs more commonly than right occipital petalia or occipital pole symmetry (Chui & Damasio, 1980; LeMay, 1976, 1977; LeMay & Kido, 1978; Zilles et al., 1996). CT and MRI studies have also found asymmetry in the width of the occipital lobes (Chui & Damasio, 1980; Kertesz, Black, Polk, & Howell, 1986; LeMay, 1976, 1977; LeMay & Kido, 1978). In addition, the left occipital pole has been found to have a more medial and caudal position in stereotaxic space[20] in comparison to the right occipital pole (Amunts, Malikovic, Mohlberg, Schormann, & Zilles, 2000).

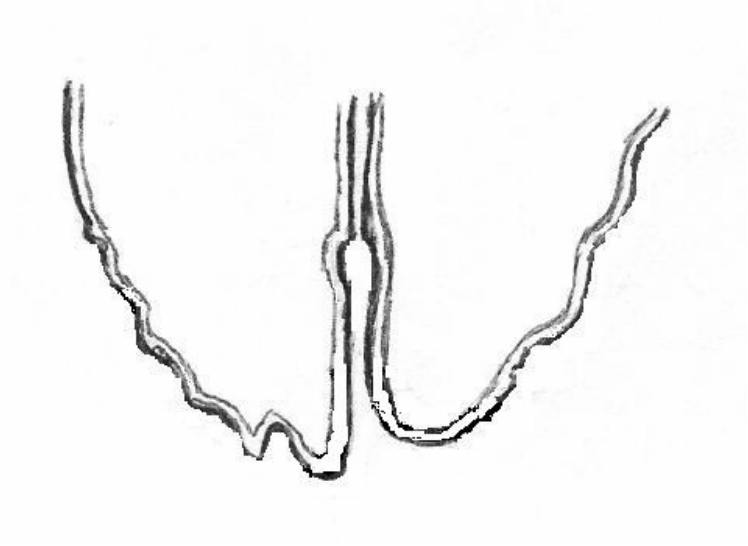

Figure 4.4: An example of left occipital petalia as characterized by the protrusion of the left occipital pole.

Most of the cited anatomical investigations found a relationship between the distribution patterns of occipital asymmetries and handedness. In the case of

[20] That is, relative to an external three-dimensional coordinate system.

occipital petalia, left lateralization was found to dominate the frequency distribution for groups of right-handers, while the distribution for groups of left-handers was characterized by a greater balance in the occurrences of left lateralization, right lateralization, and symmetry (Chui & Damasio, 1980; LeMay, 1976, 1977; LeMay & Kido, 1978; Zilles et al., 1996). In addition, some results suggested that the pattern of petalia observed in left-handers is associated with familial left-handedness (LeMay, 1977) or with female gender (Zilles et al., 1996). Findings on occipital width patterns are, for the most part, similar to those for petalia (Kertesz et al., 1986; LeMay, 1976, 1977; LeMay & Kido, 1978; but see also Chui & Damasio, 1980).

Measurement of parietal-occipital asymmetry in a group of right-handers based on a series of MRI-based coronal cuts confirmed the predominance of the left occipital pole found in the earlier studies, particularly in its ventral aspect (Myslobodsky, Glicksohn, Coppola, & Weinberger, 1991). This leftward asymmetry was found to diminish with rostral distance from the pole, eventually shifting to rightward asymmetry in the dorsal aspect. Morphological asymmetry was observed to be maximal near the occipital poles.

Significant topological variations in the visual cortex, which are both interindividual and interhemispheric in nature, include differences in the anterior (Rademacher, Caviness, Steinmetz, & Galaburda, 1993) and posterior (Rademacher, et al., 1993; Stensaas, Eddington, & Dobelle, 1974) extent of the primary visual cortex (V1). The latter appears as variation in the extension of V1

onto the occipital poles. Variation in V1 topology is accompanied by similar variation in the topology of the adjacent visual area V2 (Amunts et al., 2000). The degree to which topological variation is systematically lateralized, or correlated with handedness or morphological variation, is unknown.

4.1.4 The Dipole Sources of VEP Components

The findings discussed in the previous subsection support the possibility that anatomical asymmetry, particularly in the area of the occipital poles, contributes significantly to VEP asymmetry. Indeed, several studies that found hemispheric differences in the potentials evoked by right and left hemifield stimulation in response to patterned stimuli tentatively attributed the differences to this anatomical asymmetry (Abe & Kuroiwa, 1990; Blumhardt et al., 1989; Jeffreys & Axford, 1972; Kuroiwa, Celesia, & Tohgi, 1987). To determine whether such asymmetry can account for the Rebai results, it is necessary to identify, locate, and characterize the major dipoles that contribute to the VEP as measured at the electrode sites used in the Rebai experiments. With that objective in mind, this subsection summarizes relevant findings on the VEP components and their dipole sources.

The N1 component is minimally evident at lateral occipital sites such as those used in the Rebai experiments (Martínez, et al., 2001). VEP-based dipole modeling studies have consistently estimated the location of the N1 dipole source to be the medial occipital cortex in or near the calcarine fissure (Baas et al., 2002;

Di Russo, et al., 2001; Kenemans et al., 2000; Martínez, et al., 2001). These estimates are consistent with N1 dipole locations found using subdural electrodes (Arroyo, Lesser, Poon, Webber, & Gordon, 1997). The N1 component is most prominent for higher (4-8 cpd) spatial frequencies (Baas, et al., 2002; Kenemans, et al., 2000; Martínez, et al., 2001; Proverbio, et al., 1996; Zani & Proverbio, 1995). Studies aimed at characterizing the N1 component have found that, in comparison to the other components, N1 exhibits relatively greater spatial frequency sensitivity (Ellemberg, et al., 2001; Plant, Zimmern, & Durden, 1983; Zani & Proverbio, 1995), saturates at high contrast (Ellemberg et al, 2001; Vassilev, Stomonyakov, & Manahilov, 1994), and arises mainly from central field stimulation (Blumhardt et al., 1989). In addition, N1 was found to exhibit inverted polarity in the case of both upper (negative) and lower (positive) visual field stimulation and contralateral (positive) and ipsilateral (negative) visual field stimulation (Di Russo et al., 2001; Blumhardt et al., 1989; Jeffreys & Axford, 1972; Onofrj et al., 1995) consistent with the retinotopic organization of the primary visual cortex (V1). The collective evidence strongly supports the widely held view that N1 is generated by the dipole sources in the part of V1 that represents the center of the visual field, known to be located medially near the occipital poles. The medial location of the N1 dipoles implies that the contributions from the two hemispheres will largely cancel one another at lateral occipital sites consistent with the lack of N1 prominence at those sites.

The P1 component is prominent at lateral occipital sites (Baas et al., 2002; Kenemans et al., 2000; Martínez et al., 2001; Proverbio et al., 1996; Zani & Proverbio, 1995). The results of dipole modeling studies suggest that multiple sources having distinct latencies and locations contribute to P1. These include an early latency (~100-110 ms) source (Di Russo et al., 2001; Martínez et al., 2001), a mid-latency (~120 ms) source (Martínez et al., 2001), and a late latency (~135-145 ms) source (Di Russo et al., 2001; Kenemans et al., 2000). The early and late latency P1 sources are prominent for high spatial frequencies, while the mid-latency P1 source is prominent for low spatial frequencies. VEP-based localization estimates place the early latency P1 source in the lateral occipital cortex contralateral to the field of stimulation (Di Russo et al., 2001; Kenemans et al., 2000; Martínez et al., 2001) within V3/V3A (Di Russo et al., 2001). However, a study based on visual evoked magnetic field measurements (Brecelj, Kakigi, Koyama, & Hoshiyama, 1998) found location estimates for the early latency sources responding to central vision to include the occipital pole, the medial occipital cortex, the lateral occipital cortex, and the calcarine fissure. Consistent with these localization estimates, subdural recordings found numerous early P1 sources with latencies of 95 to 105 ms on the occipital pole and in medial and lateral locations near the pole (Arroyo et al., 1997). Martínez et al. (2001) locates the mid-latency P1 source in the lateral occipital cortex of the contralateral hemisphere, a finding that is supported by subdural recordings (Arroyo et al., 1997). Di Russo et al. (2001) locates the late latency P1 source in the ventro-

occipital cortex ipsilateral to the field of stimulation within area V4, while the Kenemans et al. (2000) investigation locates it medially near the occipital pole.

The N2 component is prominent at all occipital-parietal locations. The N2 is attributed to the combined contributions of multiple dipole sources (Di Russo et al., 2001); however, at lateral occipital sites, a source with latency ~ 148 ms appears to predominate. The location of this N2 source is estimated to be in the lateral occipital cortex near the early latency P1 source (Di Russo et al., 2001). Subdural recordings found a source with latency 158 ms in the lateral cortex near the occipital pole, as well as several sources with latencies ~ 143 ms located medially and at the occipital pole (Arroyo et al., 1997).

These findings suggest that occipital pole asymmetries have the potential to produce asymmetry in each of the main VEP components observed at lateral occipital sites. However, of the major dipole sources just discussed, the early latency P1 source seems the most likely to be significantly affected by anatomical asymmetries due to its heavy representation both on and around the occipital pole.

4.1.5 The Spatial Frequency Sensitivity of the VEP Components

As mentioned earlier, dipole response depends on the spatial frequency of the visual stimulus. In fact, spatial frequency affects both the latency and the amplitude of dipole response and these effects are reflected in the major VEP components. This section summarizes findings on the effect of spatial frequency on the latency and amplitude of the N1, P1 and N2 VEP components.

The relationship between latency and spatial frequency is the same for all components, that is, latency generally increases as a function of spatial frequency (Onofrj et al., 1995; Parker & Salzen, 1977; Plant et al., 1983). Latency increases in the range of 6-8ms/octave have been observed in the P1 component (measured at a mid-line occipital position) for phased-reversed sine gratings of spatial frequency greater than 2 cpd (Jakobsson & Johansson, 1992; Plant et al., 1983; Tobimatsu, Kurita-Tashima, Nakayama-Hiromatsu, & Kata, 1993). For frequencies less than 2 cpd, P1 latency appears to dip before beginning its steady climb with increasing spatial frequency. At least one investigator (Plant et al., 1983) has suggested that this is attributable to the combined effects of two separate P1 dipole sources that differ in latency and spatial frequency sensitivity. These hypothesized P1 sources would appear to correspond to the early latency P1 source, prominent at high spatial frequencies, and the mid-latency P1 source, prominent at low spatial frequencies. Although evidence suggests the rate of increase is not identical for all VEP components, the rate differences do not appear large enough to cause much change in relative component latencies as spatial frequency varies (Onofrj et al., 1995; Parker & Salzen, 1977).

In contrast, the relationship between amplitude and spatial frequency does differ significantly among VEP components. The spatial frequency sensitivity of a VEP component depends on the processing stage (as defined by visual areas V1, V2, etc.) and the visual field location (central or peripheral) of its origin. In general, cortical areas associated with earlier processing stages and more central

field locations exhibit greater sensitivity to spatial frequency, especially at the high end of the spectrum, than do areas associated with later processing stages and more peripheral field locations. Thus, components originating in the vicinity of the occipital pole, which is associated with early stage, central field processing, can be expected to exhibit a high degree of spatial frequency sensitivity.

Empirical data on VEP component amplitude variation as a function of spatial frequency, particularly in response to the type of stimuli used in the Rebai experiments (high contrast, phase-reversed sinusoidal grating stimuli, in the central visual field area of 6.25° by 5°), are limited. However, such data were obtained for both the N1 and P1 components in a study that employed circular stimuli of varying diameters including 5° and 10° (Plant et al., 1983) and for the P1 component in a study that employed a stimulus of 10.6° by 6.9° (Tobimatsu et al., 1993). In addition, data for the N1 component were obtained in a study that used an 18° by 18° stimulus while varying contrast up to a high of 90% (Ellemberg et al., 1993). Although in this case the stimulus extended well into the peripheral field, it is reasonable to assume that this extension has little effect on the N1 component, if the N1 source is located in the central visual field as is generally conjectured. Normalized amplitude functions based on the mean amplitudes for the N1 and P1 components generated in response to stimuli of 1 Hz temporal frequency are shown in Figures 4.5 and 4.6, respectively.

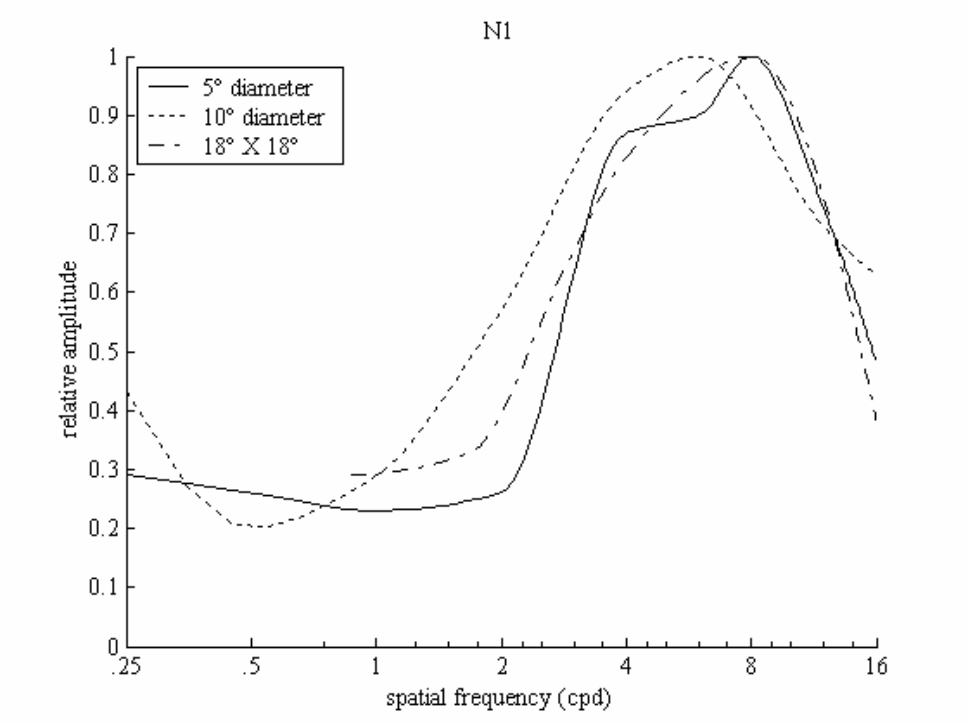

Figure 4.5: Normalized spatial frequency sensitivity functions for the N1 component, as measured at mid-line, for sinusoidal gratings presented in the central field. The functions corresponding to the 5° and 10° diameter stimuli are based on data from Plant et al. (1983). The function corresponding to the18° by 18° stimulus is based on data from Ellemberg et al. (1993). Normalization values are relative to a maximum sensitivity value of 1.

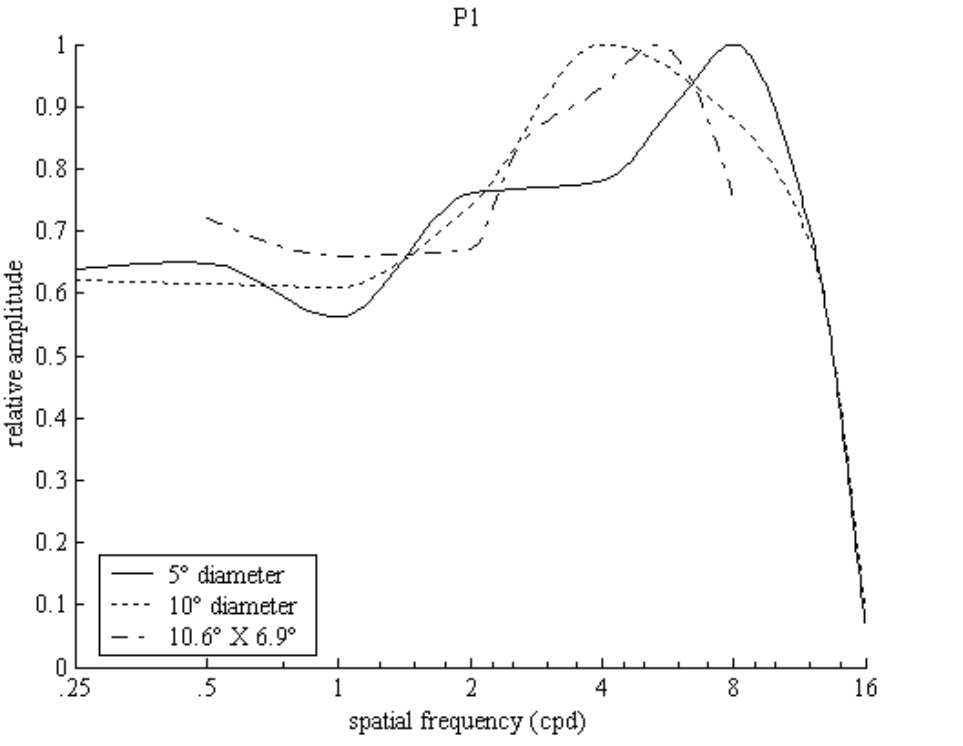

Figure 4.6: Normalized spatial frequency sensitivity functions for the P1 component, as measured at mid-line, for sinusoidal gratings presented in the central field. The functions corresponding to the 5° and 10° diameter stimuli are based on data from Plant et al. (1983). The function corresponding to the10.6° by 6.9° stimulus is based on data from Tobimatsu et al. (1993). Normalization values are relative to a maximum sensitivity value of 1.

In each of the experiments cited, the VEP was measured at a mid-line occipital location (either 2.5 cm or 5cm above the inion). Because the early latency P1 source is likely to dominate the P1 component for central field stimuli when measured at mid-line (in contrast to lateral) occipital locations, the frequency sensitivity functions determined in these experiments should be representative of early latency P1 dipole sensitivity, at least for frequencies of 2 cpd or greater. The leveling off of sensitivity attenuation below 2 cpd most likely

reflects the increased contribution of the mid-latency P1 dipole source at low spatial frequencies.

In addition to the findings on N1 and P1 just presented, the study by Plant et al. (1983) found that the VEP amplitude defined as N2-P2 was not sensitive to spatial frequency (for a circular stimulus with diameter 10°). The normalized sensitivity function for N2-P2 based on these finding is displayed in Figure 4.7. Given the lack of P2 component prominence for pattern reversal stimuli, this finding suggests that the N2 component may exhibit minimal spatial frequency sensitivity, although the relationship between N2 measured at mid-line and N2 measured at lateral sites is unknown.

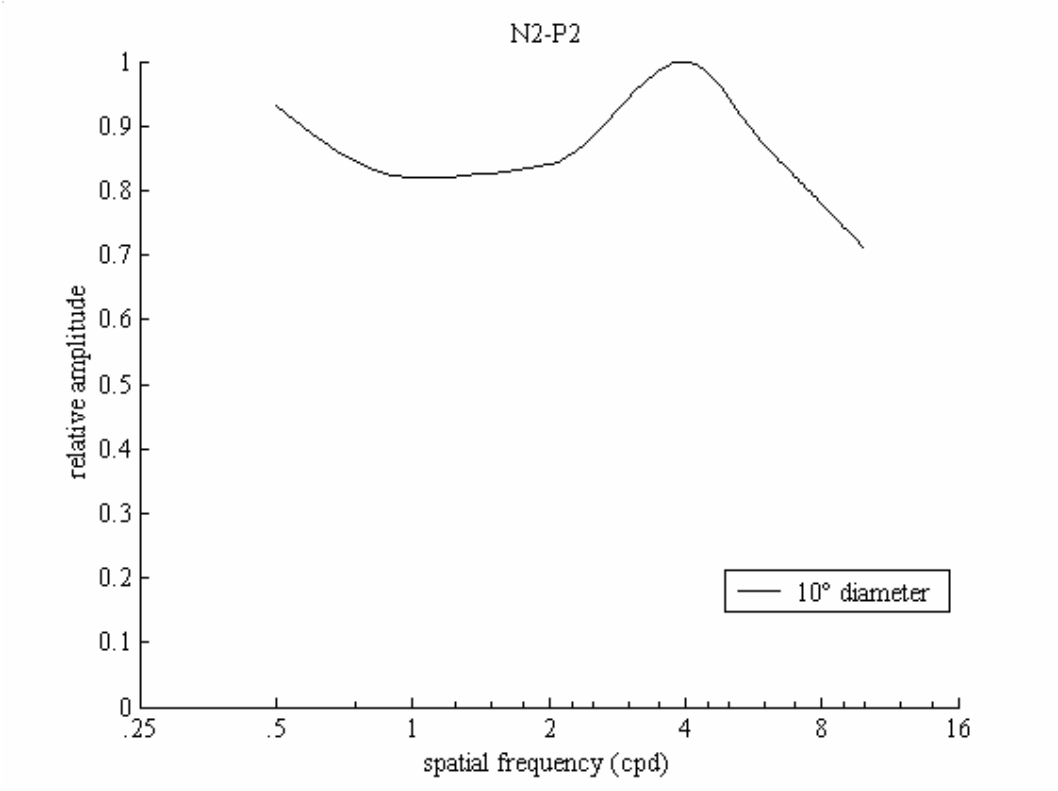

Figure 4.7: Normalized spatial frequency sensitivity function for N2-P2, as measured at mid-line, for sinusoidal gratings, 10° in diameter, presented in the central field. The function is based on data from Plant et al. (1983). Normalization values are relative to a maximum sensitivity value of 1.

4.2 Model Design and Analytical Methods

4.2.1 Overview

The investigation utilizes a general model of the dipole potential-VEP wave relationship. The model that assumes that the phase reversal of a grating stimulus activates a certain set of dipoles and that each activated dipole[21]

[21] Each dipole implicitly represents the combined contribution of a pair of dipole sources, that is, a dipole source in the right hemisphere and the corresponding dipole source in the left hemisphere.

produces a specified change in electric potential at an arbitrary electrode location.[22] Based on these assumptions, the model computes the transient VEP wave that would result (at that electrode location) from a single phase reversal and the steady state waves that would result from continuous phase reversals presented at various temporal frequencies. Thus, the model allows the effects that amplitude variations in the electric potential generated by individual dipoles would have on the transient and steady state waves to be examined.

As discussed in more detail in the design section (Section 4.2.3), the effect of dipole amplitude[23] variation on the steady-state wave can be determined by either of two methods. The first method requires the computation and Fourier analysis of a steady-state wave for every temporal frequency of interest. In contrast, the second method requires the computation and Fourier analysis of only the underlying transient wave. The analysis of modeling results presented in this chapter is based predominately on the latter method.

Ultimately, the model is used to demonstrate that hemispheric differences in steady state waves observed at lateral occipital electrode sites in the Rebai experiments (1986, 1989) can be largely explained by asymmetry in the amplitude of the potential produced by a particular dipole. This is accomplished by

[22] Note that the hypothetical change in potential produced by a dipole at an electrode location is specified rather than computed based dipole distance and orientation relative to electrode location. This approach is appropriate to the purpose of the model, which is the exploration of the effects that variation in the amplitude of the potential generated by a dipole has on resulting VEP waves.

[23] The term "dipole amplitude" is used throughout the document to refer to the amplitude of the electric potential generated by the dipole at an electrode location. Similarly, "dipole latency" refers to the latency of the peak potential generated by the dipole at an electrode location.

obtaining model results for each experimental condition of interest using two sets of hypothetical amplitude values for this dipole. One set represents amplitudes that are hypothesized to result at the lateral occipital electrode site in right hemisphere and the other, amplitudes that are hypothesized to result at the mirror site in left hemisphere.

4.2.2 Assumptions

As previously mentioned, the VEP wave model assumes that the phase reversal of a grating stimulus activates a certain set of dipoles and that each activated dipole produces a specified change in electric potential at an arbitrary electrode location. Consistent with the properties of electric dipoles discussed in Section 4.1.1, the model also assumes that:

1. Transient VEP waves represent the linear summation of the electric potentials produced (at a particular electrode location in response to a visual stimulus) by dipoles that differ in their amplitudes and latencies.

2. Steady-state VEP waves represent the linear summation of transient VEP waves generated in response to each presentation or reversal of the stimulus.

Use of the model to demonstrate the effects that hypothetical asymmetries in dipole potentials would have on the transient and steady state wave produced at mirror electrode locations further assumes that:

3. The amplitude of the change in electric potential generated by a dipole may differ at mirror electrode locations (due to anatomical asymmetries)[24] but time-course of the change in potential does not.

4. Any effect that temporal frequency has on dipole response is the same at mirror electrode locations.

Assumption 3 is consistent with the properties of electric dipoles discussed in Section 4.1.1. Assumption 4 is consistent with the study hypothesis that presumes dipole asymmetry reflects anatomical rather than processing asymmetry.

4.2.3 Design

The model computes the transient VEP wave generated at an arbitrary electrode as the sum of the electric potentials produced at that electrode by the set of dipoles activated by the stimulus (e.g., N1, early P1, late P1, and N2). Thus, the transient wave generated at electrode *x* is given by

[24] Again, amplitudes differences are not computed within the model. Rather, two sets of hypothesized amplitude values are used in separate model computations for mirror electrodes.

$$v^x(t, f_{sp}) = \sum_k^D d_k^x(t, f_{sp}), \text{ for } 0 \leq t \tag{4.1}$$

where $d_k^x(t, f_{sp})$ is the electric potential produced by dipole $k \in D$ at electrode x and time t for a stimulus of spatial frequency f_{sp}, and D is the set of all activated dipoles.

The model computes steady-state VEP waves as the sum of the transient waves generated in response to the phase reversals. Specifically, the steady-state VEP wave generated at electrode x by a phase-reversed stimulus of temporal frequency f_{tp} (in Hz) is computed as the sum of N transient waves starting at time 0 and separated in time by an interval of $1/2f_{tp}$, that is,

$$ss^x(t, f_{tp}, f_{sp}) = \sum_{n=0}^{N} v^x(t', f_{sp}), \qquad \text{for } 0 \leq t \leq T \tag{4.2}$$

where N is determined by the length of the simulation interval T (in seconds) such that N is the integer part of $2f_{tp}T$ and $t' = t - n/2f_{tp}$.

The electric potential produced (at electrode x) by an activated dipole ($d_k^x(t, f_{sp})$ in Equation 4.1) is represented by a time-dependent Gaussian function whose amplitude depends on the spatial frequency of the stimulus. Thus, the electric potential produced by dipole k at electrode x, in response to a stimulus of spatial frequency f_{sp} presented (or reversed) at time 0, is given by

$$d_k^x(t, f_{sp}) = A_k^x(f_{sp}) e^{-(t - t_{\text{lat}\,k}(f_{sp}))^2 / 2\sigma_k^2}, \text{ for } 0 \leq t \tag{4.3}$$

where $A_k^x(f_{sp})$ is amplitude as a function of spatial frequency measured at electrode *x*, $t_{\text{lat}\,k}(f_{sp})$ is the dipole's latency of peak response as a function of spatial frequency, and σ_k is a constant that determines the length of the dipole's response period.

The amplitude function $A_k^x(f_{sp})$ can be expressed as the product of a dipole's strength and its spatial frequency sensitivity as given by

$$A_k^x(f_{sp}) = A\max_k^x S_k^x(f_{sp}) \tag{4.4}$$

where $A\max_k^x$ is the maximum amplitude of dipole *k* across all spatial frequencies at electrode *x* (for dipoles of negative polarity, $A\max_k^x$ is the largest negative amplitude) and $S_k^x(f_{sp})$ is the normalized relative spatial frequency sensitivity function (function value at peak sensitivity is 1) of dipole *k* at electrode *x*. This formulation allows for asymmetries in both the strength (maximum amplitude) and the spatial frequency sensitivity of a dipole at mirror electrodes. As will be discussed in more detail in Section 4.3, the former represent the presumed effect of morphological asymmetry while the latter represent the presumed effect of topological asymmetry.

The change in latency as a function of spatial frequency is similar for all dipole sources (see Section 4.1.5). Thus, if $t_{\text{lat}_k}(f_{\text{ref}})$ is the latency of peak response for dipole *k* for an arbitrary but fixed reference stimulus of spatial frequency $f_{\text{ref},}$ and $t_{\text{lat}_k}(f_{sp})$ is the latency of peak response for dipole *k* for a

stimulus of spatial frequency f_{sp}, then $t_{\mathrm{lat}_k}(f_{sp}) - t_{\mathrm{lat}_k}(f_{\mathrm{ref}}) = \delta(f_{sp})$ for all k. Thus, Equation 4.1 can be rewritten as

$$v^x(t, f_{sp}) = \sum_k^D A_k^x(f_{sp}) e^{-(t-\delta(f_{sp})-t_{\mathrm{lat}_k}(f_{\mathrm{ref}}))^2 / 2\sigma_k{}^2} \tag{4.5}$$

The wave defined by Equation 4.5 constitutes a time shift, equal to $\delta(f_{sp})$, of the transient wave given by:

$$v^x(t, f_{sp}) = \sum_k^D A_k^x(f_{sp}) e^{-(t-t_{\mathrm{lat}_k}(f_{\mathrm{ref}}))^2 / 2\sigma_k{}^2} \tag{4.6}$$

According to the shifting property of the Fourier transform, the waves defined by Equations 4.5 and 4.6 have the same amplitude spectra. Because the analysis of results is based on the amplitude spectra of the computed waves (see next paragraph), wave computations can be based on Equation 4.6.

A main concern of the modeling investigation is the relationship between asymmetry in the amplitude of a contributing dipole at mirror electrode locations and asymmetry in the corresponding temporal frequency amplitude functions[25]. This relationship is easily examined because, as the analysis provided in Appendix A demonstrates, the relative amplitudes of the second harmonic component for steady-state waves generated at the same temporal frequency but at different electrodes is equivalent to the relative amplitudes of that frequency component in amplitude spectra of their underlying transient waves (under the

[25] The temporal frequency amplitude function associated with a grating stimulus is defined as the amplitude of the second harmonic frequency component ($2f_{tp}$) in the amplitude spectrum of the steady-state wave produced by the phase reversal of the stimulus, as a function of the temporal frequency (f_{tp}) of the counter-phase modulation.

model assumptions). Thus, a comparison of the effects of different dipole amplitudes on the amplitude of the second harmonic frequency component of steady-state waves generated by a phase-reversed stimulus can be made on the basis of the Fourier transform of the underlying transient wave, eliminating the need to generate and analyze steady-state waves at various temporal frequencies. As mentioned previously, this methodology is used throughout most of the investigation.

All model equations and computations of associated amplitude functions used to produce the results discussed in the next section are implemented in MATLAB 6 release 12. The Fourier transforms are computed using the Fast Fourier Transform function in MATLAB. Model computations are performed on a Dell Dimension 8200 (2.2 GHz Pentium 4 processor and 256 MB RAM) under Windows XP.

4.3 Results

4.3.1 The Effect of Dipole Asymmetry on VEP Latency Measurements

The investigations (Rebai et al., 1993, 1997, 1998) that based hemispheric comparisons on transient VEP measurements assume that shorter latency in a VEP component, in particular the P1, indicates faster activation of some corresponding process. However, if a VEP component is produced by the combined effects of multiple equivalent dipoles, then its latency is a function of the amplitudes as well as the latencies of the contributing dipoles. Consequently,

hemispheric asymmetry in VEP component latency may reflect amplitude differences related to anatomical asymmetry affecting the dipole pairs in the two hemispheres rather than differences in the latency of process activation.

The transient VEP wave model (Equation 4.6) can be used to illustrate this point. In this model implementation, the set D of activated dipoles comprises an early latency P1, a late latency P1, and an N2 dipole, each representing a separate process activated by a stimulus of spatial frequency $f_{sp} = f_{\text{ref}}$ where f_{ref} represents an arbitrary reference frequency. The peak latency and amplitude values assumed for each dipole are shown in Table 4.1. Symmetric values are hypothesized for the late latency P1 and N2 dipole amplitudes at the mirror electrodes in the right (R) and left (L) hemispheres. The amplitude of the early latency P1 dipole, however, is hypothesized to differ at the mirror electrodes. The parameter σ_k is set to 8ms for all $k \in D$ such that onset latency occurs approximately 25 ms earlier than peak.

Table 4.1: Model Parameter Values for P1 Latency Example

dipole k	*latency* (ms) $t_{\text{lat}}(f_{\text{ref}})$	*amplitude* (R) $A^R(f_{\text{ref}})$	*amplitude* (L) $A^L(f_{\text{ref}})$
early latency P1	105	0.6	0.4
late latency P1	120	0.5	0.5
N2	145	-1.0	-1.0

Using these parameter values in Equation 4.6, the transient wave generated at the right electrode is computed as

$$v^R(t) = 0.6e^{-(t-105)^2/2(8)^2} + 0.5e^{-(t-120)^2/2(8)^2} - e^{-(t-145)^2/2(8)^2}$$

Similarly, the transient wave generated at the left electrode is computed as

$$v^L(t) = 0.4e^{-(t-105)^2/2(8)^2} + 0.5e^{-(t-120)^2/2(8)^2} - e^{-(t-145)^2/2(8)^2}$$

The computed waves, shown in Figure 4.8, appear to differ in the latency (and amplitude) of their P1 component. Thus, asymmetry in the amplitude of early P1 dipole appears as a latency difference, although no difference in process latency actually exists.

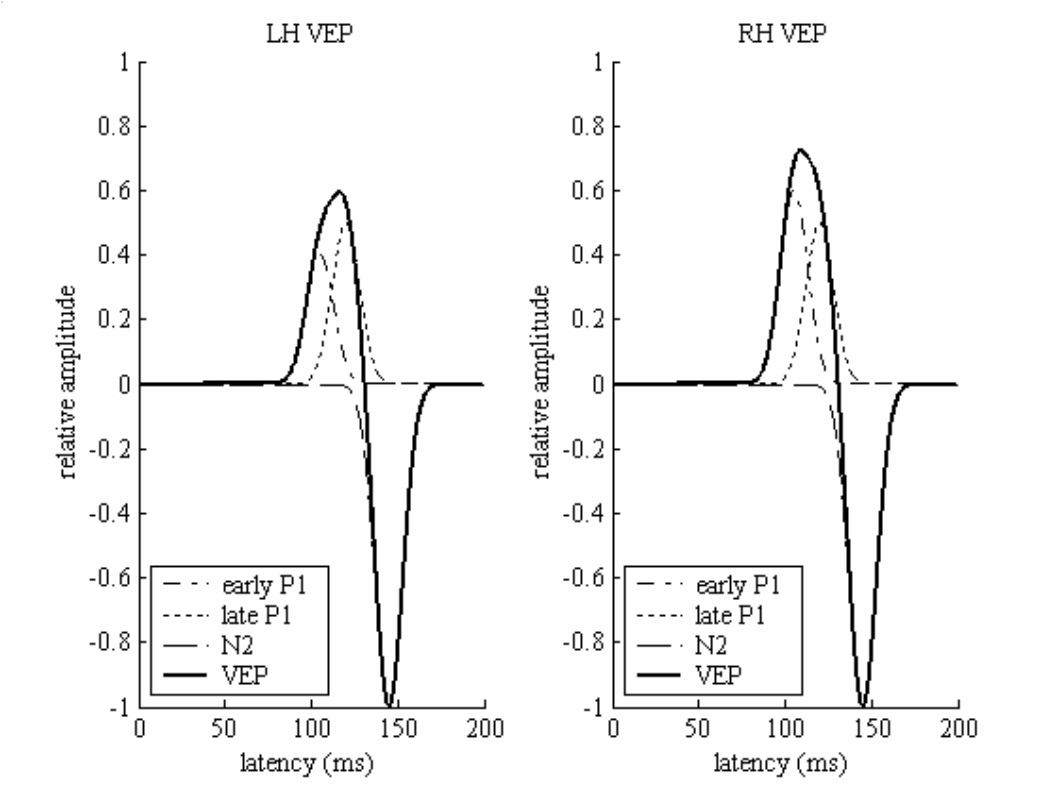

Figure 4.8: The VEP waves represent the combined responses of three dipoles as generated at mirror electrodes in the left (LH) and right (RH) hemispheres. Dipole latencies are the same at both locations, namely, 105, 120, and 145 ms for early latency P1, late latency P1, and N2, respectively. Dipole amplitudes are also the same for late latency P1 and N2. However, the amplitude of early latency P1 is greater in the right than in the left hemisphere. This asymmetry in dipole amplitude causes the P1 component of the VEP wave to differ in latency as well as amplitude between the two hemispheres, with the right hemisphere exhibiting the shorter latency and greater amplitude.

4.3.2 The Effect of Dipole Asymmetry on Steady-State Waves

The investigations that utilized steady-state VEP measurements as the basis for hemispheric comparisons (Rebai et al., 1986, 1989) assumed that larger amplitude for the second harmonic component in the frequency spectrum of a phase-reversal steady-state wave indicates greater sensitivity to the temporal frequency of the stimulus. However, as stated in Section 4.2.3 and established in Appendix A, the amplitude of the second harmonic depends on the frequency

spectrum of the transient VEP waves underlying the steady-state wave. The frequency spectrum of a transient wave, in turn, depends on the time varying amplitudes of dipoles from which it is formed. Thus, hemispheric asymmetry in the amplitude of the second harmonic may arise from differences in the corresponding sets of active dipoles that are caused by anatomical asymmetries and are unrelated to temporal frequency sensitivity.

The transient wave model (Equation 4.6) and the steady-state wave model (Equation 4.2) can be used to illustrate this point. As in the model implementation discussed in the previous section, a stimulus of spatial frequency $f_{sp} = f_{\text{ref}}$ is assumed (again f_{ref} represents an arbitrary reference frequency), with the set D of activated dipoles consisting of an early latency P1, a late latency P1, and an N2 dipole. Hypothetical peak latency and amplitude values for each dipole are shown in Table 4.2. The amplitude values are symmetric in the case of the N2 dipole but asymmetric in the case of the early latency P1 and the late latency P1 dipole. The parameter σ_k is again set to 8ms for all $k \in D$.

Table 4.2: Model Parameter Values for the Steady-State Example

dipole k	*latency* (ms) $t_{\text{lat}}(f_{\text{ref}})$	*amplitude* (R) $A^R(f_{\text{ref}})$	*amplitude* (L) $A^L(f_{\text{ref}})$
early latency P1	105	0.9	0.1
late latency P1	120	0.1	0.9
N2	145	-1.0	-1.0

Applying these parameter values to Equation 4.6, the transient wave generated at the right hemisphere electrode is computed as

$$v^R(t) = 0.9e^{-(t-105)^2/2(8)^2} + 0.1e^{-(t-120)^2/2(8)^2} - e^{-(t-145)^2/2(8)^2}$$

Similarly, the transient wave generated at the corresponding left hemisphere electrode is computed as

$$v^L(t) = 0.1e^{-(t-105)^2/2(8)^2} + 0.9e^{-(t-120)^2/2(8)^2} - e^{-(t-145)^2/2(8)^2}$$

As can be seen in Figure 4.9a, this dipole amplitude asymmetry produces asymmetric transient waves that have P1 components that are very similar in amplitude but very different in latency.

The corresponding steady-state waves generated in response to stimuli of temporal frequencies (f_{tp}) of 4, 12, and 18 Hz, as computed using Equation 4.2, are shown in Figure 4.9b. A 2 second simulation interval, T, starting at time t= 0 is used for the wave computations. Figure 4.9b depicts a 250 ms portion of the interval in which the overlapping transient waves form a steady-state wave (i.e., this portion of the interval does not contain stimulation start and end effects).

Figure 4.9 also shows the amplitude spectra for both the transient and the steady-state waves. The amplitude spectra were calculated by first computing the power spectra values for the waves using a Fast Fourier Transform (FFT) with a sampling rate of 1000 Hz. For the transient waves, the FFT is based on 512 samples from the time interval 0 to 511 ms. For the steady-state waves, the FFT is

based on 1024 samples from the time interval 489 to 1512 ms in the center of the 2000 ms simulation interval. The amplitude spectra were then computed by taking the square root of the power spectra values. In the case of the steady state waves, the power spectra values were multiplied by a factor of $1000/f_{tp}$ prior to the square root operation in order to compensate for the variation in the number of waves contained in the analysis interval for the various temporal frequencies.

As can be seen in Figure 4.9, dipole asymmetry results in asymmetry in the amplitude spectra of both the transient and the steady-state waves. The magnitude and direction of the amplitude asymmetry depends on frequency but is the same for both the steady-state waves and their underlying transient waves. In this case, the dipole asymmetry results in the right lateralization of the second harmonic amplitude for temporal frequencies of 4 and 18 Hz, and the left lateralization of the second harmonic amplitude for a temporal frequency of 12 Hz. This apparent lateralization of response is evident in the steady-state waves themselves at the higher temporal frequencies of 12 and 18 Hz. At these frequencies, consecutive transient waves overlap causing components of opposite polarity to cancel one another, thus reducing the amplitude of the steady-state wave. Asymmetry in the dipole components leads to asymmetry in the degree of cancellation that, in turn, appears as asymmetry in the amplitude of the steady-state wave.

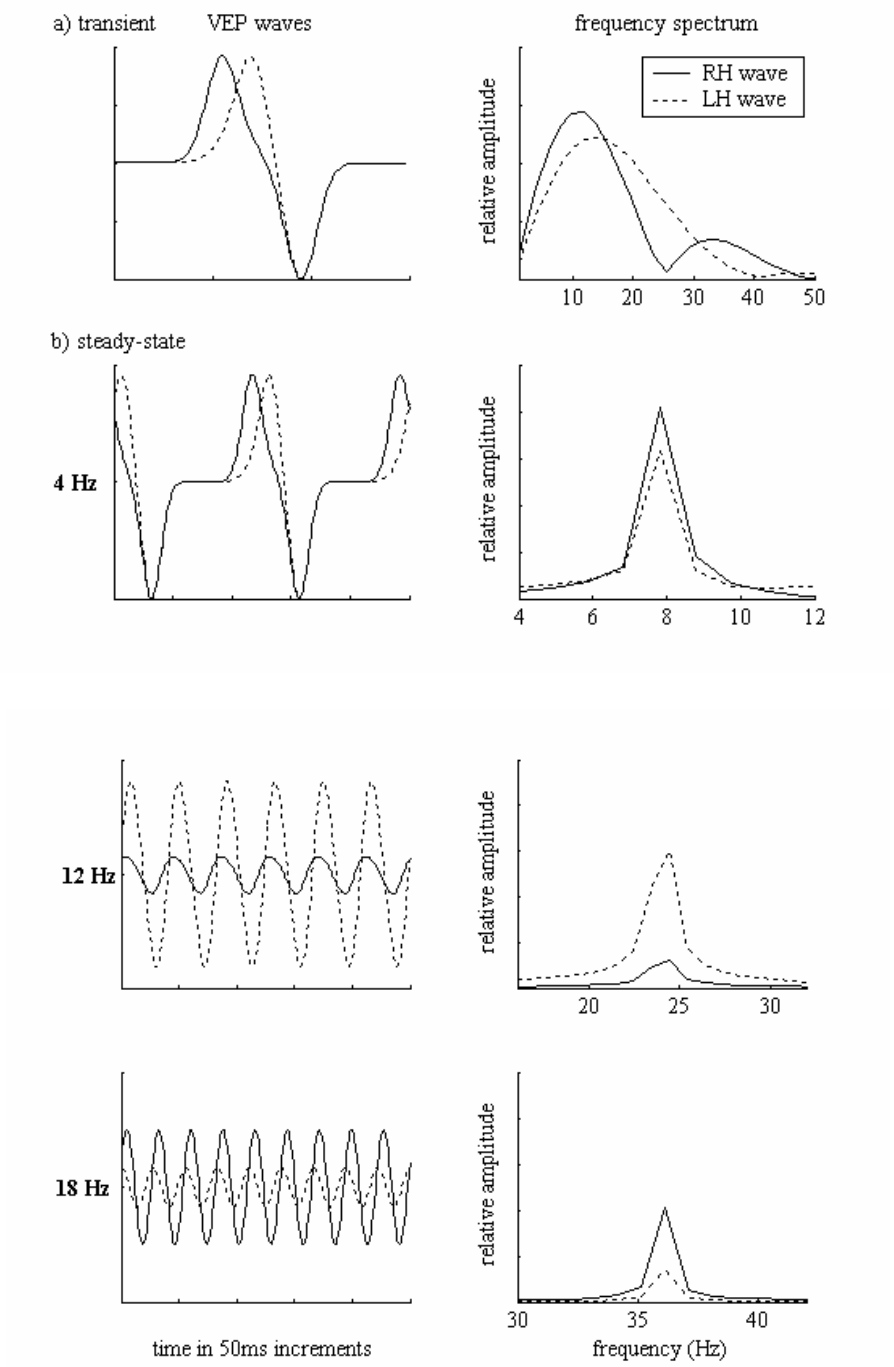

Figure 4.9: VEP waves (left) and their amplitude spectra (right). a) The right hemisphere (RH) transient wave appears to have shorter latency in the positive component than the left hemisphere (LH) wave resulting in spectral differences. b) The steady-state waves formed from these transient VEP waves, in response to phase-reversed stimuli at temporal frequencies 4, 12, and 18 Hz, have amplitude spectra with a peak at the second harmonic of the temporal frequency. The asymmetry in the amplitude of the second harmonic component corresponds to the asymmetry in the amplitude spectra of the underlying transient waves at that same frequency.

The model results discussed in this section imply that a steady-state waveform generated in response to a particular stimulus at a particular electrode location may exhibit greatly reduced amplitude at certain temporal frequencies despite strong dipole responses to the stimulus. If the psychophysical response to the stimulus is a function of the dipole response, then the model predicts that a reduction in response, as measured by a reduction in the amplitude of the second harmonic component, may be observed at certain temporal frequencies in the absence of any reduction in psychophysical response. Such a phenomenon appears to have been observed in a number of experiments that examined steady-state VEP response as a function of stimulus characteristics (Parry, Murray, & Hadjizenonos, 1999; Strasburger, Murray, & Remky, 1993). Thus, the validity of the VEP wave model used in this investigation is supported by empirical evidence.

4.3.3 Early P1 Asymmetry and Temporal Frequency Lateralization Effects

This section examines the hypothesis that asymmetry in the early P1 component due to morphological asymmetry in the occipital poles can account for the temporal frequency lateralization effects observed in the Rebai et al. (1986) investigation. The hypothesis is based on the theory that left occipital petalia is present in the right-handed subjects used the Rebai study. The potential impact of this asymmetry on the location and orientation of early P1 dipole sources in the two hemispheres is illustrated in Figure 4.10. The asymmetry results in a more

medial set of early P1 sources in the left hemisphere and a more lateral set of early P1 sources in the right hemisphere. The combined potentials of the two sets of early P1 sources at mirror lateral occipital sites should produce greater early P1 amplitude in the right than in the left hemisphere, and could even produce *negative* amplitude for the early P1 component in the left hemisphere.

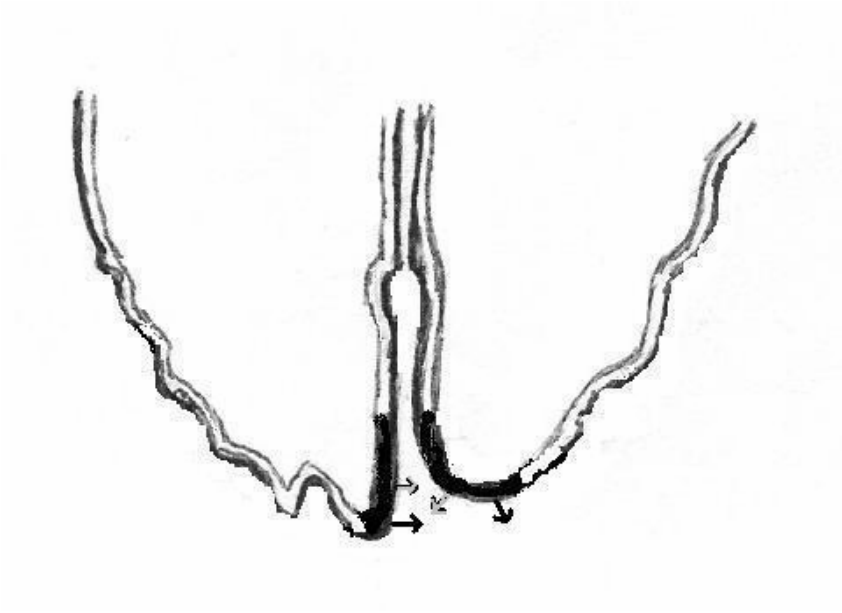

Figure 4.10: Left occipital petalia, typically found in right-handers, produces asymmetry in both the location and the orientation of early P1 dipole sources, as shown. The darkened cortex represents the early P1 dipole source area. The dipole sources are indicated by arrows that point in the direction of positive potential. Dark arrows represent sources originating in a more central part of the visual field. Light arrows represent sources originating in a less central part of the visual field. Compared with their counterparts in the left hemisphere, the right hemisphere sources are located more laterally, with orientations that produce relatively greater positive potential at lateral occipital electrode sites over the source hemisphere and relatively less positive potential at mirror electrode sites over the opposite hemisphere.

The examination of the study hypothesis proceeds by using the VEP wave model to investigate the relationship between dipole amplitude and the temporal frequency amplitude function. As demonstrated in Appendix A, the relative

amplitude spectrum of a transient wave is equivalent to the relative temporal frequency amplitude function. Thus, the investigation is accomplished by computing transient waves (based on Equation 4.6) while varying dipole amplitude values, and then computing the associated amplitude spectra. In the process, amplitude values are sought which produce temporal frequency amplitude functions similar to those observed in the Rebai experiment. Success in finding such values demonstrates that a simple dipole model can account for the temporal frequency amplitude function and determines a plausible set of dipole amplitudes. Temporal frequency amplitude functions associated with various early P1 amplitudes are then compared to those observed in the right and left hemispheres in order to evaluate the potential for asymmetry in the amplitude of the early P1 component to account for the empirically-observed temporal frequency lateralization effects.

The dipole set D used in this implementation of the model includes those that can be expected to exhibit significant activation in response to a stimulus of moderately high spatial frequency (~3 cpd), namely, the N1, the early latency P1, the late latency P1, and the N2 dipoles (see Section 4.1.4). The values assigned to the peak latency parameter $t_{\text{lat}}(f_{\text{ref}})$ for these dipoles, shown in Table 4.3, are consistent with the experimental findings on dipole latencies associated with a stimulus frequency of 3 cpd (i.e., f_{ref} = 3 cpd). The spatial frequency of the stimulus is assumed to be equal to the reference frequency, that is, f_{sp} = 3 cpd. As in the model implementations previously discussed, the value of σ_k is set to 8 ms

for all $k \in D$ such that the onset of dipole response occurs approximately 25 ms earlier than the response peak.

The investigation begins by examining the characteristics of the temporal frequency amplitude spectrum as a function of the amplitude of dipoles that are assumed both prominent and symmetric at lateral occipital sites (the lateral occipital electrode is designated as $x = O$ in the discussion that follows), namely, the late latency P1 and the N2. Because N2 is the more prominent of the two, its amplitude is held constant at -1.0, while the amplitude of late P1, designated by the variable A, takes on the values of 0.3, 0.5, and 0.7. The amplitude values for the N1 and early P1 dipoles are set to 0. These dipole amplitude assignments are summarized in Table 4.3.

Table 4.3: Model Parameter Values with Variable Late P1

dipole k	*latency* (ms) $t_{\text{lat}}(3)$	*amplitude* (O) $A^O(3)$
N1	75	0.0
early latency P1	105	0.0
late latency P1	135	A
N2	148	-1.0

With these parameter values applied to Equation 4.6, the transient wave generated at the lateral occipital electrode given these dipole amplitudes is computed as

$$v^{O}(t) = 0.0e^{-(t-75)^2/2(8)^2} + 0.0e^{-(t-105)^2/2(8)^2} + Ae^{-(t-135)^2/2(8)^2} - e^{-(t-148)^2/2(8)^2}$$

with the late P1 dipole amplitude taking on hypothetical values of A = 0.3, 0.5 and 0.7 in successive implementations.

The amplitude spectra of the transient waves corresponding to the three hypothetical values for the late P1 amplitude are shown in Figure 4.11. These results indicate that, as the late P1 amplitude increases relative to the N1 amplitude, the amplitude function decreases for temporal frequencies below approximately 6.5 Hz while increasing for frequencies above that point. These changes transform the function from low-pass to band-pass with a peak appearing near 8 Hz for a late P1 amplitude value of 0.5 and shifting higher toward 9 Hz as the amplitude increases to .7. The shape of the amplitude function for the higher late P1 amplitude values resembles that observed empirically in the left hemisphere (see Figure 4.2) suggesting that the late P1 and N2 components are sufficient to account for the basic characteristics of the temporal frequency amplitude function in the left hemisphere.

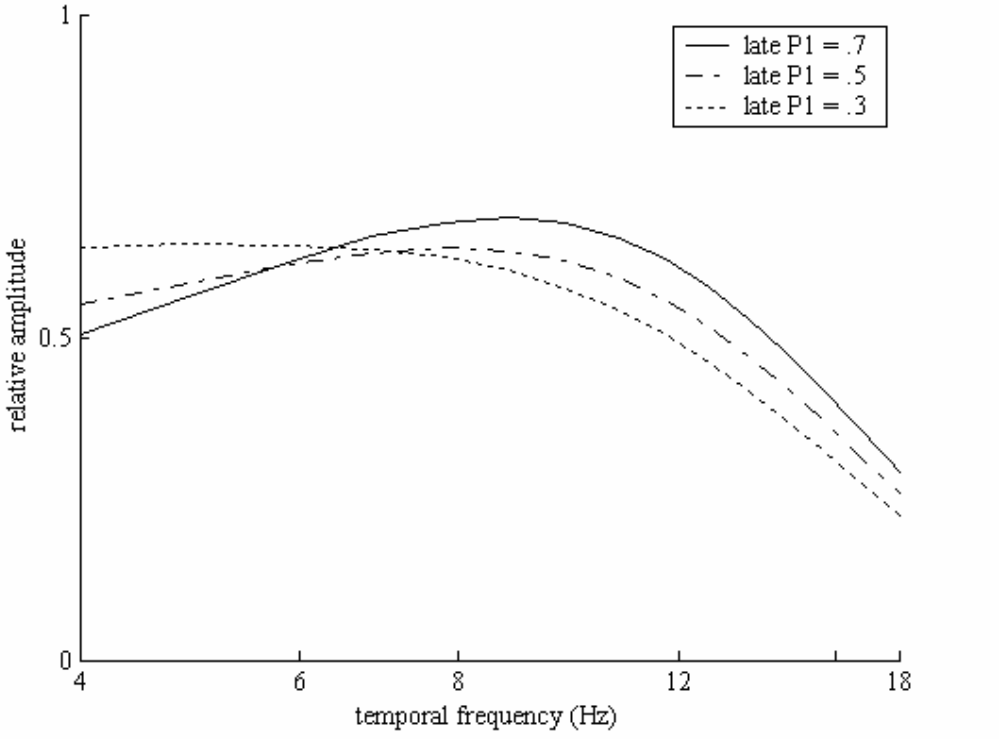

Figure 4.11: The effect on the temporal frequency amplitude function produced by varying the amplitude of late P1. N2 amplitude is fixed at -1.0. Late P1 amplitudes are varied as indicated.

As just demonstrated, the late P1 and the N2 dipoles alone can produce an amplitude function similar to that observed empirically in the left hemisphere. According to the study hypothesis then, the amplitude function should begin to resemble that observed in the right hemisphere as the amplitude of the early latency P1 component takes on values greater than 0. The model is used to examine this assertion by holding late P1 and N2 amplitudes at values that produced a left hemisphere-like amplitude function (0.7 and -1.0, respectively), while increasing early P1 amplitude from 0 (designated as the variable *A*) to 0.2

and then 0.4. The N1 amplitude remains set to 0. These dipole amplitude assignments are summarized in Table 4.4.

Table 4.4: Model Parameter Values with Variable Early P1

dipole k	*latency* (ms) $t_{lat}(3)$	*amplitude* (O) $A^O(3)$
N1	75	0.0
early latency P1	105	A
late latency P1	135	0.7
N2	148	-1.0

Using these parameter values in Equation 4.6, the transient wave generated at the lateral occipital electrode is computed as

$$v^O(t) = 0.0e^{-(t-75)^2/2(8)^2} + Ae^{-(t-105)^2/2(8)^2} + .0.7e^{-(t-135)^2/2(8)^2} - e^{-(t-148)^2/2(8)^2} \quad (4.7)$$

with the early P1 dipole amplitude taking on the hypothetical values of A = 0.0, 0.2 and 0.4 in successive implementations.

The amplitude spectra of the transient waves corresponding to the three hypothetical values for the early P1 amplitude are shown in Figure 4.12. Evidently, as early P1 amplitude increases, the amplitude function increases for temporal frequencies below approximately 7 Hz but decreases for temporal

frequencies in the range of 7 to 13 Hz. Furthermore, the 9 Hz peak is replaced by peak near 6 Hz, which shifts lower with increasing P1 amplitude. A comparison of these results with empirical data (see Figure 4.2) shows that the amplitude function does develop the characteristics of the amplitude function observed in right hemisphere with increasing P1 amplitude, as hypothesized.

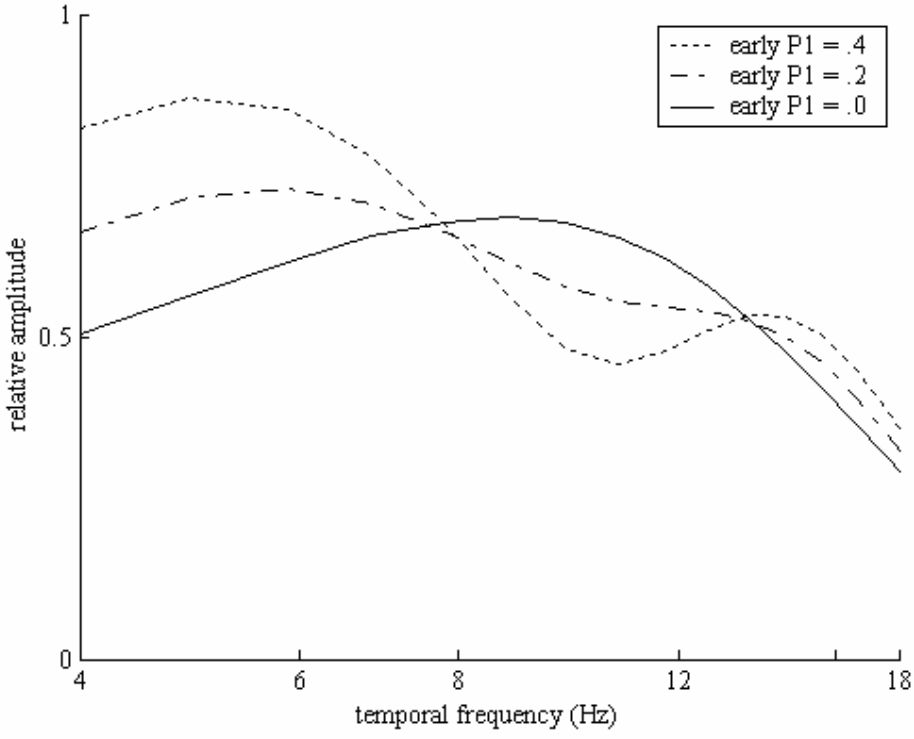

Figure 4.12: The effect on the temporal frequency amplitude function produced by increasing the amplitude of early P1. Late P1 and N2 amplitudes are fixed at 0.7 and -1.0, respectively. Early P1 amplitudes are varied as indicated.

As theorized earlier, the morphological asymmetry impacting the early P1 dipole sources could result in a negative value for early P1 amplitude in the left hemisphere. To explore the effect of negative early P1 amplitude values on the temporal frequency amplitude function, model results are obtained for early P1 amplitude values of 0, -0.1 and -0.2 with late P1 and N2 amplitudes again fixed at 0.7 and -1.0, respectively. The transient waves are again given by Equation 4.7, but with the early P1 amplitude successively assigned hypothetical values of A = 0, -0.1, and -0.2.

The amplitude spectra of the transient waves corresponding to the three hypothetical values for the early P1 amplitude are displayed in Figure 4.13. The amplitude spectra show that negative early P1 amplitude values cause the amplitude function to decrease for temporal frequencies below approximately 7 Hz and increase for temporal frequencies between 7 to 13 Hz. Thus, negative values for the early P1 amplitude amplify the characteristics of the temporal frequency amplitude function that most resemble those found in the left hemisphere.

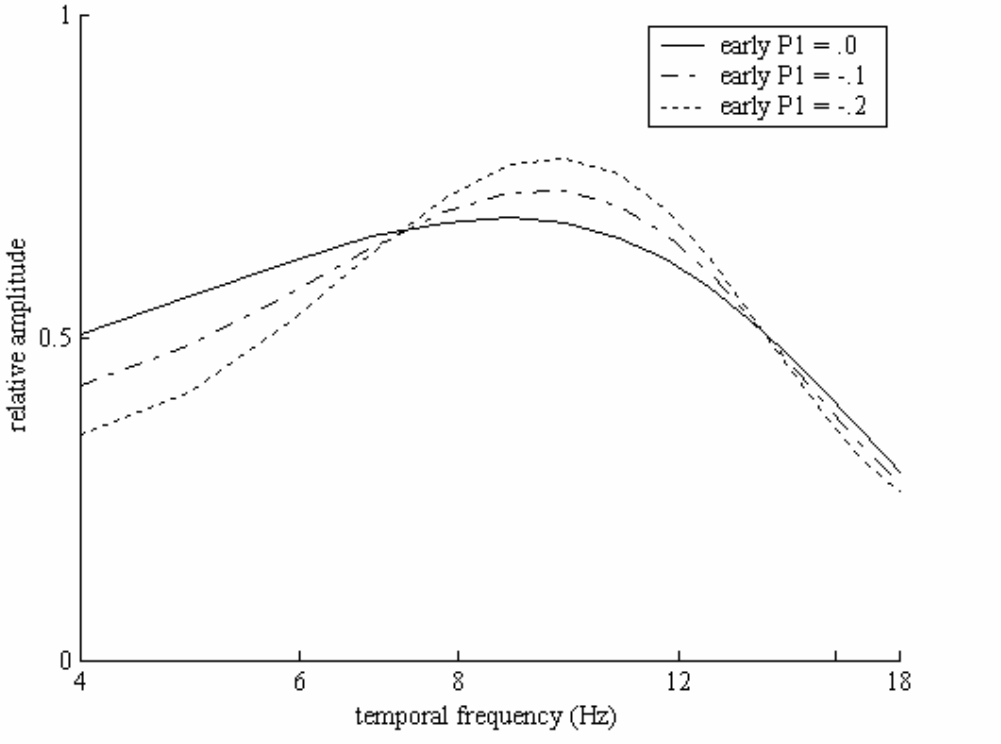

Figure 4.13: The effect on the temporal frequency amplitude function produced by negative amplitude values for early P1. Late P1 and N2 amplitudes are fixed at 0.7 and -1.0, respectively. Early P1 amplitudes are varied as indicated.

The N1 component is not prominent at lateral occipital sites suggesting its impact on the temporal frequency amplitude function is minimal. Its potential effect is explored using the VEP wave model by varying N1 amplitude (designated by the variable *A*) in relation to fixed early P1, late P1 and N2 amplitudes (0, 0.7, and -1, respectively). N1 is allowed to take on amplitude values of 0, -0.1, and -0.2. These dipole amplitude assignments are summarized in Table 4.5.

Table 4.5: Model Parameter Values with Variable N1

dipole k	*latency* (ms) $t_{lat}(3)$	*amplitude* (O) $A^O(3)$
N1	75	A
early latency P1	105	0.0
late latency P1	135	0.7
N2	148	-1.0

Applying these parameter values to Equation 4.6, the transient wave generated at the lateral occipital electrode given these dipole amplitudes is computed as

$$v^O(t) = Ae^{-(t-75)^2/2(8)^2} + 0.0e^{-(t-105)^2/2(8)^2} + .0.7e^{-(t-135)^2/2(8)^2} - e^{-(t-148)^2/2(8)^2}$$

with the N1 dipole amplitude taking on the hypothetical values of A = 0.0, -0.1 and -0.2 in successive implementations.

The amplitude spectra of the transient waves corresponding to the three hypothetical values for the N1 amplitude are displayed in Figure 4.14. The results demonstrate that as N1 amplitude increases, amplitude for temporal frequencies between 4 and 7.5 Hz increases while amplitude for frequencies between 7.5 and 11 Hz decreases, shifting the peak from 9 to 6 Hz. Thus, within the 4 to 11 Hz range, variation in N1 amplitude tends to enhance the effects on the temporal frequency amplitude function produced by similar variation in early P1 amplitude.

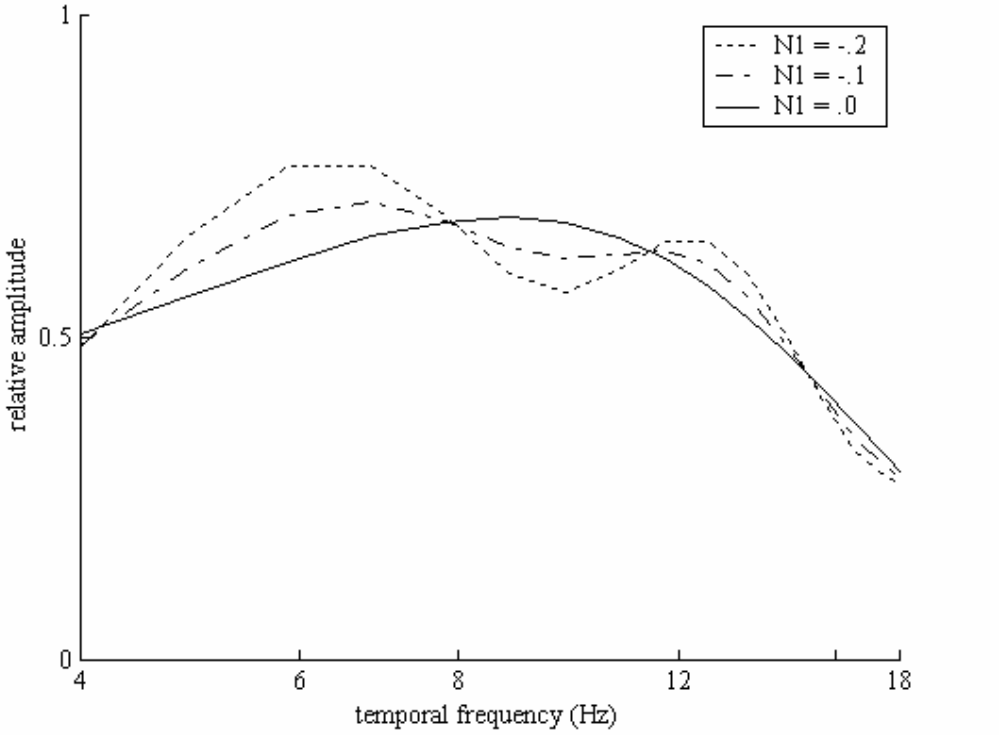

Figure 4.14: The effect on the temporal frequency amplitude function produced by varying the amplitude of N1. Early P1, late P1, and N2 amplitudes are fixed at 0, 0.7, and 1.0, respectively. Early N1 amplitudes are varied as indicated.

The modeling results indicate that asymmetry in the early P1 component can produce asymmetry in the temporal frequency amplitude function that is qualitatively similar to that observed empirically. In particular, the results demonstrate that if the amplitude of the early P1 component is greater in the right hemisphere than in the left, the right hemisphere will appear to have the greater response for temporal frequencies below ~7Hz, while the left hemisphere will appear to have the greater response for temporal frequencies above ~7 Hz (up to

13 Hz). This point is illustrated again in Figure 4.15 which shows the temporal frequency amplitude functions obtained for early P1 amplitude values ranging from -.1 to 3 with a late P1 amplitude value of .7 and an N2 amplitude value of 1 (N1 amplitude is 0). The model producing this effect fixed the value of σ (which determines the dipole response period) at 8ms and the values for the dipole latencies at early P1 – 105 ms, late P1 – 135 ms, and N2 – 148 ms.

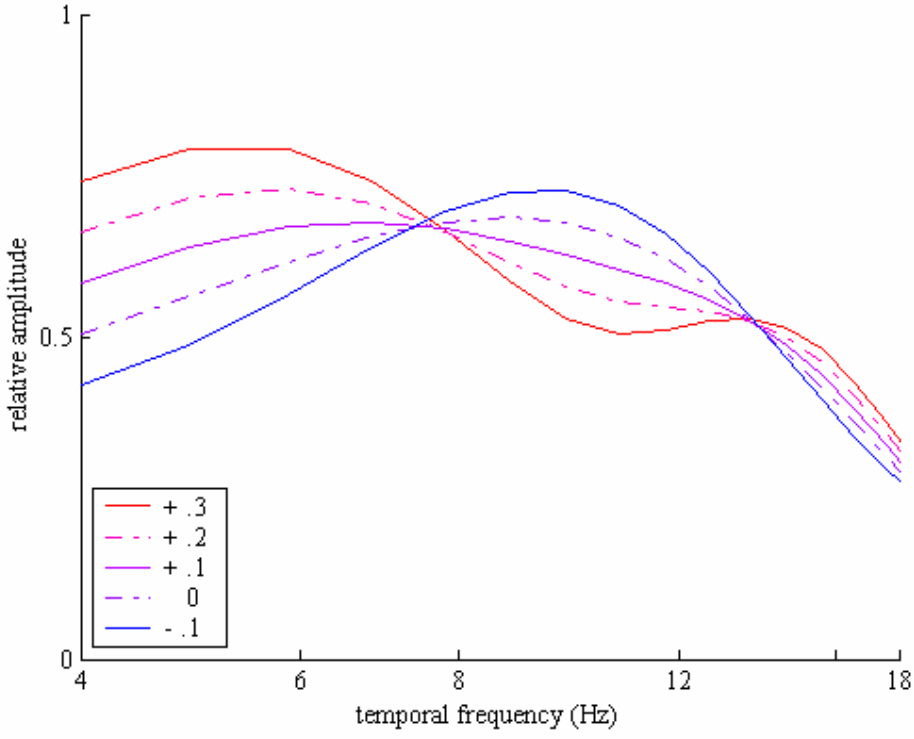

Figure 4.15: The variation in the temporal frequency amplitude function resulting from variation in the early P1 amplitude. The legend shows the values used for the early P1 amplitude. Late P1 amplitude is .7, N2 amplitude is 1.0. Amplitudes for temporal frequencies below ~7 Hz increase, while amplitudes for temporal frequencies above ~7 Hz decrease (up to ~13 Hz), as early P1 amplitude increases. The model producing this effect assumed a value of 8 ms for σ and dipole latencies of early P1 – 105 ms, late P1 – 135 ms, and N2 – 148 ms.

The values for σ and the dipole latency parameters were chosen to be consistent with empirical findings and, therefore, should represent reasonable estimates of the mean values that occur in a sample population of subjects. To determine the sensitivity of the model to small variations in these parameter values, variation in the temporal frequency amplitude function resulting from variation in the early P1 amplitude was again computed (using the same dipole amplitude values) for two conditions. First, values of 7 and 9 ms were used for σ while dipole latencies were held at their original values. Second, the original value of 8 ms was used for σ, while dipole peak latencies were changed either to decrease (early P1 – 108, N2 – 145) or to increase (early P1 – 102, N2 – 151) the time interval between peaks. The latency of the late P1 dipole was not varied as only variation in relative dipole latencies affects the temporal frequency amplitude function. The results of these variations are shown in Figure 4.16.

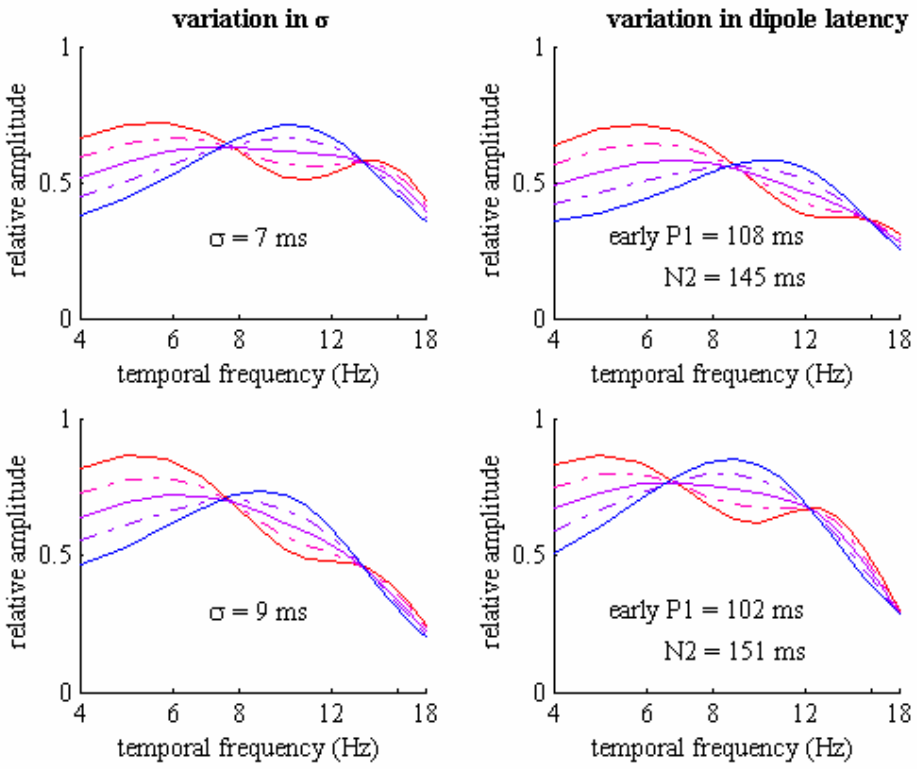

Figure 4.16: The graphs on the left show the effect on model behavior of variation in the value of σ with dipole latencies set to their original values (early P1 - 105 ms, late P1 - 135 ms, N2 - 148 ms). The graphs on the right show the effect on model behavior of variation in dipole latency values with σ set to its original value (8 ms). All graphs depict the variation in the temporal frequency amplitude function resulting from variation in early P1 amplitude. The legend in Figure 4.15, which shows the early P1 amplitude values associated with each of the lines, applies to these graphs.

Increasing σ shifts lower temporal frequency amplitudes upwards and higher temporal frequency amplitudes downward, consistent with a longer dipole response period, but does not affect the crossover point at which increasing early P1 amplitude produces opposite effects on temporal frequency amplitudes (~ 7 Hz). Increasing the time separating dipole peak latencies produces an increase in amplitude for all but the highest temporal frequencies. Such an increase also shifts

the crossover point toward lower frequencies. These results indicate that the model is sensitive to variation in these model parameters but not excessively so. The fundamental effect that variation in early P1 amplitude has on the temporal frequency amplitude function remains the same. That is, an increase in early P1 amplitude produces an increase in amplitude for temporal frequencies below a crossover point in the range of 6.5 to 8.5 Hz and decrease in amplitude for temporal frequencies above that point. Thus, the aspect of model behavior that is critical to the hypothesis that asymmetry in early P1 amplitude can account for temporal frequency lateralization does not depend on the precise values of the fixed parameters in the model.

A final demonstration of the potential for the empirical data to be explained by asymmetry in the amplitude of the early P1 dipole is provided by modeling results produced by the parameter values given in Table 4.6.

Table 4.6: Parameter Values Underlying Model Results

dipole k	*latency* (ms) $t_{lat}(3)$	*amplitude* (R) $A^R(3)$	*amplitude* (L) $A^L(3)$
N1	75	0	0
early latency P1	105	0.2	-0.1
late latency P1	135	0.77	0.77
N2	148	-1.1	-1.1

Using these parameter values In Equation 4.6, the transient waves generated at lateral occipital sites in the right and left hemispheres are computed as

$$v^{R}(t) = 0.0e^{-(t-75)^2/2(8)^2} + 0.2e^{-(t-105)^2/2(8)^2}$$

$$+ .0.77e^{-(t-135)^2/2(8)^2} - 1.1e^{-(t-148)^2/2(8)^2}$$

and

$$v^{L}(t) = 0.0e^{-(t-75)^2/2(8)^2} - .1e^{-(t-105)^2/2(8)^2}$$

$$+ .0.77e^{-(t-135)^2/2(8)^2} - 1.1e^{-(t-148)^2/2(8)^2}$$

Figure 4.17 displays the temporal frequency amplitude function evaluated at temporal frequencies 4, 6, 8, 12, and 18 Hz (based on the amplitude spectra of the computed transient waves). The similarity of temporal frequency lateralization pattern produced by the model and that observed in the experimental data (also shown in Figure 4.15) supports the study hypothesis, and suggests that asymmetry in the amplitude of the early P1 dipole alone is sufficient to account for the basic characteristics of the lateralization.

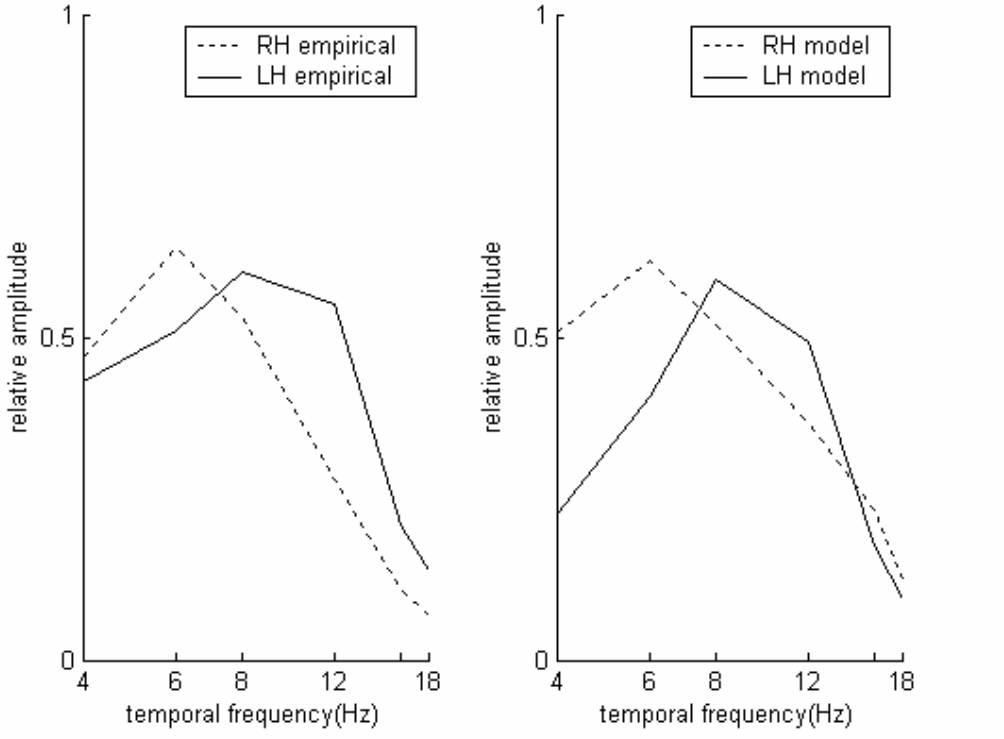

Figure 4.17: Empirical data (Rebai et al., 1986) and model results for the temporal frequency amplitude functions in the right (RH) and left (LH) hemispheres. The empirical data represent the mean of individual (normalized) amplitude functions. The model results are based on N1, late P1, and N2 values of 0, 0.77 and -1.1, respectively, with early P1values of 0.2 for the right hemisphere and -0.1 for the left hemisphere.

4.3.4 Early P1 Asymmetry and Spatial Frequency Lateralization Effects

This section examines the hypothesis that asymmetry in the amplitude of the early P1 dipole at mirror electrode locations due to anatomical asymmetries can account for the spatial frequency lateralization effects observed in the Rebai et al. (1989) investigation. The hypothesis specifically proposes that asymmetry in the strength of the early P1 dipole, defined as its maximum amplitude across all spatial frequencies, can account for the lateralization effects observed in the right-

handed group, while asymmetry in the spatial frequency sensitivity of the early P1 dipole can account for the lateralization effects observed in the left-handed group. This hypothesis is based on the theory that left occipital petalia is present in the right-handed group, but that the occipital poles of the left-handed group are, on average, morphologically symmetric (Chui & Damasio, 1980; LeMay, 1976, 1977; LeMay & Kido, 1978; Zilles et al., 1996). It is further reasoned that the absence of morphological asymmetry in the left-handed group allows the less salient effects of topological asymmetry, which could be present in both groups, to become evident.

While morphological asymmetry can be expected to have a similar effect on the amplitude of the early P1 dipole across all spatial frequencies, topological asymmetry can be expected to have a differential effect on amplitude as a function of spatial frequency. Specifically, slight differences between the hemispheres in the location and orientation of the early P1 dipole source pairs originating in more or less central parts of the visual field can be expected to produce asymmetry with respect to the part of the visual field that dominates the early P1 dipole at mirror lateral occipital locations (see Figure 4.18). The early P1 dipole sensitivity peak will occur at a higher spatial frequency for the hemisphere in which the more central field dipoles are the dominant sources.

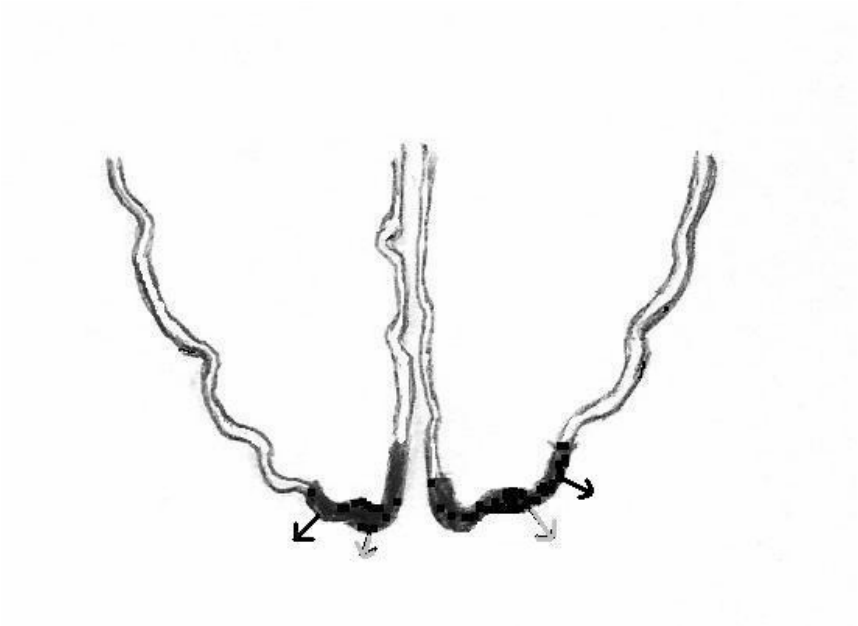

Figure 4.18: Morphological symmetry associated with left-handedness may allow the effects of topological asymmetry in the vicinity of the occipital pole to become more evident. The darkened cortex represents the early P1 dipole source area. The dipoles sources are indicated by arrows that point in the direction of positive potential. Dark arrows represent sources originating in a more central part of the visual field. Light arrows represent sources originating in a less central part of the visual field. Differences in topology at the occipital poles produce asymmetry in both the location and the orientation of corresponding pairs of early P1 dipole sources, as shown. The spatial frequency sensitivity of the early P1 component observed in a particular hemisphere depends on the relative contributions of the various early P1sources throughout the visual field that, in turn, depend on dipole location and orientation.

The hypothesis is examined using a model implementation in which the set *D* of activated dipoles includes the early, mid and late latency P1 and the N2 dipoles. N1, which is not a prominent component at the electrode sites used in the experiments and did not play an important role in the previous model implementations, is not included. The mid-latency P1 represents the dipole source associated with low spatial frequency mentioned in Section 4.1.3. The dipole latencies, which are based on a reference spatial frequency of f_{ref} = 3 cpd, are

shown in Table 4.7. As in the previous model implementations, a value of 8 ms is assigned to σ_k for all $k \in D$.

To investigate the hypothesis that asymmetry in the maximum amplitude of the early P1 dipole can produce the lateralization effects observed in the right-handed group, normalized spatial frequency sensitivity functions were determined for each dipole based on empirical findings on dipole sensitivities (see Sections 4.1.4 and 4.1.5). These functions (represented as $S(f_{sp})$ in the model), together with the maximum amplitude values (A_{max}) for each dipole, were then manually tuned until the spatial frequency amplitude functions of the computed waves for temporal frequencies 4 and 12 Hz (i.e., the model results) closely resembled the empirical data for the right hemisphere[26]. The maximum amplitude values ($A_{max}{}^{R}$) resulting from this process are given in Table 4.7. The resulting sensitivity functions are shown in Figure 4.19, with the function values for spatial frequencies used as the stimulus frequency f_{sp} in the model wave computations provided in Table 4.8. The parameter values shown in Tables 4.7 and 4.8 for the right hemisphere were used to compute transient waves (based on Equations 4.4 and 4.6) for each spatial frequency listed in Table 4.8. As in the model implementation discussed previously, Fourier transforms of the resulting transient

[26] Manual tuning was accomplished by computing the transient waves (based on Equation 4.6) and their amplitude spectra for a given set of dipole sensitivity and maximum amplitude values. The amplitudes of the second harmonic for temporal frequencies 4 and 12 Hz as a function of spatial frequency (referred to as the spatial frequency amplitude functions for 4 and 12 Hz) were then compared with the empirical data for the right hemisphere and the dipole sensitivity and maximum amplitude values adjusted to improve the fit. This process was repeated until a good fit was obtained. Adjustments were minimal and the initial consistency with empirical findings on dipole spatial frequency sensitivity was maintained.

waves were performed to evaluate the temporal frequency amplitude function at the frequencies 4 and 12 Hz. The close match between the model results produced using these parameter values and the empirical data for the right hemisphere can be seen in the graphs displayed in Figure 4.20.

Table 4.7: Model Parameter Values for Right-Handed Condition

dipole k	*latency* (ms) $t_{lat}(3)$	*max amplitude* (R) $A\max^R$	*max amplitude* (L) $A\max^L$
early latency P1	105	2.9	1.3
mid latency P1	115	1.8	1.8
late latency P1	135	7.0	7.0
N2	148	-7.4	-7.4

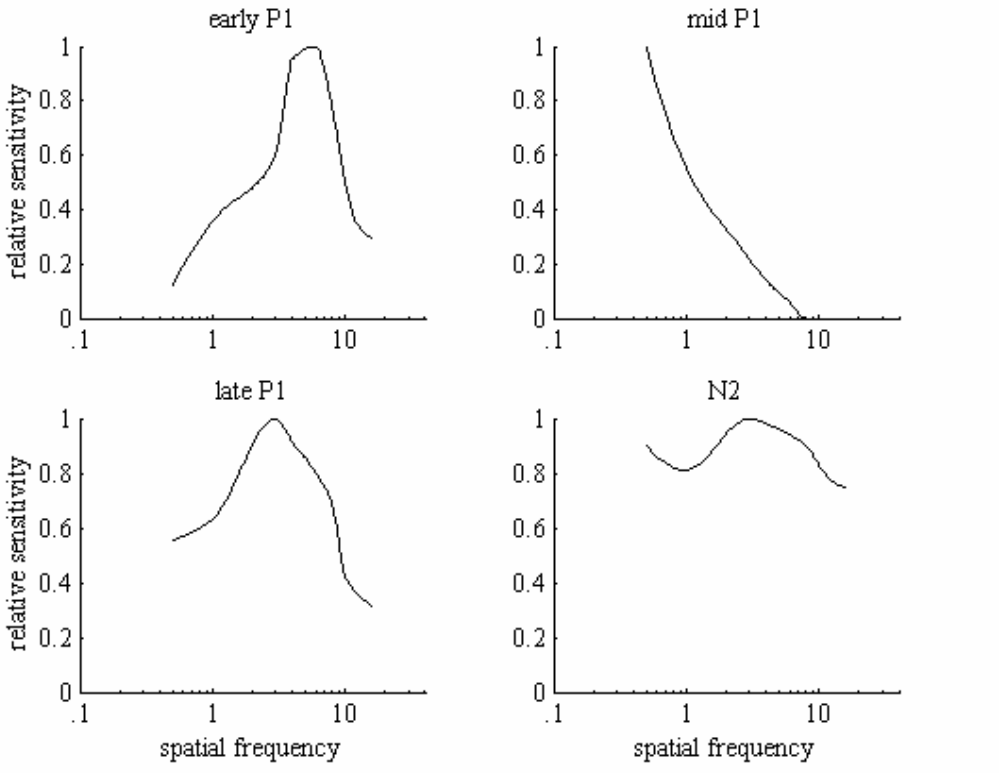

Figure 4.19: Relative spatial frequency sensitivity values for the early, mid, and late latency P1 and the N2 components used in the model to produce results corresponding to the right-handed group data.

Table 4.8: Dipole Spatial Frequency Sensitivity - Right-Handed Condition

spatial frequency f_{sp} (cpd)	*early latency P1* S^R ($=S^L$)	*mid latency P1* S^R ($=S^L$)	*late latency P1* S^R ($=S^L$)	*N2* S^R ($=S^L$)
0.5	0.12	1.00	0.58	0.90
1	0.36	0.55	0.63	0.81
3	0.60	0.22	1.00	1.00
4	0.95	0.14	0.92	0.98
6	1.00	0.06	0.80	0.94
8	0.77	0	0.68	0.90
10	0.50	0	0.42	0.83
12	0.36	0	0.37	0.78
16	0.30	0	0.32	0.75

The potential validity of the hypothesis was examined by computing (using the same methodology) the spatial frequency amplitude functions for the left hemisphere using a reduced value for the maximum amplitude of the early P1 dipole as shown in Table 4.7 ($A_{max}{}^L$). No change was made in the maximum amplitude values of the other dipoles or in any of the dipole sensitivity functions, including that for the early P1 dipole. As shown in Figure 4.20, the reduction in the amplitude of the early P1 dipole was sufficient to produce model results that are qualitatively similar to the empirical data for the left hemisphere. In particular, the left hemisphere shows little sensitivity to spatial and temporal frequency in

comparison with the right hemisphere. Furthermore, the model results for the two hemispheres exhibit the same lateralization patterns as seen in the empirical data. Specifically, low temporal frequency amplitudes are right lateralized and high temporal frequency amplitudes are left lateralized with a reduced lateralization effect at the spatial frequency extremes. These results suggest that asymmetry in the maximum amplitude of the early P1 component is sufficient to explain the essential difference in VEP amplitudes as a function of the spatial and temporal frequency of the stimulus in the right-handed group.

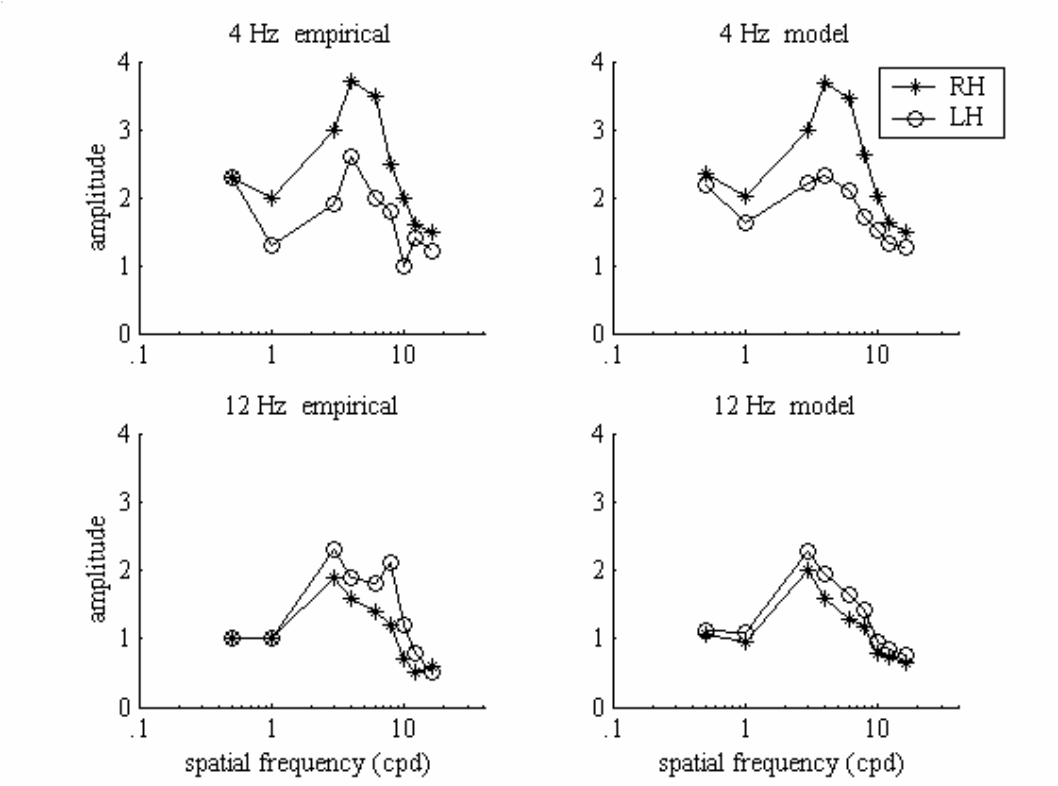

Figure 4.20: For the right-handed condition, empirical data and model results for low (4 Hz) and high (12 Hz) temporal frequency stimuli for both right (RH) and left (LH) hemispheres. Empirical data is taken from Rebai et al. (1989). Model results were obtained with mid P1, late P1 and N2 maximum amplitudes of 1.8, 7.0, and -7.4, respectively, in both hemispheres, and early P1 maximum amplitude of 2.9 in the right and 1.3 in the left hemisphere. Sensitivity functions for all dipoles were symmetric.

To investigate the hypothesis that asymmetry in the spatial frequency sensitivity of the early P1 component can produce the lateralization effects observed in the left-handed group, the spatial frequency sensitivity functions for each dipole, together with the maximum amplitude values, were again manually tuned until the model results closely resembled the empirical data for the right hemisphere. The maximum amplitude values resulting from this process are

shown in Table 4.9. The resulting dipole sensitivity functions are shown in Figure 4.21, with the function values for spatial frequencies used as the stimulus frequency f_{sp} in the model wave computations provided in Table 4.10 (S^R). The parameter values shown in Tables 4.9 and 4.10 for the right hemisphere were used to compute transient waves (based on Equations 4.4 and 4.6) for every spatial frequency listed in Table 4.10. Again, Fourier transforms of the resulting transient wave were performed to evaluate the temporal frequency amplitude function at the frequencies 4 and 12 Hz. The close match between the model results obtained using these parameter values and the empirical data for the right hemisphere can be seen in the graphs displayed in Figure 4.22.

Table 4.9: Model Parameter Values for Left-Handed Condition

dipole k	*latency* (ms) $t_{lat}(3)$	*max amplitude* $A\max^R (= A\max^L)$
early latency P1	105	2.6
mid latency P1	115	1.5
late latency P1	135	7.7
N2	148	-8.3

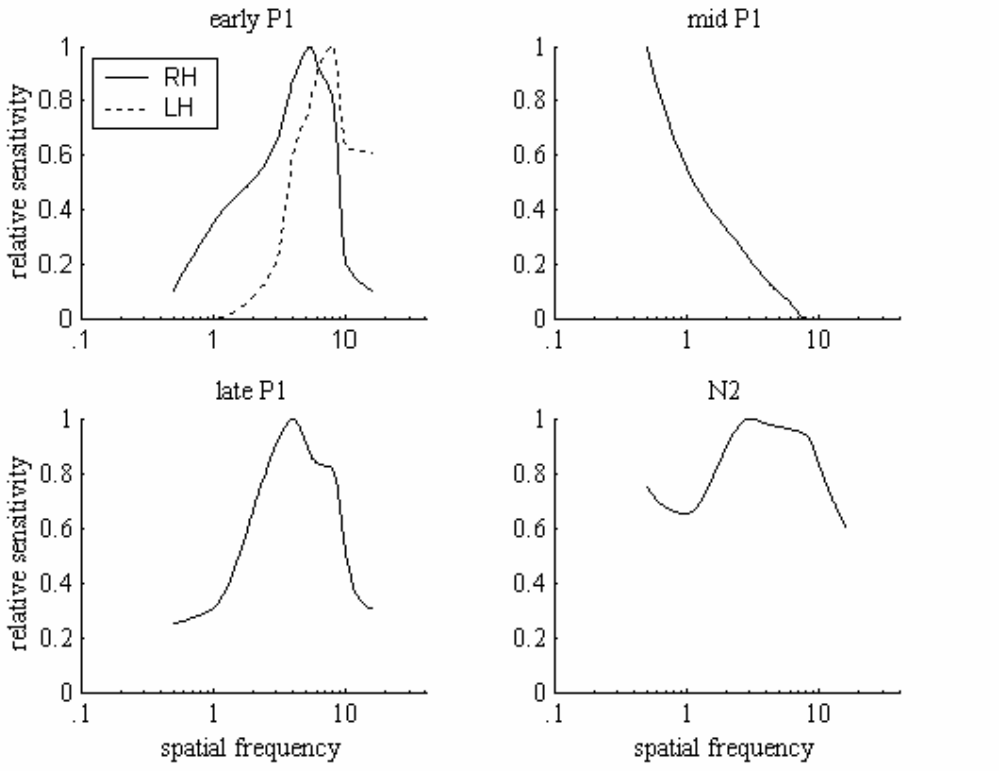

Figure 4.21: Relative spatial frequency sensitivity values used in the model to produce results corresponding to the left-handed group data. Early P1 sensitivity is asymmetric with the left hemisphere (LH) sensitivity function tuned toward higher spatial frequencies than the right hemisphere (RH) function. The sensitivity functions for the mid P1, late P1, and N2 components are the same for both hemispheres.

Table 4.10: Dipole Spatial Frequency Sensitivity - Left-Handed Condition

spatial frequency f_{sp} (cpd)	*early latency P1* S^R	S^L	*mid latency P1* S^R ($=S^L$)	*late latency P1* S^R ($=S^L$)	*N2* S^R ($=S^L$)
0.5	0.10	0	1.00	0.26	0.75
1	0.35	0	0.55	0.31	0.65
3	0.64	0.20	0.22	0.90	1.00
4	0.87	0.60	0.14	1.00	0.98
6	0.94	0.90	0.06	0.84	0.96
8	0.80	1.00	0	0.82	0.94
10	0.20	0.63	0	0.51	0.83
12	0.15	0.62	0	0.36	0.73
16	0.10	0.61	0	0.31	0.60

The potential validity of the hypothesis was examined by tuning the early P1 sensitivity function so that the model results for amplitude as a function of spatial frequency for temporal frequency 4 Hz closely resemble the empirical data for the left hemisphere. If the hypothesis is correct, then the tuning process should produce a change in the early P1 dipole sensitivity function that is consistent with a difference in the part of the visual field in which it originates. Furthermore, the model results for amplitude as a function of spatial frequency for temporal frequency 12 Hz should qualitatively resemble the empirical data for the left hemisphere.

The resulting early P1 dipole sensitivity function is shown in Figure 4.21 (LH in early P1 graph). The early P1 sensitivity function values for spatial frequencies used as the stimulus frequency f_{sp} in the model wave computations are also provided in Table 4.10 (*early latency P1*, S^L). As predicted, the early P1 dipole sensitivity function for the left hemisphere differs from that for the right hemisphere in a manner consistent with a difference in the field of origin. Specifically, the function shifts toward higher spatial frequencies for the left hemisphere, consistent with an early P1 dipole source that originates in a more central part of the visual field.

As shown in Figure 4.22, the model results obtained for the left hemisphere (using the same methodology and the left hemisphere sensitivity values) closely resemble the empirical data for 4 Hz temporal frequency condition, especially for spatial frequencies above 1 cpd. The model results for the 12 Hz condition are also qualitatively similar to the empirical data. For both model results and experimental data, the spatial frequency amplitude function is right lateralized for spatial frequencies below 7cpd and left lateralized for spatial frequencies above 7cpd in the low (4 Hz) temporal frequency condition. For the high (12 Hz) temporal frequency condition, lateralization of the spatial frequency amplitude function is minimal in both the model results and the empirical data. The model results exhibit slightly lateralized amplitudes in the reverse direction from those obtained at 4 Hz, that is, amplitudes that are left lateralized for spatial frequencies below 7cpd and right lateralized for spatial frequencies above 7cpd.

Although the empirical data exhibit a somewhat more variable lateralization pattern for frequencies below 7 cpd, they are similarly right lateralized for frequencies above 7 cpd. These results suggest that asymmetry in the spatial frequency sensitivity of the early P1 component is sufficient to explain the essential difference in VEP amplitudes as a function of the spatial and temporal frequency of the stimulus in the left-handed group.

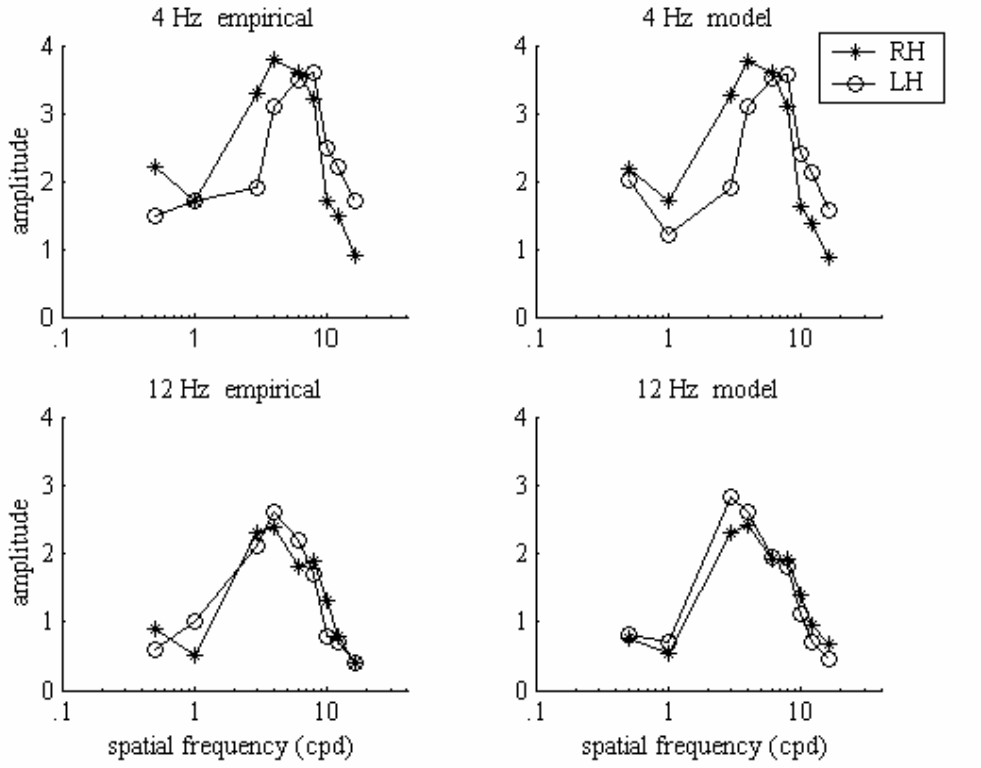

Figure 4.22: For the left-handed condition, empirical data and model results for low (4 Hz) and high (12 Hz) temporal frequency stimuli for both right (RH) and left (LH) hemispheres. Empirical data were taken from Rebai et al. (1989). Model results were obtained with early P1, mid P1, late P1 and N2 maximum amplitudes of 2.6, 1.5, 7.7, and -8.3, respectively, in both hemispheres. Asymmetric sensitivity functions were used for the early P1 component. Sensitivity functions for all other components were symmetric.

4.3.5 Early P1 Asymmetry and Other Lateralization Effects

The lateralization effects observed in the later Rebai et al. (1993, 1997, and 1998) experiments are also explained by the early latency P1 amplitude asymmetry hypothesis. Because the early P1 dipole originates in an area that processes the central visual field, it can be expected to display characteristics that are consistent with a strong contribution from the parvocellular (sustained) system. If pattern onset stimulation activates the parvocellular (sustained) system more efficiently than pattern reversal stimulation, as argued in Rebai et al. (1993), then the amplitude of the early P1 dipole should be enhanced by pattern onset stimulation for patterns of medium-to-high spatial frequency. When the enhanced amplitude of the early P1 dipole is large enough to dominate the P1 amplitude, P1 amplitude should be increased by the use of pattern onset stimulation. When the enhanced amplitude of the early P1 dipole is not large enough to dominate, P1 amplitude should be minimally affected by the use of pattern onset stimulation.

In the case of right-handers, the study hypothesis suggests that the former scenario is more likely to occur in the right hemisphere and the latter in the left hemisphere, a situation akin to that depicted in Figure 4.8. Thus, the use of onset stimulation in right-handers should produce a right-lateralized enhancement of amplitude measurements involving P1, as observed in Rebai et al. (1993). Because the early P1 dipole is more sensitive to spatial frequency than the other P1 dipoles, asymmetry in the dominance of the early P1 dipole should also result

in greater sensitivity to spatial frequency in the right hemisphere in amplitude measurements involving the P1 component of the VEP. This effect was observed in Rebai et al. (1997). Furthermore, because the early P1 is the shortest latency dipole contributing to the P1 component, the asymmetry should result in earlier mean P1 latencies in the right hemisphere for all but the lowest spatial frequencies, as was observed in Rebai et al. (1998).

In the case of left-handers, the study hypothesis suggests that the amplitude of the early P1 dipole is likely to dominate the P1 component amplitude in both hemispheres. Consequently, greater sensitivity to spatial frequency should be displayed by both hemispheres in response to onset stimulation. This effect was observed in Rebai et al. (1997) and was more clearly present in the subgroup of left-handers with a family history of left-handedness.

4.4 Discussion

The results of this study support the hypothesis that asymmetry in the early latency P1 dipole amplitude due to anatomical asymmetry in the vicinity of the occipital poles is the primary cause of apparent lateralization in frequency processing observed in the Rebai experiments. The model results demonstrate that greater early P1 amplitude in the right hemisphere can produce temporal frequency lateralization effects similar to those observed in right-handed subjects. In addition, the model results show that such amplitude asymmetry is consistent with the observed earlier P1 latency and greater spatial frequency sensitivity (as

reflected in VEP amplitude) for the right hemisphere of right-handed subjects. The model results also indicate that asymmetry in the spatial frequency sensitivity of the early P1 dipole can account for the spatiotemporal frequency lateralization effects observed in left-handed subjects. The early P1 amplitude asymmetry posited in the case of right-handers is consistent with the presence of morphological asymmetry in the form of left occipital petalia. The asymmetry in early P1 spatial frequency sensitivity posited in the case of left-handers is consistent with the presence of topological asymmetry at the occipital pole in the absence of morphological asymmetry.

The hypothesis of early P1 amplitude asymmetry due to anatomical asymmetry can also explain the findings of other studies that used VEP methodology to investigate the spatial frequency hypothesis (Proverbio et al., 1996; Zani & Proverbio, 1995). In these studies, the P1 component was observed at lateral occipital sites over both the right and left hemispheres following central visual field stimulation in pattern onset mode for groups of right-handed subjects. In the Zani and Proverbio experiment, significantly greater P1 amplitudes with latencies of approximately 95 ms were observed over the right hemisphere for spatial frequencies of 3, 4.5, and 6 cpd. Similarly, the Proverbio et al. investigation found that P1 was of greater amplitude and earlier latency (~90 ms) over the right hemisphere for spatial frequencies of 1.5, 3, 6 and 12 cpd.

The hypothesis that the amplitude of the early P1 dipole is asymmetric, and that the asymmetry is attributable to anatomical asymmetry, finds support in

the Blumhardt et al. (1989) investigation of the effect of field size on the pattern reversal VEP. This study observed that stimulation of the right or left half-fields produces an ipsilateral N1-P1-N2 wave complex and a contralateral iN1-iP1-iN2 wave complex of inverted polarity (indicated by the prefix "i") with similar latencies for corresponding components (N75-P100-N145 and P75-N105-P135, respectively). Reduction of the stimulus field size was accompanied by a marked reduction of amplitudes in the contralateral components, with a lesser reduction in the ipsilateral amplitudes, and was most pronounced for the P100 and N105 components. As field size was reduced, the topographical distribution of the P100 component (corresponding to the early latency P1) changed, spreading to the contralateral scalp in the majority of subjects, although contralateral sites generally retained a negative potential even for a field size of 5 ° radius. The Blumhardt study hypothesized that a redistribution of the P100 with the reduction of field size would be observed for a hemisphere in which the location of P100 dipole sources shifts outward and laterally (from the medial cortex to the occipital pole, and then to the lateral cortex) as the visual field of the source changes from peripheral to central. Thus, for central field presentation, medial sources of the P100 (which also generate the contralateral N105) yield to pole and lateral sources that reduce, and possibly even invert the polarity of, the N105 resulting in greater positive amplitude of the P1 component in the 100-105 ms timeframe. Variations in the redistribution of the P100 among subjects and between hemispheres within a single subject would then reflect anatomical differences

affecting the locations of the P100 dipole sources. Substantial interindividual and interhemispheric differences in P100 redistribution patterns were observed that suggest a high degree of anatomical variability and possibly some degree of systematic hemispheric asymmetry.

The existence of significant interindividual variation in P100 anatomy is confirmed in a study (Brecelj et al., 1998) that examined the effect of field size on both visual evoked magnetic field and VEP measurements. This study used source analysis combined with MRI imaging to estimate dipole locations; however, no data on interhemispheric variation were obtained as effects were observed for the right hemisphere only. The observed sensitivity of the P100 to the visual field of the stimulus is consistent with the considerable effect that visual field has on both transient and steady-state VEP amplitudes as measured at lateral occipital sites (Mecacci & Spinelli, 1987; Mecacci, Spinelli & Viggiano, 1990).

Several predictions follow from the study hypothesis that can be tested empirically. First, the degree and direction of temporal frequency lateralization exhibited in VEP amplitudes, measured at lateral occipital sites (PO_7 and PO_8) in response to pattern-reversal stimuli of medium-to-high spatial frequency (~2 to12 cpd) present in the central visual field (~ 6°), should correlate with the degree and direction of occipital petalia. Similarly, the degree and direction of P1 latency differences observed in response to such stimulation presented in the pattern onset mode should correlate the degree and direction of occipital petalia. These predictions further imply that the degree and direction of P1 latency differences

observed in response to pattern onset stimulation should correlate with the degree and direction of temporal frequency lateralization exhibited in VEP amplitudes.

The hypothesis proposed in this study conflicts with the researchers' interpretation of empirical data as evidence of hemispheric specialization in the Rebai studies. In particular, the Rebai studies proposed that, in right-handers, the right hemisphere specializes in the processing of low temporal frequencies, spatial frequency information, and the output of the parvocellular (sustained) system, while the left hemisphere specializes in the processing of high temporal frequencies and the output of the magnocellular (transient) system. The analysis presented in this study, however, supports the contention that the apparent specialization is an artifact of anatomically-based asymmetry in the early P1 component. *Therefore, no conclusions regarding hemispheric specialization can be validly drawn on the basis of the Rebai experiments*.

The results of this study raise serious questions regarding past findings on hemispheric specialization in visual frequency processing that have been based on VEP methodology. Furthermore, the results suggest that the use of VEP methodology in lateralization research, particularly as it relates to temporal frequency processing, may be problematic. Thus, the results support the view, advanced by some researchers in the field of electroencephalography (Myslobodsky & Bar-Ziv, 1989; Myslobodsky, Coppola, & Weinberger, 1991; Myslobodsky, Glicksohn et al., 1991), that anatomical asymmetry may lead to ambiguity in the interpretation of VEP lateralization data, especially in the case of

data related to central visual field stimulation. This ambiguity may be reduced by obtaining structural and functional imaging data in conjunction with the electrophysiological data in lateralization investigations. The imaging data could be used to improve the symmetry of electrode placement with respect to the underlying cortical structures. It would also provide a means of assessing the potential impact of anatomical asymmetry on the electrophysiological measurements. The findings of this study suggest such assessment is a necessary step in establishing the validity of lateralization research based on electrophysiological experiments.

Chapter 5

Conclusion

This chapter begins with a summary of the research that has been presented in the previous chapters. Next, theoretical predictions that arise from the study hypotheses are discussed. Finally, the implications of the study findings are considered with respect to lateralization in frequency processing beyond the spatial domain within the visual system.

5.1 Research Summary

In this study, I developed a hypothesis about the origin and nature of spatial frequency lateralization that is grounded in the biology of the visual system, and demonstrated its potential validity using a neural network model. The lateralization is characterized as a right hemisphere advantage for low spatial frequencies, and a left hemisphere advantage for high spatial frequencies, in the processing of a visual stimulus beyond its initial processing in the primary visual cortex (V1). The hypothesis proposes that differences in the time course of maturation for the magnocellular and parvocellular pathways, in combination with asynchronous development of the right and left cortical hemispheres, can produce

lateralized spatial frequency processing. The hypothesis is based on evidence that the contribution of the parvocellular pathway to V1 spatial filters (relative to that of the magnocellular pathway) increases as filter preferred frequency increases, and that parvocellular pathway maturation is protracted in comparison to magnocellular pathway maturation in the neonate. This implies that high frequency filters take longer to mature than low frequency filters. Consequently, high frequency filters should compete more effectively for downstream connections in the visual cortex (against low frequency filters) as the maturation gap between the pathways closes. If neonatal development of the left hemisphere development lags that of the right hemisphere, as also suggested by empirical evidence, then high frequency filters should develop stronger connectivity at the expense of low frequency filters in the later developing left hemisphere, resulting in lateralized frequency processing. The model simulations performed in this study showed that the assumed developmental conditions could produce the predicted asymmetry in filter connectivity and the associated spatial frequency lateralization.

Model simulations also showed that for intermediate frequencies, the direction of lateralization could change as a function of visual field eccentricity. This occurs because the spatial frequency spectrum represented by the V1 filters associated with a visual field location shifts to a lower range with increasing visual field eccentricity. Thus, certain intermediate frequencies fall in the lower part of the range represented near the fovea, but in the higher part of the range

represented in the periphery. On the basis of these results, I formulated a hypothesis about the neural basis of the relative frequency lateralization effect and illustrated its potential validity using a theoretical model.

The relative frequency lateralization effect is characterized as a right hemisphere advantage in the processing of a component of intermediate frequency if its frequency is low relative to the other frequencies contained in a stimulus, and a left hemisphere advantage if its frequency is high relative to the other frequencies. The hypothesis proposes that the interaction of eccentricity-dependent frequency lateralization and task-driven spatial attention can produce such an effect. The hypothesis is based on evidence that for tasks that involve the processing of relatively high spatial frequencies, spatial attention may be directed to the less eccentric portion of the presentation area, where representation of high frequencies is most robust. Similarly, for tasks that involve the processing of relatively low spatial frequencies, spatial attention may be directed to the more eccentric portion of the presentation area. If spatial attention amplifies the signal from the attended area while suppressing the signal from the unattended area of a stimulus, as empirical evidence suggests, then the area to which attention is directed during task performance should determine the lateralization associated with the processing a stimulus component of intermediate frequency. Thus, the direction of lateralization could change depending on the frequency characteristics of the stimulus and the requirements of the task.

In constructing the computational model demonstrating the basis of asymmetric development and lateralized spatial frequency processing, and the theoretical model illustrating the basis of the relative frequency lateralization effect, I specified both models in terms of neural structures and processes in the visual system. By providing this biological specification, I effectively made two theories, which previously were developed only at an abstract level, operational: namely, the Hellige (1993) theory on lateralized spatial frequency development and the Ivry and Robertson (1998) DFF theory of relative frequency lateralization (as applied to the visual system). Hence, the models can be viewed as evidence that supports the plausibility of these theories.

In investigating the nature of the hard-wired asymmetry that developed in the simulation experiments, I found that the asymmetry exhibited a hemispheric bias based primarily on spatial frequency. However, I also found evidence of a secondary bias related to visual pathway: specifically, a slight right hemisphere bias toward the output of the magnocellular pathway, and a slight left hemisphere bias toward the output of the parvocellular pathway. This pathway bias is opposite in direction from that proposed by other researchers to explain the effects observed in certain electrophysiological investigations on frequency processing lateralization. I addressed this contradiction through the development of a hypothesis on the neural basis of the electrophysiological lateralization effects that effectively eliminates the conflict. In particular, I proposed that the effects observed in the electrophysiological experiments arise from gross anatomical

asymmetries in the vicinity of the occipital poles rather than from actual processing differences. In support of this contention, I used a computational model of the dipole potential-VEP wave relationship to demonstrate that dipole asymmetry attributable to anatomical differences could produce the observed lateralization effects.

5.2 Theoretical Predictions

My hypothesis on the development of spatial frequency lateralization leads to two predictions that may lend themselves to empirical testing. Both are predicated on the condition that an experiment based on the identification of a low versus a high frequency sinusoidal grating produces results consistent with the spatial frequency hypotheses in the subjects comprising the test group. First, a frequency identification experiment employing a range of frequencies should produce right lateralization of low frequencies, and left lateralization of high frequencies, that increases on either side of a cross-over point, and then diminishes or reverses towards the frequency extremes. Second, this type of testing should reveal a change in the spatial frequency lateralization function with increasing eccentricity such that the cross-over lateralization point shifts to lower frequencies. Verification of these predictions is of interest because it provides support not only for the specific theory of spatial frequency lateralization proposed in this study, but also more generally for the developmental paradigm on which it is based. That is, it supports the hypothesis that asynchronous

maturation of homologous regions of the hemispheres interacts with the developmental timing of systems that provide input to those regions to produce lateralized functionality.

The predictions that follow from the study hypothesis on the neural basis of the electrophysiological lateralization effects have already been delineated (see Section 4.4). They essentially are specifications of the basic prediction that a correlation exists between the degree and direction of occipital petalia and the degree and direction of lateralization exhibited in certain electrophysiological measurements. Verification of this prediction is of interest as it would greatly affect the interpretation of electrophysiological results in the study of lateralization in visual pattern processing, and could raise questions, in general, regarding the use of electrophysiological methodology in lateralization research.

5.3 Implications of Findings

5.3.1 Temporal Frequency Processing

In discussions of temporal processing lateralization, the results of the Rebai et al. (1986, 1989) electrophysiological experiments are cited as key evidence of left hemisphere dominance in the processing of high temporal frequencies (i.e., in temporal resolution) in the visual domain. In this study, I have proposed a hypothesis on the neural basis of the lateralization effects observed in these experiments that implies that their use as evidence of temporal frequency processing lateralization is invalid. Psychophysical evidence related to the

processing of fine temporal information in the visual domain is inconsistent in its support of a left hemisphere advantage (for review, see Nicholls, 1996). Consequently, any discounting of the electrophysiological evidence significantly weakens support for a general theory of left hemisphere superiority in the processing of high temporal frequencies that encompasses all domains and derives from a common mechanism (Nicholls, 1996).

5.3.2 Auditory Frequency Processing

The DFF theory suggests that common processes or mechanisms are involved in amplifying low frequencies in the right hemisphere and high frequencies in the left hemisphere for the spectral domains of both visual (spatial frequency) and auditory (pitch) processing (Ivry & Robertson, 1998; Robertson & Ivry, 2000). Although the hypotheses developed in this study explain how the DFF theory could be implemented in the visual system and how the asymmetry at the heart of that implementation could develop, the auditory system counterparts of the essential visual system elements, and therefore, the common processes or mechanisms, are not obvious. For example, in the visual cortex, the hard-wired asymmetry arises from competition among filter outputs at each retinotopic location that collectively represent virtually the entire spatial spectrum. In the auditory cortex, however, the tonotopic mapping of the spectral filters suggests that such direct competition between outputs representing the low and high ends of the spectrum is improbable. Still, it is possible that competition between

outputs representing the low and high ends of the range of spectral frequencies represented at each location in the tonotopic map produces a local hard-wired asymmetry that lateralizes frequency processing around the mid-point of the represented range. If so, then attention directed to the place in the tonotopic map where a particular frequency is maximally represented could produce lateralized processing of frequencies immediately above and below the attended frequency that is oppositely directed in the two hemispheres. This sort of lateralization was observed in the experiments of Ivry and Lebby (1993).

In any case, it is conceivable that the same basic forces, that is, asynchronous hemispheric development coupled with differences in the timing of development of systems providing input to the spectral filters in the cortex, can explain spectral frequency lateralization in audition. It is also possible that such processes underlie the development of lateralization in the processing of temporal frequency information within the auditory system. The development of hypotheses addressing these possibilities presents an interesting topic for future research.

5.4 Main Conclusions

Several major conclusions can be drawn on the basis of the results of this investigation:

1. *Developmental conditions can interact to produce a hard-wired asymmetry that affects the processing of spatial frequencies.* Specifically, a lag in the development of the left hemisphere relative to that of the right hemisphere could interact with the later maturation of the parvocellular pathway relative to that of the magnocellular pathway to produce right-lateralized processing of low frequencies and left-lateralized processing of high frequencies.

2. *The resulting hard-wired asymmetry is consistent with the relative, as well as the absolute, frequency lateralization effects that have been observed in psychophysical experiments.* The relative frequency lateralization effects can be explained by the interaction of eccentricity-dependent differences in the hard-wired asymmetry (predicted by the development model) and the direction of spatial attention to the eccentricity within the visual field of the stimulus that optimizes task performance.

3. *Lateralization effects observed in electrophysiological experiments employing central visual field stimuli can be explained by hemispheric differences in the amplitude of the potential generated by the activated dipoles located on or near the occipital pole as measured at lateral-occipital sites.* Such amplitude differences can result from asymmetry in the mirror dipole sources located in the vicinity of the occipital poles that

are associated with central visual field processing. The asymmetry results from morphological and topological asymmetries that affect the orientation and location of these dipoles. The amplitude differences can account for the apparent lateralization of steady-state wave amplitudes as well as the apparent hemispheric differences in transient wave amplitudes and latencies. Thus, for electrophysiological experiments employing central visual field stimuli, the interpretation of the results as evidence of hemispheric specialization is invalid.

4. *There is no inherent conflict between the findings of the psychophysical experiments and those of the electrophysiological experiments.* The lateralization effects observed in the psychophysical experiments reflect actual differences in hemispheric processing that can be explained by microanatomical asymmetries. The lateralization effects observed in the electrophysiological experiments do *not* reflect actual differences in hemispheric processing. Rather, they are apparent differences that can be explained by gross anatomical asymmetries in the hemispheres. The apparent lateralization effects may even mask the effects of actual hemispheric processing differences in electrophysiological experiments.

5.5 Final Comments

This investigation has provided evidence in support of a paradigm of asymmetric development that can potentially account for lateralization on a broad scale. In this paradigm, asynchronous development of homologous cortical regions results in asymmetry if three conditions apply: 1) multiple pathways supply distinctive input to these regions, 2) the input pathways differ from one another in their time course of maturation, 3) at least one input pathway is still maturing during the time of the regions' development. Evidence suggests that homologous cortical regions are subject to asynchronous development throughout the entire twenty year span of cortical maturation. It seems probable that the conditions delineated above occur for many cortical systems and occur repeatedly throughout the course of cortical development. If so, asynchronous development of homologous cortical regions could be a powerful force driving the hemispheres toward functional specialization.

This investigation has also provided evidence that the use of electrophysiological methodology in lateralization research is problematic. Interpretation of the results of such experiments as evidence of hemispheric specialization is valid if and only if the potential-generating dipole source pairs are anatomically symmetric with respect to the measurement locations. Anatomical findings suggest that a significant violation of the symmetry assumption is likely in the case of occipital pole dipole pairs, and some deviation from anatomical symmetry seems likely affect dipole pairs throughout the cortex.

Consequently, any meaningful interpretation of lateralization effects observed in electrophysiological experiments must be grounded in an assessment of anatomical asymmetry and its potential impact on the results.

Appendix A

Implications of the Steady-State Linearity Assumption

The assumption that steady-state VEP waves represent the linear summation of a series of transient VEP waves (Assumption 2 in Section 4.2.2) has a useful implication that is exploited in the modeling investigation of Chapter 4. Specifically, it implies that the relative amplitudes of the second harmonic component of the two steady-state waves generated in response to a pattern reversal stimulus of the same temporal frequency is equivalent to the relative amplitudes of that frequency component in their underlying transient waves. The mathematical basis of this equivalence is as follows.

If the transient VEP wave generated in response to a stimulus presented at time 0 is given by the function $v(t)$, then, under the assumption of linearity, the steady-state VEP wave generated by N reversals of the stimulus, counter-phase modulated at the temporal frequency f_{tp}, is represented as:

$$ss(t) = \sum_{n=0}^{N} v(t - n/2f_{tp}) \qquad \text{(A.1)}$$

The Fourier transform of the steady-state VEP wave $ss(t)$ is then given by:

$$SS(f) = \mathsf{F}(ss(t)) = \mathsf{F}\left(\sum_{n=0}^{N} v(t - n/2f_{\text{tp}})\right) \tag{A.2}$$

The linear property of the Fourier transform allows this to be reformulated as

$$SS(f) = \mathsf{F}(ss(t)) = \sum_{n=0}^{N} \mathsf{F}(v(t - n/2f_{\text{tp}})) \tag{A.3}$$

If the Fourier transform of the transient wave given by $v(t)$ is $V(f) = \mathsf{F}(v(t))$, then by the shifting property of the Fourier transform,

$$\mathsf{F}(v(t - n/2f_{\text{tp}})) = V(f)e^{-i2\pi fn/2f_{\text{tp}}} \tag{A.4}$$

Thus,

$$SS(f) = \mathsf{F}(ss(t)) = \sum_{n=0}^{N} V(f)e^{-i2\pi fn/2f_{\text{tp}}} \tag{A.5}$$

$$= V(f)\sum_{n=0}^{N} e^{-i2\pi fn/2f_{\text{tp}}} \tag{A.6}$$

Therefore, the ratio of the Fourier transforms for two steady-state waves, SS_1 and SS_2, generated at the same temporal frequency but with underlying transient waves V_1 and V_2, is equal to the ratio of the Fourier transforms of their underlying transient waves, that is:

$$\frac{SS_1(f)}{SS_2(f)} = \frac{V_1(f)}{V_2(f)} \tag{A.7}$$

Consequently, the ratio of the amplitude spectrum values for the steady state waves is equal to the ratio of the amplitude spectrum values for the underlying transient waves as given by:

$$\frac{|SS_1(f)|}{|SS_2(f)|} = \frac{|V_1(f)|}{|V_2(f)|} \tag{A.8}$$

Therefore, the ratio of the relative amplitudes of the second harmonic component of the two steady-state waves is equivalent to the ratio of the relative amplitudes of that frequency component in their underlying transient waves, that is,

$$\frac{|SS_1(2f_{\text{tp}})|}{|SS_2(2f_{\text{tp}})|} = \frac{|V_1(2f_{\text{tp}})|}{|V_2(2f_{\text{tp}})|} \tag{A.9}$$

Thus, the temporal frequency amplitude functions (for definition, see Footnote 25 in Section 4.2.3) associated with transient waves V_1 and V_2 can be compared simply by comparing the amplitude spectra of the transient waves themselves.

Bibliography

Abe, Y., & Kuroiwa, Y. (1990). Amplitude asymmetry of hemifield pattern reversal VEPs in healthy subjects. *Electroencephalography and clinical neurophysiology, 77,* 81-85.

Abel, P.L., O'Brien, B.J., & Olavarria, J.F. (2000). Organization of callosal linkages in visual area V2 of macaque monkey. *The Journal of Comparative Neurology, 428,* 278-293.

Allison, J.D., Melzer, P., Ding, Y., Bonds, A.B., & Casagrande, V.A. (2000). Differential contributions of magnocellular and parvocellular pathways to the contrast response of neurons in bush baby visual cortex (V1). *Visual Neuroscience, 17,* 71-76.

Amunts, K., Malikovic, A., Mohlberg, H., Schormann, T., & Zilles, K. (2000). Brodmann's areas 17 and 18 brought into stereotaxic space – where and how variable? *NeuroImage, 11,* 66-84.

Arroyo, S., Lesser, R.P., Poon, W., Webber, W.R.S., & Gordon, B. (1997). Neuronal generators of visual evoked potentials in humans: Visual processing in the human cortex. *Epilepsia, 38,* 600-610.

Azzopardi, P., Jones, K.E., & Cowey, A. (1999). Uneven mapping of magnocellular and parvocellular projections from the lateral geniculate nucleus to the striate cortex in the macaque monkey. *Vision Research, 39,* 2179-2189.

Baas, J.M.P., Kenemans, J.L., & Mangun, G.R. (2002). Selective attention to spatial frequency: An ERP source localization analysis. *Clinical Neurophysiology, 113,* 1840-1854.

Baker, D.P., Chabris, C.F., & Kosslyn, S.M. (1999). Encoding categorical and coordinate spatial relations without input-output correlations: New simulation models. *Cognitive Science, 23*, 33-51.

Banks, M.S., & Dannemiller, J.L. (1987). Infant visual psychophysics. In P. Salapatek & L. Cohen (Eds.), *Handbook of infant perception*: *Vol. 1* (pp. 115-184). London: Academic Press, Inc.

Best, C.T. (1988). The emergence of cerebral asymmetries in early human development: a literature review and a neuroembryological model. In D.L. Molfese & S.J. Segalowitz (Eds.). *Brain lateralization in children* (pp. 1-34). New York: The Guilford Press.

Blumhardt, L.D., Barrett, G., Halliday, A.M., & Kriss, A. (1989). The effect of field size on the pattern reversal visual evoked response (PRVER). *Clinical Vision Sciences, 4,* 27-40.

Boynton, G.M., & Hedgé, J. (2004). Visual cortex: The continuing puzzle of area V2. *Current Biology, 14,* R523-R524.

Bracco, L., Tiezzi, A., Ginanneschi, A., Campanella, C., & Amaducci, L. (1984). Lateralization of choline acetyltransferase (Ch.AT) activity in foetus and adult human brain. *Neuroscience Letters, 50,* 301-305.

Brecelj, J., Kakigi, R., Koyama, S., & Hoshiyama, M. (1998). Visual evoked magnetic responses to central and peripheral stimulation: Simultaneous VEP recordings. *Brain Topography, 10,* 227-237.

Brefcznski, J.A., & DeYoe, E.A. (1999). A physiological correlate of the 'spotlight' of attention. *Nature Neuroscience, 1999,* 370-374.

Brown, J.W., & Jaffe, J. (1975). Note: Hypothesis on cerebral dominance. *Neuropsychologia, 13,* 107-110.

Burkhalter, A. (1993). Sequential development of intracortical processing channels in human visual cortex. In B. Gulyas, D. Ottoson, & P.E. Roland (Eds.), *Functional organisation of the human visual cortex* (pp. 151-163). Oxford: Permagon Press Ltd.

Cave, K.R., & Bichot, N.P. (1999). Visuospatial attention: Beyond a spotlight model. *Psychonomic Bulletin and Review, 6,* 204-223.

Chi, J.G., Dooling, E.C., & Gilles, F.H. (1977). Gyral development of the human brain. *Annals of Neurology, 1,* 86-93.

Chiron, C., Jambaque, I., Nabbout, R. Lounes, R., Syrota, A., & Dulac, O. (1997). The right hemisphere is dominant in human infants. *Brain, 120,* 1057-1065.

Christman, S. D. (1997). Hemispheric asymmetry in the processing of spatial frequency: Experiments using grating and bandpass filtering. In S. Christman (Ed.). *Cerebral asymmetries in sensory and perceptual processing* (pp. 3-30). Amsterdam: Elsevier Science B.V.

Christman, S., Kitterle, F. L., & Hellige, J.B. (1991). Hemispheric asymmetry in the processing of absolute versus relative spatial frequency. *Brain and Cognition, 16*, 62-73.

Chui, H.C., & Damasio, A.R. (1980). Human cerebral asymmetries evaluated by computed tomography. *Journal of Neurology, 43,* 873-878.

Connolly, M., & Van Essen, D. (1984). The representation of the visual field in parvicellular and magnocellular layers of the lateral geniculate nucleus in the macaque monkey. *The Journal of Comparative Neurology, 226,* 544-564.

Cook, N.D. (1995). Correlations between input and output units in neural networks. *Cognitive Science, 19*, 563-574.

Cook, N.D., Fruh, H., & Landis, T. (1995). The cerebral hemispheres and neural network simulations: Design considerations. *Journal of Experimental Psychology: Human Perception and Performance, 21*(2), 410-422.

Corballis, M.C. (1991). *The lopsided ape.* New York: Oxford University Press.

Corballis, M.C., & Morgan, M.J. (1978). On the biological basis of human laterality: I. Evidence for a maturational left-right gradient. *The Behavioral and Brain Sciences, 2,* 261-269.

Crowell, D.H., Jones, R.H., Kapuniai, L.E., & Nakagawa, J.K. (1973). Unilateral cortical activity in humans: An early index of cerebral dominance? *Science, 180,* 205-208.

Davis, E.T. (1981). Allocation of attention: Uncertainty effects when monitoring one or two visual gratings of non-contiguous spatial frequencies. *Perception and Psychophysics, 29,* 618-622.

Davis, E.T., & Graham, N. (1981). Spatial frequency uncertainty effects in the detection of sinusoidal gratings. *Vision Research, 1981,* 705-712.

Dayan, P., & Abbott, L.E. (2001). *Theoretical neuroscience: Computational and mathematical modeling of neural systems.* Cambridge, MA: The MIT Press.

de Schonen, S., & Mathivet, E. (1989). First come, first served: A scenario about the development of hemispheric specialization in face recognition during infancy. *European Bulletin of Cognitive Psychology, 9,* 3-44.

Desimone, R., & Duncan, J. (1995). Neural mechanisms of selective visual attention. *Annual Reviews of Neuroscience, 18,* 193-222.

De Valois, R.L., Albrecht, D.G., & Thorell, L.G. (1982). Spatial frequency selectivity of cells in the macaque visual cortex. *Vision Research, 22,* 545-559.

De Valois, R.L., & De Valois, K.K. (1988). *Spatial vision*. New York, NY: Oxford University Press.

Di Russo, F., Martinez, A., Sereno, M.I., Pitzalis, S., & Hillyard, S.A. (2001). Cortical sources of the early components of the visual evoked potential. *Human Brain Mapping, 15,* 95-111.

Dobkins, K.R., Anderson, C.M., & Lia, B. (1999). Infant temporal contrast sensitivity functions (tCSFs) mature earlier for luminance than for chromatic stimuli: Evidence for precocious magnocellular development? *Vision Research, 39,* 3223-3239.

Dobkins, K.R., & Teller, D.Y. (1996). Infant motion: Detection (M:D) ratios for chromatically defined and luminance-defined moving stimuli. *Vision Research, 36,* 3293-3310.

Dobson, V., & Teller, D.Y. (1978). Visual acuity in human infants: A review and comparison of behavioral and electrophysiological studies. *Vision Research, 18*, 1469-1483.

Dooling, E.C., Chi, J.G., & Gilles, F.H. (1983). Telencephalic development: Changing gyral patterns. In F.H. Gilles, A. Leviton, & E.C. Dooling (Eds.), *The developing human brain: Growth and epidemiologic neuropathy* (pp. 94-104). Boston: John Wright, PSG.

Dow, B.M., Snyder, A.Z., Vautin, R.G., & Bauer, R. (1981). Magnification factor and receptive field size in foveal striate cortex of the monkey. *Experimental Brain Research, 44,* 213-228.

Ellemberg, D., Hammarrenger, B., Lepore, F., Roy, M.-S., & Guillemot, J.P. (2001). Contrast dependency of VEPs as a function of spatial frequency: The parvocellular and magnocellular contributions to human VEPs. *Spatial Vision, 15,* 109-121.

Eriksen, C.W., & St. James, J.D. (1986). Visual attention within and around the field of focal attention: A zoom lens model. *Perception and Psychophysics, 40,* 225-240.

Eriksen, C.W., & Yeh, Y. (1985). Allocation of attention in the visual field. *Journal of Experimental Psychology: Human Perception and Performance, 11,* 583-597.

Fiorentini, A. (1992). Parallel processes in human visual development. In J.R. Brannan (Ed.), *Applications of parallel processing in vision* (pp. 81-118). Amsterdam: Elsevier Science Publishers B.V.

Fiorentini, A., & Berardi, N. (1984). Right-hemisphere superiority in the discrimination of spatial phase. *Perception, 13,* 695-708.

Fiorentini, A., Pirchio, M., & Spinelli, D. (1980). Scotopic contrast sensitivity in infants evaluated by evoked potentials. *Investigative Ophthalmology and Visual Science, 19,* 950-955.

Foley, J.M. (1994). Human luminance pattern vision mechanisms: Masking experiments require a new model. *Journal of the Optical Society of America A, 11,* 1710-1719.

Geschwind, N., & Galaburda, A. (1987). *Cerebral lateralization*. Cambridge, MA: The MIT Press.

Grabowska, A., & Nowicka, A. (1996). Visual-spatial-frequency model of cerebral asymmetry: A critical survey of behavioral and electrophysiological studies. *Psychological Bulletin, 120*, 434-449.

Graham, N.V.S. (1989). *Visual pattern analyzers*. New York, NY: Oxford University Press.

Gwiazda, J., Bauer, J., Thorn, F., & Held, R. (1997). Development of spatial contrast sensitivity from infancy to adulthood: Psychophysical data. *Optometry and Vision Science, 74,*785-799.

Hammarrenger, B., Lepore, F., Lippe, S., Labrosse, M., Guillemot, J.-P., & Roy, M.S., (2003). Magnocellular and parvocellular developmental course in infants during the first year of life. *Documenta Ophthalmologica, 107,* 225-233.

Hartmann, E.E., & Banks, M.S. (1992). Temporal contrast sensitivity in human infants. *Vision Research, 32,* 1163-1168.

Hawken, M.J., Blakemore, C., & Morley, J.W. (1997). Development of contrast sensitivity and temporal-frequency selectivity in primate lateral geniculate nucleus. *Experimental Brain Research, 114,* 86-98.

Hedgé, J., & Van Essen, D.C. (2003). Strategies of shape representation in macaque visual area V2. *Visual Neuroscience, 20,* 313-328.

Heeger, D.J. (1993). Normalization of cell responses in cat striate cortex. *Visual Neuroscience, 9,* 181-198.

Hellige, J.B. (1993). *Hemispheric asymmetry: what's right and what's left*. Cambridge, Mass.: Harvard University Press.

Hellige, J.B. (1995). Hemispheric asymmetry for components of visual information processing. In R.J. Davidson & K. Hugdahl (Eds.), *Brain asymmetry* (pp. 99-121). Cambridge, MA: The MIT Press.

Hellige, J.B. (1996). Hemispheric asymmetry for visual information processing. *Acta Neurobiologiae Experimentalis*, *56*, 485-497.

Hellige, J.B., & Michimata, C. (1989). Categorization versus distance: Hemispheric differences for processing spatial information. *Memory and Cognition, 17*, 770-776.

Homan, R.W., Herman, J., & Purdy, P. (1987). Cerebral location of international 10-20 system electrode placement. *Electroencephalography and Clinical Neurophysiology, 66,* 376-382.

Howard, M.F., & Reggia, J.A. (2004). The effects of multi-task learning and time-varying hemispheric asymmetry on lateralization in a neural network model. *Laterality, 9,* 113-131.

Hubel, D.H., & Wiesel, T.N. (1974). Uniformity of monkey striate cortex: A parallel relationship between field size, scatter, and magnification factor. *Journal of Comparative Neurology, 158,* 295-306.

Huttenlocher, P.R., de Courten, C., Garey, L.J., & Van der Loos, H. (1982). Synaptogenesis in the human visual cortex – Evidence for synapse elimination during normal development. *Neuroscience Letters, 33,* 247-252.

Intriligator, J., & Cavanaugh, P. (2001). The spatial resolution of visual attention. *Cognitive Psychology, 43,* 171-216.

Ito, M., & Komatsu, H. (2004). Representation of angles embedded within contour stimuli in area V2 of macaque monkeys. *The Journal of Neuroscience, 24,* 3313-3324.

Ivry, R.B., & Lebby, P.C. (1993). Hemispheric differences in auditory perception are similar to those found in visual perception. *Psychological Science, 4,* 41-45.

Ivry, R.B., & Robertson, L.C. (1998). *The two sides of perception*. Cambridge, MA: The MIT Press.

Jacobs, R.A., & Kosslyn, S.M. (1994). Encoding shape and spatial relations: The role of receptive field size in coordinating complementary representations. *Cognitive Science, 18*, 361-386.

Jakobsson, P., & Johansson, B. (1992). The effect of spatial frequency and contrast on the latency in the visual evoked potential. *Documenta Ophthalmologica, 79,* 187-194.

Jeffreys, D.A., & Axford, J.G. (1972). Source locations of pattern-specific components of human visual evoked potentials. I. Components of striate cortical origin. *Experimental Brain Research, 16,* 1-21.

Kastner, S., & Ungerleider, L.G. (2000). Mechanisms of visual attention in the human cortex. *Annual Reviews of Neuroscience, 23,* 315-341.

Kelly, D.H. (1979). Motion and vision. II. Stabilized spatio-temporal threshold surface. *Journal of the Optical Society of America, 69,* 1340-1349.

Kelly, D.H. (1984). Retinal inhomogeneity. I. Spatiotemporal contrast sensitivity. *Journal of the Optical Society of America A, 1,* 107-113.

Kelly, J.P., Borchert, K., & Teller, D.Y. (1997). The development of chromatic and achromatic contrast sensitivity in infancy as tested with the sweep VEP. *Vision Research, 37,* 2057-2072.

Kenemans, J.L., Baas, J.M.P., Mangun, G.R., Lijffjt, M., & Verbaten, M.N. (2000). On the processing of spatial frequencies as revealed by evoked-potentials source modeling. *Clinical Neurophysiology, 111,* 1113-1123.

Kennedy, H., DeHay, C., & Bullier, J. (1986). Organization of the callosal connections of visual areas V1 and V2 in the macaque monkey. *The Journal of Comparative Neurology, 247,* 398-415.

Kertesz, A., Black, S.E., Polk, M., & Howell, J. (1986). Cerebral asymmetries on magnetic resonance imaging. *Cortex, 22,* 117-127.

Kinchla, R. A., Solis-Macias, V., & Hoffman, J. (1983). Attending to different levels of structure in a visual image. *Perception and Psychophysics, 33,* 1-10.

Kitterle, F.L., Christman, S., & Conesa, J. (1993). Hemispheric differences in the interference among components of compound gratings. *Perception and Psychophysics, 54*, 785-793.

Kitterle, F. L., Christman, S., & Hellige, J.B. (1990). Hemispheric differences are found in the identification, but not the detection, of low versus high spatial frequencies. *Perception and Psychophysics, 48*, 297-306.

Kitterle, F.L., Hellige, J.B., & Christman, S. (1992). Visual hemispheric asymmetries depend on which spatial frequencies are task relevant. *Brain and Cognition, 20*, 308-314.

Kitterle, F.L., & Selig, L. M. (1991). Visual field effects in the discrimination of sine-wave gratings. *Perception and Psychophysics, 50*, 15-18.

Kosslyn, S.M., Chabris, C.F., & Baker, D.P. (1995). Neural network models as evidence for different types of visual representations. *Cognitive Science, 19*, 575-579.

Kosslyn, S.M., Chabris, C.F., Marsolek, C.J., Jacobs, R.A., & Koenig, O. (1995). On computational evidence for different types of spatial relations encoding: Reply to Cook et al. (1995). *Journal of Experimental Psychology: Human Perception and Performance, 21*, 423-431.

Kosslyn, S.M., Chabris, C.F., Marsolek, C.J., & Koenig, O. (1992). Categorical versus coordinate spatial relations: Computational analyses and computer simulations. *Journal of Experimental Psychology: Human Perception and Performance, 18*, 562-577.

Kosslyn, S.M., Koenig, O., Barrett, A., Cave, C.B., Tang, J., & Gabrieli, J.D.E. (1989). Evidence for two types of spatial representations: Hemispheric specialization for categorical and coordinate relations. *Journal of Experimental Psychology: Human Perception and Performance, 15*, 723-735.

Kuroiwa, Y., Celesia, G.G., & Tohgi, H. (1987). Amplitude difference between pattern-evoked potentials after left and right hemifield stimulation in normal subjects. *Neurology, 37,* 795-799.

Kutas, M., & Dale, A. (1997). Electrical and magnetic readings of mental functions. In M.D. Rugg (Ed.). *Cognitive neuroscience* (pp. 197-242). Cambridge, MA: The MIT Press.

LeMay, M. (1976). Morphological cerebral asymmetries of modern man, fossil man, and nonhuman primate. *Annals of the New York Academy of Sciences, 280,* 349-366.

LeMay, M. (1977). Asymmetries of the skull and handedness. *Journal of the Neurological Sciences, 32,* 243-253.

LeMay, M., & Kido, D.K. (1978). Asymmetries of the cerebral hemispheres on computed tomograms. *Journal of Computer Assisted Tomography, 2*, 471-476.

LeVay, S., Wiesel, T.N., & Hubel, D.H. (1980). The development of ocular dominance columns in normal and visually deprived monkeys. *Journal of Comparative Neurology, 191,* 1-51.

Levitan, S., & Reggia, J.A. (2000). A computational model of lateralization and asymmetries in cortical maps. *Neural Computation, 12,* 2037-2062.

Levitt, J.B., Kiper, D.C., & Movshon, J.A. (1994). Receptive fields and functional architecture of macaque V2. *Journal of Neurophysiology, 71,* 2517-2542.

Lezak, M. (1995). *Neurological assessment.* New York: Oxford University Press.

Livingstone, M., & Hubel, D. (1988a). Segregation of form, color, movement, and depth: Anatomy, physiology, and perception. *Science, 240,* 740-749.

Livingstone, M., & Hubel, D. (1988b). Do the relative mapping densities of the magno- and parvocellular systems vary with eccentricity? *The Journal of Neuroscience, 8,* 4334-4339.

Luck, S.J., Chelazzi, L., Hillyard, S.A., & Desimone, R. (1997). Neural mechanisms of spatial selective attention in areas V1, V2, and V4 of macaque visual cortex. *Journal of Neurophysiology, 77,* 24-42.

Mangun, G.R. (1995). Neural mechanisms of selective visual attention. *Psychophysiology, 32,* 4-18.

Marsolek, C.J. (1995). Abstract visual-form representations in the left cerebral hemisphere. *Journal of Experimental Psychology: Human Perception and Performance, 21*, 375-386.

Martin, M. (1979). Hemispheric specialization for local and global processing. *Neuropsychologia, 17,* 33-40.

Martínez, A., Di Russo, F., Anllo-Vento, L., & Hillyard, S.A. (2001). Electrophysiological analysis of cortical mechanisms of selective attention to high and low spatial frequencies. *Clinical Neurophysiology, 112,* 1980-1998.

Martínez, A., Di Russo, F., Anllo-Vento, L., Sereno, M.I., Frank, L.R., Buxton, R.B., Dubowitz, D.J., Wong, E.C., Hinrichs, H., Heinze, H.J., & Hillyard, S.A. (1999). Involvement of striate and extrastriate visual cortical areas in spatial attention. *Nature Neuroscience, 2,* 364-369.

Mecacci, L. (1993). On spatial frequencies and cerebral hemispheres: Some remarks from the electrophysiological and neuropsychological points of view. *Brain and Cognition, 22,*199-212.

Mecacci, L. (1997). Temporal frequency processing. In S. Christman (Ed.). *Cerebral asymmetries in sensory and perceptual processing* (pp. 31-54). Amsterdam: Elsevier Science B.V.

Mecacci, L., & Spinelli, D. (1987). Hemispheric asymmetry of pattern reversal visual evoked potentials in healthy subjects. *International Journal of Psychophysiology, 4,* 325-328.

Mecacci, L., Spinelli, D., & Viggiano, M.P. (1990). The effects of visual field size on hemispheric asymmetry of pattern reversal visual evoked potentials. *International Journal of Neuroscience, 51,* 141-151.

Merigan, W.H., Byrne, C., & Maunsell, J.H.R. (1991). Does primate motion perception depend on the magnocellular pathway? *Journal of Neuroscience, 11,* 3422-3429.

Merigan, W.H., Katz, L.M., & Maunsell, J.H.R. (1991). The effects of parvocellular lateral geniculate lesions on the acuity and contrast sensitivity of macaque monkeys. *Journal of Neuroscience, 11,* 994-1101.

Merigan, W.H., & Maunsell, J.H.R. (1993). How parallel are the primate visual pathways? *Annual Review of Neuroscience, 16,* 369-402.

Moran, J., & Desimone, R. (1985). Selective attention gates visual processing in the extrastriate cortex. *Science, 229,* 782-784.

Movshon, J.A., & Kiorpes, L. (1988). Analysis of the development of spatial contrast sensitivity in monkey and human infants. *The Journal of the Optical Society of America A, 5,* 2166-2172.

Myslobodsky, M.S., & Bar-Ziv, J. (1989). Locations of occipital EEG electrodes verified by computed tomography. *Electroencephalography and clinical neurophysiology, 72,* 362-366.

Myslobodsky, M.S., Coppola, R., & Weinberger, D.R. (1991). EEG laterality in the era of structural brain imaging. *Brain Topography, 3,* 381-390.

Myslobodsky, M.S., Glicksohn, J., Coppola, R., & Weinberger, D.R. (1991). Occipital lobe morphology in normal individuals assessed by magnetic resonance imaging (MRI). *Vision Research, 31,* 1677-1685.

Nakayama, K., & Mackeben, M. (1989). Sustained and transient components of focal attention. *Vision Research, 29,* 1631-1647.

Nealy, T.A., & Maunsell, J.H.R. (1994). Magnocellular and parvocellular contributions to the responses of neurons in macaque striate cortex. *The Journal of Neuroscience, 14,* 2069-2079.

Niebauer, C.L., & Christman, S.D. (1999). Visual field differences in spatial frequency discrimination. *Brain and Cognition, 41*, 381-389.

Nicholls, M.E.R. (1994). Hemispheric asymmetries for temporal resolution: A signal detection analysis of threshold and bias. *Quarterly Journal of Experimental Psychology, 47A,* 291-310.

Nicholls, M.E.R. (1996). Temporal processing asymmetries between the cerebral hemispheres: Evidence and implications. *Laterality, 1*, 97-137.

Norcia, M.A., Tyler, C.W., & Hamer, R.D. (1990). Development of contrast sensitivity in the human infant. *Vision Research, 30,* 1475-1486.

Onofrj, M., Fulgente, T., Thomas, A., Curatola, L., Peresson, M., Lopez, L., Locatelli, T., Martinelli, V., & Comi, G. (1995). Visual evoked potentials generator model derived from different spatial frequency stimuli of visual field regions and magnetic resonance imaging coordinates of V1, V2, V3 areas in man. *International Journal of Neuroscience, 83*, 213-239.

Parker, D.M., & Salzen, E.A. (1977). Latency changes in the human visual evoked response to sinusoidal gratings. *Vision Research, 17,* 1201-1204.

Parry, N.R.A., Murray, I.J., & Hadjizenonos, C. (1999). Spatio-temporal tuning of VEPs: Effect of mode of stimulation. *Vision Research, 39,* 3491-3497.

Parsons, O.A., Majumder, R.K., & Chandler, P.J. (1967). Impaired flicker detection in visual fields subserved by non-damaged hemispheres. *Cortex, 3,* 307-316.

Peterzell, D.H., Harvey, L.O., Jr., & Hardyck, C.D. (1989). Spatial frequencies and the cerebral hemispheres: Contrast sensitivity, visible persistence, and letter classification. *Perception and Psychophysics, 46,* 443-455.

Peterzell, D.H., & Kelly, J. P. (1997). Development of spatial frequency tuned "covariance" channels: Individual differences in the electrophysiological (VEP) contrast sensitivity function. *Optometry and Vision Science, 74,* 800-807.

Peterzell, D.H., & Teller, D.Y. (1996). Individual differences in contrast sensitivity functions: The lowest spatial frequency channels. *Vision Research, 36,* 3077-3085.

Peterzell, D.H., Werner, J.S., & Kaplan P.S. (1993). Individual differences in contrast sensitivity functions: The first four months of life in humans. *Vision Research, 33,* 381-396.

Peterzell, D.H., Werner, J.S., & Kaplan P.S. (1995). Individual differences in contrast sensitivity functions: Longitudinal study of 4-, 6-, and 8-month-old human infants. *Vision Research, 35,* 961-979.

Plant, G.T., Zimmern, R.L., & Durden, K. (1983). Transient visually evoked potentials to the pattern reversal and onset of sinusoidal gratings. *Electroencephalography and Clinical Neurophysiology, 56,* 147-158.

Posner, M.I., & Peterson, S.E. (1990). The attention system of the human brain. *Annual Review of Neuroscience, 13,* 25-42.

Posner, M.I., Snyder, C.R., & Davidson, B.J. (1980). Attention and the detection of signals. *Journal of Experimental Psychology, 109,* 160-174.

Proverbio, A.M., Zani, A., & Avella, C. (1996). Differential activation of multiple current sources of foveal VEPs as a function of spatial frequency. *Brain Topography, 9,* 59-68.

Proverbio, A.M., Zani, A., & Avella, C. (1997). Hemispheric asymmetries for spatial frequency discrimination in a selective attention task. *Brain and Cognition, 34,* 311-320.

Rademacher, J., Caviness, V.S., Steinmetz, H., & Galaburda, A.M. (1993). Topographical variation of the human primary cortices: Implications for neuroimaging, brain mapping, and neurobiology. *Cerebral Cortex, 3,* 313-329.

Rasengane, T.A., Allen, D., & Manny, R.E. (1997). Development of temporal contrast sensitivity in human infants. *Vision Research, 37,* 1747-1754.

Rebai, M., Bagot, J.-D., & Viggiano, M.-P. (1993). Hemispheric asymmetry in transient visual evoked potentials induced by the spatial factor of the stimulation. *Brain and Cognition, 23,* 263-278.

Rebai, M., Bernard, C., Lannou, J., & Jouen, F. (1998). Spatial frequency and right hemisphere: An electrophysiological investigation. *Brain and Cognition, 36*, 21-29.

Rebai, M., Lannou, J., Bernard, C., Bonnet, C., & Rochetti, G. (1997). Hemispheric asymmetries of visual evoked potentials in relation to spatial frequency, handedness and familial left-handedness. *International Journal of Psychophysiology, 25,* 85-95.

Rebai, M., Mecacci, L., Bagot, J.-D., & Bonnet, C. (1986). Hemispheric asymmetries in the visual evoked potentials to temporal frequency: Preliminary evidence. *Perception, 15,* 589-594.

Rebai, M., Mecacci, L., Bagot, J.-D., & Bonnet, C. (1989). Influence of spatial frequency and handedness on hemispheric asymmetry in visually steady-state evoked potentials. *Neuropsychologia, 27,* 315-324.

Regal, D.M. (1981). Development of critical flicker frequency in human infants. *Vision Research, 21,* 549-555.

Reggia, J.A., Goodall, S., & Shkuro, Y. (1998). Computational studies of lateralization of phoneme sequence generation. *Neural Computation, 10,* 1277-1297.

Reynolds, J.H., Chelazzi, L., & Desimone, R. (1999). Competitive mechanisms subserve attention in macaque area V2 and V4. *Journal of Neuroscience, 19,* 1736-1753.

Robertson, L.C., Egly, R., Lamb, M.R., & Kerth, L. (1993). Spatial attention and cuing to global and local levels of hierarchical structure. *Journal of Experimental Psychology: Human Perception and Performance, 19,* 471-487.

Robertson, L.C., & Ivry, R. (2000). Hemispheric asymmetries: Attention to visual and auditory primitives. *Current Directions in Psychological Science, 9,* 59-63.

Robson, J.G. (1966). Spatial and temporal contrast-sensitivity functions of the visual system. *Journal of the Optical Society of America, 56,* 1141-1142.

Rose, D. (1983). An investigation into hemispheric differences in adaptation to contrast. *Perception & Psychophysics, 34,* 89-95.

Roth, E. C., & Hellige, J.B. (1998). Spatial processing and hemispheric asymmetry: Contributions of the transient/magnocellular visual system. *Journal of Cognitive Neuroscience, 10,* 472-484.

Rovamo, J., & Virsu, V. (1979). An estimation and application of the human cortical magnification factor. *Experimental Brain Research, 37,* 495-510.

Rovamo, J., Virsu, V., & Näsänen (1978). Cortical magnification factor predicts the photopic contrast sensitivity of peripheral vision. *Nature, 271,* 54-56.

Rugg, M.D., & Coles, M.G.H. (1995). *Electrophysiology of mind: Event-related brain potentials and cognition.* Oxford: Oxford University Press.

Sasaki, Y., Hadjikhani, N., Fischl, B., Liu, A.K., Marrett, S., Dale, A.M., & Tootell, R.B.H. (2001). Local and global attention are mapped retinotopically in human occipital cortex. *Proceedings of the National Academy of Sciences USA, 98,* 2077-2082.

Sawarti, A., & Callaway, E.M. (1996). Convergence of magno- and parvocellular pathways in layer 4B of macaque primary visual cortex. *Nature, 380,* 442-446.

Scheibel, A.B. (1984). A dendritic correlate of human speech. In N. Geschwind & A.M. Galaburda (Eds.), *Cerebral dominance: The biological foundations* (pp. 43-52). Cambridge, MA: Harvard University Press.

Schiller, P.H., Finlay, B.L., & Volman, S.F. (1976). Quantitative studies of single-cell properties in the monkey striate cortex: III. Spatial frequency. *Journal of Neurophysiology, 39,* 1334-1351.

Schiller, P.H., & Logothetis, N.K. (1990). The color-opponent and broad-band channels of the primate visual system. *Trends in Neuroscience, 13,* 392-398.

Sergent, J. (1982). The cerebral balance of power: Confrontation or cooperation? *Journal of Experimental Psychology: Human Perception and Performance, 8*, 253-272.

Sergent, J. (1987). Failures to confirm the spatial frequency hypothesis: Fatal blow or healthy complication? *Canadian Journal of Psychology*, *41*, 412-428.

Shapley, R. (1990). Visual sensitivity and parallel retinocortical channels. *Annual Review of Psychology, 41,* 635-658.

Shapley, R. (1992). Parallel retinocortical channels: X and Y and P and M. In J.R. Brannan (Ed.), *Applications of parallel processing in vision* (pp. 3-36). Amsterdam: Elsevier Science Publishers B.V.

Sharbrough F., Chatrian G.-E., Lesser R.P., Lüders H., Nuwer M., Picton T.W. (1991). American Electroencephalographic Society Guidelines for Standard Electrode Position Nomenclature. *Journal of Clinical Neurophysiology, 8*, 200-2.

Shevtsova, N., & Reggia, J.A. (1999). A neural network model of lateralization during letter identification. *Journal of Cognitive Neuroscience, 11*, 167-181.

Smith, A.T., Singh, K.D., Williams, A.I., & Greenlee, M.W. (2001). Estimating receptive field size from fMRI data in human striate and extrastriate visual cortex. *Cerebral Cortex, 11,* 1182-1190.

Somers, D.C., Dale, A.M., Seiffert, A.E., & Tootell, R.B.H. (1999). Functional MRI reveals spatially specific attentional modulation in human primary visual cortex. *Proceedings of the National Academy of Sciences USA, 96,* 1663-1668.

Stensaas, S.S., Eddington, D.K., & Dobelle, W.H. (1974). The topography and variability of the primary visual cortex in man. *The Journal of Neurosurgery, 40,* 747-755.

Strasburger, H., Murray, I.J., & Remky, A. (1993). Sustained and transient mechanisms in the steady-state visual evoked potential: Onset presentation compared to pattern reversal. *Clinical Vision Sciences, 8,* 211-234.

Swanson, W.H., & Birch, E.E. (1990). Infant spatiotemporal vision: Dependence of spatial contrast sensitivity on temporal frequency. *Vision Research, 30,* 1033-1048.

Taylor, D.C. (1969). Differential rates of cerebral maturation between sexes and between hemispheres. *Lancet, 2,* 140-142.

Thatcher, R.W. (1992). Cyclic cortical reorganization during early childhood. *Brain and Cognition, 20,* 24-50.

Thatcher, R.W., Walker, R.A., & Giudice, S. (1987). Human cerebral hemispheres develop at different rates and ages. *Science, 236*, 1110-1113.

Tobimatsu, S., Kurita-Tashima, S., Nakayama-Hiromatsu, M., & Kata, M. (1993). Effect of spatial frequency on transient and steady-state VEPs: Stimulation with checkerboard, square-wave grating and sinusoidal grating patterns. *Journal of the Neurological Sciences, 118,* 17-24.

Tootell, R.B.H., Hadjikhani, N., Hall, E.K., Marrett, S., Vanduffel, W., Vaughan, J.T., & Dale, A.M. (1998). The retinotopy of visual spatial attention. *Neuron, 21,* 1409-1422.

Tootell, R.B.H., Silverman, M.S., Hamilton, S.L., Switkes, E., & De Valois, R.L. (1988). Functional anatomy of macaque striate cortex. V. Spatial frequency. *The Journal of Neuroscience, 8*, 1610-1624.

Tootell, R.B.H., Silverman, M.S., Switkes, E., & De Valois, R.L. (1982). Deoxyglucose analysis of retinotopic organization of primate striate cortex. *Science, 218,* 902-904.

Turkewitz, G. (1988). A prenatal source for the development of hemispheric specialization. In D.L. Molfese & S.J. Segalowitz (Eds.). *Brain lateralization in children* (pp. 1-34). New York: The Guilford Press.

Turrigiano, G.G., & Nelson, S.B. (2004). Homeostatic plasticity in the developing nervous system. *Nature Neuroscience, 5,* 97-107.

Van Essen, D.C., & DeYoe, E.A. (1995). Concurrent processing in the primate visual cortex. In M. Gazzaniga (Ed.), *The cognitive neurosciences* (pp. 383-400).

Van Essen, D.C., Newsome, W.T., & Maunsell, J.H.R. (1984). The visual field representation in striate cortex of the macaque monkey: Asymmetries, anisotropies, and individual variability. *Vision Research, 24,* 429-448.

Van Kleek, M.H. (1989). Hemispheric differences in global versus local processing of hierarchical visual stimuli by normal subjects: New data and a meta-analysis of previous studies. *Neuropsychologia, 27*(9), 1165-1178.

Van Orden, K.F., & House, J.F. (1996). Spatial frequency-dependent asymmetry of visual evoked potential amplitudes. *Perceptual and Motor Skills, 82,* 1011-1018.

Vassilev, A., Stomonyakov, V., & Manahilov, V. (1994). Spatial-frequency specific contrast gain and flicker masking of human transient VEP. *Vision Research, 34,* 863-872.

Vidyasagar, T.R., Kulikowski, J.J., Lipnicki, D.M., & Dreher, B. (2002). Convergence of parvocellular and magnocellular information channels in the primary visual cortex of the macaque. *European Journal of Neuroscience, 16,* 945-956.

Virsu, V. & Rovamo, J. (1979). Visual resolution, contrast sensitivity, and the cortical magnification factor. *Experimental Brain Research, 37,* 475-494.

Wilson, H.R. (1988). Development of spatiotemporal mechanisms in infant vision. *Vision Research, 28*, 611-628.

Wilson, H.R., & Gelb, D.J. (1984). Modified line-element theory for spatial frequency and width discrimination. *The Journal for the Optical Society of America A, 1,* 124-131.

Wilson, H.R., Levi, D. Maffei, L., Rovamo, J., & De Valois, R. (1990). The perception of form: Retina to striate cortex. In L. Spillmann & J.S. Werner (Eds.), *Visual perception: The neurophysiological foundations* (pp. 231-272). San Diego, CA: Academic Press, Inc.

Wilson, H.R., & Wilkinson, F. (2004). Spatial channels in vision and spatial pooling. In L.M. Chalup & J.S. Werner (Eds.), *The visual neurosciences* (pp. 1060-1068). Cambridge, MA: The MIT Press.

Youdelis, C., & Hendrickson, A. (1986). A qualitative and quantitative analysis of the human fovea during development. *Vision Research, 26,* 847-855.

Zani, A., & Proverbio, A.M. (1995). ERP signs of early selective attention effects to check size. *Electroencephalography and Clinical Neurophysiology, 95,* 277-292.

Zani, A., & Proverbio, A.M. (Eds.) (2003). *The cognitive electrophysiology of the mind*. San Diego, CA: Academic Press.

Zilles, K., Dabringhaus, A., Geyer, S., Amunts, K., Meishu, Q., Schleicher, A., Gilissen, E., Schlaug, G., & Steinmetz, H. (1996). Structural asymmetries in the human forebrain and the forebrain of non-human primates and rats. *Neuroscience and Behavioral Reviews, 20,* 593-605.